FINAL REPORT: The Role of RUB (related to ubiquitin) Family of Proteins in the Hormone Response

FINAL REPORT

DOE AWARD No. DE-FG02-03ER15416 entitled:
The Role of RUB (related to ubiquitin) Family of Proteins in the Hormone Response
08/01/2003-07/31/2010

Judy Callis, PI
Professor and Vice-Chair
Department of Molecular and Cellular Biology
University of CA-Davis
1 Shields Avenue
Davis, CA 95616

March 22, 2013

Disclaimer Statement

Signature Page

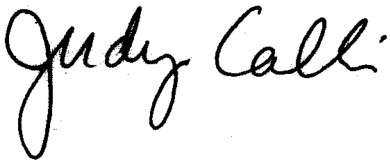

March 21, 2013

Abstract

The Rub pathway is a conserved protein modification pathway. RUB (called Rubp1 in budding yeast, Nedd8 in animals and RUB in plants) is a ubiquitin-like 76-amino acid protein. It covalently attaches to protein using an enzymatic machinery analogous to the enzymes that attach ubiquitin to its substrate proteins. However, the nature of the complement of Rub-modified proteins in organisms was not clear. From bioinformatics analyses, one can identify a Rub activating enzymes and Rub conjugating enzymes. However, in many cases, their biochemical properties were not described.

In DOE-funded work, we made major advances in our understanding of the Rub pathway in yeast and plants, work that is applicable to other organisms as well. There is a multi-subunit enzyme called SCF in all eukaryotes. The SCF consists of several subunits that serve as a scaffold (the cullin, SKP and RBX subunits) and one subunit that interacts with the substrate. This cullin protein (called Cdc53p in yeast and CULLIN 1 in plants and animals) was a known Rub target. In this work, we identified additional Rub targets in yeast as the other cullin-like proteins Cul3p and Rtt101p. Additionally we described the conservation of the Rub pathway because plant RUB1 can conjugated to yeast Cdc53p- in yeast. In the model plant *Arabidopsis thaliana*, we characterized the Rub activating enzymes and showed that they are not biochemically equivalent. We also showed that the Rub pathway is essential in plants and characterized plants with reduced levels of rub proteins. These plants are affected in multiple developmental processes. We discovered that they over-produce ethylene as dark-grown seedlings. We characterized a mutant allele of CULLIN1 in Arabidopsis with impaired interaction with RBX and showed that it is unstable *in vivo*. We used our knowledge of monitoring protein degradation to map the degradation determinants in a plant transcription factor. Finally, we took a mass spectrometric approach to identify novel Rub targets in plants and identified DDB1a, a subunit of an different ubiquitin ligase as a potential Rub-modified protein. Altogether, these studies have advanced our knowledge of the Rub pathway in all organisms.

Table of Contents

Executive Summary

The Rub pathway is a conserved protein modification pathway. RUB (called Rubp1 in budding yeast, Nedd8 in animals and RUB in plants) is a ubiquitin-like 76-amino acid protein. It covalently attaches to protein using an enzymatic machinery analogous to the enzymes that attach ubiquitin to its substrate proteins. The enzymes that catalyze ubiquitin attachment are E1 (ubiquitin activating), E2 (ubiquitin conjugating) and E3 (ubiquitin ligase). E1 and E2 covalently link to ubiquitin in a labile thioester linkage. The third enzyme, E3 or ubiquitin ligase, recognizes the substrate protein and also binds to the E2 carrying activated ubiquitin for transfer. Similarly, related E1-like and E2-like enzymes for Rub attachment can be identified in organisms by virtue of their identity to E1 and E2. In yeast, the Rub1p activating enzyme is a heterodimer of proteins called Enr1p and Uba3p. The E2 is called Ubc12p. While ubiquitin covalently modifies a large number of proteins, the nature of the complement of Rub-modified proteins in organisms was not clear. One Rub1p substrate had been identified; Cdc53p, a cullin-like protein that is a subunit of an ubiquitin E3 ligase called a SCF was shown to be a Rub1p target. We hypothesized that there were additional Rub1p targets. We first utilized yeast as our model organism, where the Rub activating and conjugating activities were described and these activities could be eliminated because they were encoded by single genes, which could easily by disrupted using standard molecular biology techniques. We expressed an epitope-tagged form of Rubp1, which using immunoblotting identified multiple possible Rub1p targets. Using bioinformatics, we tested whether the Cdc53p-related proteins, Cul3p and Rtt101p, were also Rub1p targets. From multiple approaches, including epitope tagging Cul3p and Rtt101p and eliminating their expression, we proved that they are indeed modified by Rub1p *in vivo* and modification depends on the known Rub1p activating enzyme. In addition we discovered that Rt101p is also modified in a Rubp1p- and Rubp1 activating enzyme-independent manner; this is the first description of a protein dually modified by Rub1p. We also identified the site required for Rub1p attachment and showed that it is also required for the Rub1p-independent attachment.

The nature of the Rub pathway was much less well characterized. There are multiple RUB-encoding genes in Arabidopsis and two different Enr1p-like proteins whose relative roles were not clear (called AXR1 and AXL1). AXR1 mutants had been characterized as dwarf with a resistant to the growth inhibitory effects of the hormone auxin. Nothing was known about the second Enr1p-like protein. Two RUB conjugating enzymes are present in Arabidopsis, and their relative contributions are unknown. Two RUB genes encode proteins that differ by only one amino acid (RUB1 and RUB2), while the third RUB-like encoding gene is more diverged (RUB3). We first used the yeast system to determine that RUB1 can conjugate to Cdc53p in yeast, but not RUB3, the first indication of divergence of function between the RUBs. Second, we were the first to discover that RUBS can be conjugated by the ubiquitin E1 under certain circumstances. In our case over-expression of plant RUB1 lead to conjugation to a myriad of protein in a manner independent of the Rub1p activating enzyme, indicating that the ubiquitin pathway was recognizing RUB. We showed that yeast ubiquitin E1 fails to discriminate RUB from ubiquitin when the plant C-terminal half of RUB is present.

We hypothesized that RUB1 and RUB2 proteins, given their high degree of identity are functionally redundant. This was proven by looking at plants with disruptions in individual *RUB* genes. We showed these disruptions eliminate expression from the gene and plants with only a single *RUB1* or *RUB2* gene are not different from wild type plants containing 4 *RUB1/2* – encoding genes. However, loss of the remaining *RUB* gene causes many gametes to die and all

homozygous mutant embryos to die. Thus, in stark contrast in yeast where the Rub pathway can be eliminated with no phenotypic consequences, loss of all *RUB*-encoding genes is lethal. This was an important finding, establishing the functional significance of the Rub pathway in plants. These studies also showed the RUB3 protein is NOT functionally equivalent to RUB1/2 because it cannot prevent death upon loss of RUB1/2. To further study RUB1/2 function, we generated and carefully analyzed a large number of plants with reduced RUB expression, called *dsrub* plants. These plants had many developmental defects, from early seedling growth to flowering, demonstrating that the Rub pathway plays important roles during vegetative growth. We discovered that dark-grown *dsrub* seedlings synthesized more ethylene than wild type and that *axr1* mutant seedlings synthesized less than wild type. This was a surprising result, given that AXR1, participating in RUB1 activation, should be in the same pathway as RUB and loss of function mutants should have the same phenotype. However, we showed that the regulation of ethylene biosynthetic genes is different between *dsrub* lines and *axr1* lines, indicating complexities.

We hypothesized that plant RUB would conjugate to the multiple cullin-like proteins present in higher eukaryotes. Using epitope-tagged forms of RUB1/2 and a RUB-specific antibody that we developed, we demonstrated that plant RUB1/2 proteins attach to the multiple cullin-like proteins present in Arabidopsis, CUL3 and CUL4. We undertook a mass spectrometry approach to identify addition, novel RUB targets in Arabidopsis. After an extensive effort, ten candidates were further tested in transient expression assays that we showed had a high degree of specificity. One of these proteins, DDB1a, was clearly RUB1-modified in these assays by multiple criteria. Expression of parts of the protein identified a preferred rubylation region. This protein is a new, not previously identified potential in vivo rubylated protein.

We also carefully studied the second Enr-like protein in Arabidopsis, AXL1. We showed for the first time that AXL1, at least in the in vitro assays that we conducted, behaved identically to AXR1 in RUB thioester formation and transfer to E2. We then hypothesized that these two proteins are functionally redundant. To our surprise, AXL1 cannot substitute for AXR1, suggesting that these two have distinct biological roles, suggesting complex regulation of RUB activation.

Through isolation of a mutation in Arabidosis CUL1 in a genertic screen, we show here that the interaction of CUL1 with RBX1 is important for the stability of CUL1. This viable line with impaired CUL1 function is a useful reagent to identify its potential substrates. Finally, we utilize our knowledge of monitoring proten degradation with LUC protein fusions to measure the degradation rate od AFR1, a transcription factor.

These studies have revealed important new information about the Rub pathway in yeast and plants and generated a number of reagent freely distributed to other laboratories: clones, yeast strains, transgenic plant lines, expression vectors, etc. Our work has provided invaluable information for others who are further exploring the role of Rtt101p and Cul3p in yeast. DOE supported research provided support for these studies to gain a deeper understanding of this essential regulatory mechanism.

Report Details

Introduction

Plant growth and biomass production is an important area of research. Understanding how plants grow can contribute to plants better able to utilize solar energy for biomass production. The current interest in using plants as a renewable resource makes it even more imperative that we understand the fundamental mechanisms for plant growth and development. Once we have a better understanding, we may use this information to increase productivity, either by optimizing the growth environment or by genetic engineering mechanisms. Our lab is focusing on how proteolysis is regulating seedling growth, but what we learn is applicable to other phases of the life cycle, such as vegetative growth, flowering, fruit development, and seed set, which are other important aspects contributing to plant biomass.

Our laboratory is interested in understanding how the levels of proteins are regulated in cells. In addition to transcriptional control, regulated proteolysis is an equal partner in controlling protein concentration. By regulating the levels of key transcription factors, signaling molecules and rate limiting enzymes in biosynthetic pathways, the cell regulates growth and development. The major mechanism to regulate protein abundance is by the ubiquitin pathway. Ubiquitin is a 76-aa protein that covalently attaches typically to the lysyl amino group of other proteins. One or more ubiquitins can be attached, either at a single lysine or at multiple lysines. When attached at a single lysine, ubiquitin is covalently linked to ubiquitin at one of its 7 surface lysines. Ubiquitin linked to ubiquitin at lysine 48 is a signal for recognition by a large multi-catalytic protease, called the proteasome. Other ubiquitin-ubiquitin linkages and monoubiquitin appear to function in different pathways, such as intracellular localization and DNA repair.

The enzymes that catalyze ubiquitin attachment are E1 (ubiquitin activating), E2 (ubiquitin conjugating or UBC) and E3 (ubiquitin ligase). E1 and E2 covalently link to ubiquitin in a labile thioester linkage. The third enzyme, E3 or ubiquitin ligase, recognizes the substrate protein and also binds to the E2 carrying activated ubiquitin for transfer. Hence, E3s are key to understanding the specificity and can control the ubiquitination pathway.

One type of E3, called the SCF for SKP-cullin-F box, is a major type of E3 in all organisms, including plants, with likely over 700 different ligases of this type in one species. In plants, three different cullins have been described, CULLIN1, CULLIN3a/b and CULLIN4. While all share the same E2 binding subunit, the RING protein called RBX, each assembles with a different substrate interacting subunit that brings the substrate to be ubiquitinated close to the activated ubiquitin-E2. As well as positioning the E2 for ubiquitin transfer, recent evidence suggests that the RING domain protein allosterically activates the E2 to facilitate transfer of ubiquitin from the E2 to the substrate protein.

One major mechanism that serves to activate this ligase family is modification of the cullin subunit by the ubiquitin-like protein, RUB for Related to Ubiquitin (called Nedd8 in animals). RUB/Nedd8 proteins share 50-60% amino acid identity with ubiquitin. Covalent attachment of RUB/Nedd8 proteins to cullin subunit requires an E1-like, an E2-like and an E3-like activity. In all species, the E1-like activity is a heterodimeric enzyme called Enr1p/Uba3p

in budding yeast, AXR1/ECR1 in Arabidopsis, and APP-BP1/hUba3 in mammals. AXR1 was previously identified as a protein required for a proper auxin response in plants, though at the time of isolation its biochemical identity was mysterious (Leyser *et al.,* 1993). ECR1 (for E1-like C-terminal region) was found subsequently through homology searches for proteins with similarity to the C-terminus of ubiquitin E1 (del Pozo *et al.,* 2002). Recombinant AXR1 and ECR1 together are capable of thioester formation with Arabidopsis RUB1 and human Nedd8, but not ubiquitin (del Pozo et al., 2002). Similarly, the Nedd8 activating enzyme is a heterodimeric enzyme consisting of a subunit related to the ubiquitin E1 N-terminal region named APP-BP1 (for beta-amyloid precursor protein-binding protein) and a subunit related to the ubiquitin E1 C-terminal region called Uba3. The RUB/Nedd8 E2 activity is called Ubc12p in budding yeast, RCE1 in Arabidopsis, and hUBc12 in mammals. The E3 activity is curious; it appears to require RBX, a subunit of the SCF complex, so this protein has a dual function in catalyzing both ubiquitination and rubylation.

In the DOE funded period, we identified additional Rub substrates in yeast, studied the role this subfamily of ubiquitin-like proteins in *Arabidopsis thaliana* and developed a methodology to identify novel Rub-modified substrates in plants. The following section details our findings.

Results and Discussion

1. Studies of yeast Rub pathway identifies additional *in vivo* substrates and is used to demonstrate conservation and divergence of aspects of the Rub pathways between yeast and plants

1.1. Identification of new RUB-modified proteins in *Saccharomyces cerevisaie*- Rub1p attaches to the two cullin-like proteins in *S. cerevisaie,* Cul3p and Rtt101p.

A single ubiquitin-like protein Rub1p covalently attaches to cullin protein Cdc53p in yeast (Lammer *et al.,* 1998) and to the mammalian homologous protein, Cullin 1 (Feldman *et al.,* 1997). To further understand the biological roles of the ubiquitin-like protein Rub1p, we asked whether other proteins in addition to Cdc53p were modified by Rub1p *in vivo* in yeast. As likely potential Rub1p substrates, we sought to determine whether other cullin-like proteins in yeast were also Rub1p modified in yeast. A TFASTA search of the *S. cerevisiae* genome revealed two open reading frames with significant identity to Cdc53p. Open reading frame YGR003w encodes an 86 kDa protein with 22% identity to Cdc53p named Cul3p. The second open reading frame, YJL047c, encodes a 99 kDa protein named Rtt101p with 21% identity in the carboxyl-terminal 400 amino acids to the corresponding region of Cdc53p. In addition to having identity to Cdc53p, both proteins contain the conserved lysine shown to be required for Rub1p attachment (the rubylation site) in mammalian cullins (Wada *et al.,* 1999). Neither protein had been linked to the ubiquitin pathway at the time of this study. Nothing was known about Cul3p, and Rtt101p was known for its role in regulating transposition of the Ty transposable element and *rtt101* mutants are hypersensitive to DNA damaging reagents (Scholes *et al.,* 2001), but the molecular mechanisms were unknown.

We generated yeast strains that expressed epitope tagged forms of Rub1p (3xHA:Rub1p) and/or epitope tagged forms of the other two cullin-like proteins so that the forms of these

proteins can be visualized in immunoblot blots. These expression constructs were introduced into different yeast strains, either wild-type or ones with a deletion in either Rub1p or in one of the cullin-like proteins. While deletion of Cdc53p is lethal, yeast lacking Rtt101p or Cul3p are viable. In addition, a mutant form of Cdc53p lacking the rubylation site is viable and was used in a few experiments. We generated two important strains. One has a deletion in the single *RUB* gene so that no rubylated (Rub1p-modified) proteins could be present. The second strain expresses 3xHA:Rub1p in the *Δrub1* strain, so that the only form of Rub1p present in these cells is detectable due to the epitope tag, HA, with anti-HA antibodies. After growth of these various yeast strains on the appropriate selection media, indicating the presence of the expression plasmids, we then made protein extracts and detected the presence and molecular masses of the epitope tagged proteins after SDS-PAGE to separate the proteins and immunoblot blots analyses to visualize the epitope tag.

Rub1p is a 7.5 kDa protein, and with the HA epitope tag, it migrates as an ~10 kDa protein. If Rub1p covalently attaches to other proteins, these proteins will now be visualized with anti-HA Ab and these additional anti-HA proteins will migrate at molecular masses greater than 10 kDa on denaturing acrylamide gels (SDS-acrylamide). Such HA-immunoreactive proteins can be detected in yeast, indicating covalent attachment of 3xHA:Rub1p to other proteins (compare Figure 1, lane a, yeast with no 3xHA:Rub present, to lane c, yeast expressing 3xHA:Rub1p). The higher molecular mass forms depend on the presence of ENR2p, the enzyme postulated to activate Rub1p for attachment to proteins, and as expected 3xHA:Rub higher molecular weight forms are lost in the *Δenr2* strain (Figure 1, lane b). To further demonstrate that these higher molecular weight forms are authentic Rub1p covalently bound to proteins (referred to as conjugates), we expressed a tagged form of Rub1p lacking its 2 C-terminal amino acids (3xHA:RubΔGG). The analogous deletion form of ubiquitin cannot attach to proteins. Neither can 3xHA:RubΔGG (Figure 1, lane d). We also tested if the pattern of Rub1p conjugates requires lysine-48. This residue in ubiquitin is the major site of ubiquitin-ubiquitin linkages, allowing the formation of ubiquitin ladders. However, for Rub1p, the pattern of rubylated proteins from strains expressing 3xHA:Rub1p and 3xHA:RubK48R were identical (compare Figure 1c to e), indicating that Rub1p conjugation to proteins does not require lysine-48. All together, these data indicated that Rub1p is covalently attached to multiple polypeptides in an ENR2-dependent manner that requires an intact Rub1p C-terminus, but is independent of Rub1p K-48. The latter result suggests that a single Rub1p is attached to its target proteins.

Figure 1 demonstrated that multiple bands are detected with anti-HA antibodies in a strain expressing 3xHA:Rub1p. If Rtt101p exists as a Rub1p conjugate, then this conjugate should disappear in a *Δrtt101* strain. *RTT101* was disrupted in the strain expressing 3xHA:Rub1p (Figure 2) and the conjugation pattern of protein extracts from two independent disruptions determined by Immunoblot analysis with anti-HA antibodies. Two 3xHA:Rub1p-modified proteins are readily detectable (Figure 2, lane b). The 110 kDa conjugate was not present in the *Δrtt101* protein extracts (Figure 2, lanes c and d) compared to a protein extract from the isogenic *RTT101* strain (Figure 2, lane b). These bands were dependent on 3xHA:Rub1p because they were not detected in a strain not expressing 3xHA:Rub1p (Figure 2, lane a). The band remaining is likely the previously described Rub1p conjugate: Cdc53p-3xHA:Rub1p (Lammer et al., 1998).

To ensure that Rtt101p itself was being conjugated to Rub1p and not solely that this Rub1p conjugate is dependent on the presence of *RTT101*, a triple HA epitope-tagged version of Rtt101p was expressed. Immunoblot analysis using anti-HA antibodies revealed the presence of

two forms of Rtt101p (see Figure 3, lane a). If the slower migrating form of Rtt101p is a rubylated form of Rtt101p it should be dependent on *RUB1*. The triple HA epitope-tagged version of Rtt101p was expressed in isogenic *Δrub1* and *RUB1* strains and the 3xHA:Rtt101p pattern determined by Immunoblot analysis using anti-HA antibodies. Surprisingly, while there was a reduction in abundance of the slower migrating form of 3xHA:Rtt101p in a protein extract from a *Δrub1* strain when compared to a protein extract from a *RUB1* strain (Figure 3, compare lane a with lane d), the slower migrating band was not completely absent. Quantitation of the immunoreactive bands revealed that both forms are equally present in protein extracts from a *RUB1* strain (Figure 3, lane a). In contrast, in protein extracts from a *Δrub1* strain, the slower migrating form is only 60% of the faster migrating form (Figure 3, lane d). Similar experiments done in a *Δrtt101* background revealed the same pattern, a reduction of the same magnitude of the slower migrating form of 3xHA:Rtt101p in the protein extracts from a *Δrtt101 Δrub1* strain when compared to proteins extracts from a *Δrtt101 RUB1* strain (data not shown).

To determine if the slower migrating form of Rtt101p was *ENR2*-dependent, 3xHA:Rtt101p was expressed in isogenic *ENR2* and *Δenr2* strains and the forms present determined by Immunoblot analysis using anti-HA antibodies. There was a reduction of the slower migrating form of Rtt101p from protein extracts of an *Δenr2* strain when compared to protein extracts from an *ENR2* strain. Quantitation revealed the slower migrating form of Rtt101p was 60% of the faster migrating form in protein extracts from a *Δenr2* strain. In contrast, in protein extracts from an ENR2 strain the slower migrating band was 120% of the faster migrating band. This experiment (data not shown) and that shown in Figure 3 suggest that Rtt101p is modified by Rub1p in an ENR2p-dependent manner as well as modified by a Rub1p-sized modification that is ENR2p-independent. This was a very novel finding. No one had previously reported a Rub-modified protein that was additionally modified by another protein of similar size.

To determine if the conserved site is required for rubylation, *Rtt101* codons for K791 were changed to encode arginine and the protein 3xHA:Rtt101K791R was expressed in wild type and *Δrub* strains. When the 3xHA:Rtt101p form containing R791 is expressed, <u>all</u> slower migrating forms of Rtt101p are gone (Figure 3, lanes b and e), indicating that all slower migrating forms depend on that lysine and strongly suggest that is the site of attachment of Rub1p and of another protein. Given that the sizes are identical for the Rub1p-dependent and Rub1p-Independent modified forms of Rtt101p, we hypothesize that this could be ubiquitin since Rub1p and ubiquitin both contain 76 amino acids.

We next performed similar experiments to determine if the other cullin-like protein, Cul3p, is covalently modified by Rub1p. As discussed above for Rtt101p, two electrophoretic forms differing 10 kDa are expected if 3xHA:Cul3p is modified by Rub1p. That is exactly what is observed (Figure 4, lane b). In contrast to Rtt101p, the slower migrating 3xHA:Cul3p form is completely lost in the absence of Rub1p (Figure 4, lane a). We next expressed 3xHA:Rub1p in a yeast strain background expressing Cdc53K760Rp, a form of Cdc53p that cannot be rubylated, and is disrupted for *RTT101*. In this strain, only one 3xHA:Rub1p species was detected and it co-migrated with the slower migrating 3xHA-Cul3p form (Figure 4, lane c and d). When all three Rub1p substrates are present, three 3xHA-Rub1p forms are visible (Figure 4, lane e). At the same time, we confirmed that Rtt101p is Rub1p-modified (Figure 4, lanes f-h).

In summary, these experiments clearly demonstrate that Rub1p covalently attaches to the cullin-like proteins, Cul3p and Rtt101p, in addition to Cdc53p. We discovered that the

conserved lysine is required for Rub1p attachment to Rtt101p, and additionally discovered a Rub1p-independent modification of Rtt101p.

1.2. Plant RUB1 can conjugate to Cdc53p in yeast.

We had identified three Rub-encoding genes in *Arabidopsis thaliana,* our model species, with 2 encoding nearly identical proteins (AtRUB1 and AtRUB2, referred to here as RUB1 and RUB2) and the more diverged AtRUB3 with 78% identity to RUB1 and 2 (Rao-Naik *et al*., 1998a). We wanted to determine whether the two plant RUB types (RUB1/2 and RUB3) were functionally equivalent. One test is to determine whether they will conjugate to yeast Rub1p substrates. We expressed both proteins in yeast and asked if they would covalently attach to Cdc53p, a yeast Rub1p substrate (Figure 5). In lanes b-d, only Cdc53p is epitope-tagged. In lanes e-g both the Rub protein and Cdc53 are HA-tagged. Yeast Rub1p, expressed in the same vector system, conjugated to Cdc53p, as expected (Figure 5, lanes b, e). Plant RUB1 covalently attached to Cdc53p *in vivo* in yeast (Figure 5, lanes c, f). However, plant RUB3 did not (Figure 5, lanes d and g). This result suggests that plant RUB3 has a different function from plant RUB1/2.

1.3. There is cross-talk between the ubiquitin and rub pathways.

This discovery occurred during the course of our studies on the plant Rub pathway in yeast (1.2, above). In the course of these experiments, we noticed that when plant 3xHA:RUB1 was expressed in yeast, many anti-HA immune-reactive bands were visualized (Figure 6, lane b). These species were not present when yeast Rub1p nor when RUB3 was expressed. The pattern resembled that of ubiquitin conjugation to a large number of substrate proteins. Subsequent experiments indicated that AtRUB1 was recognized by the ubiquitin pathway, attaching RUB1 to ubiquitin substrates. We also demonstrated that the C-terminal half of plant RUB1 was sufficient for this conjugation via the ubiquitin pathway (Figure 6). We made two chimeric proteins. Each had half of the yeast Rub1p and half of the plant RUB1 sequences. The chimera with the N-terminal RUB1 amino acids expressed poorly in yeast (Figure 6, lane b), while the opposite chimera expressed well in yeast and conjugated to the same proteins as the fully plant RUB1 (compare lanes c and d). Hence, a heterologous protein, plant RUB in yeast, failed to have the high degree of specificity exhibited by yeast Rub1p in yeast. The RUB amino acid sequences that distinguish it from ubiquitin are in the C-terminal half of RUB. These experiments also told us that we could not use yeast as a system to express and test the plant Rub pathway as it cross-talks to the yeast ubiquitin system.

We next then turned our focus to understanding the role of the Rub pathway in plants.

2. Demonstration that Rub pathway is essential in Arabidopsis

2.1. Identification of *rub* null alleles reveal that RUB1/2 are redundant and that the presence of a single RUB1 or RUB2 allele is sufficient. However, at least one RUB1/2 gene is required for embryo development, and often for gamete development.

To understand the biological roles for RUB1 and RUB2 proteins in plants, the effect of eliminating their expression individually and collectively was analyzed through the isolation and characterization of T-DNA insertional mutants in the loci encoding RUB1 and RUB2 proteins. Two independent T-DNA insertional-mutagenesis lines were identified for the *UBQ15* locus that encodes a ubiquitin-RUB1 dimer (Figure 8A, *RUB1*). *UBQ15* will be referred to here as the *RUB1* locus for clarity and the T-DNA alleles will be *rub1-1* and *rub1-2*. *RUB1*-specific primers amplified three low abundance cDNAs from mRNA isolated from *rub1-1* homozygous plants, one the size of the endogenous band (Figure 8B, lanes 3 and 4 top panel, marked "a"), one smaller (Figure 8B, lane 3, top panel, marked "b") and one larger (not visible in Figure 1, named band "c"). DNA sequences of the three bands were determined and all have alternative splicing in the RUB1 coding region, not recognizing the second intron acceptor site. Sequences from bands "a" and "c" are missing 27 nucleotides of exon 3, eliminating RUB1 amino acids 42-51. The sequence from band "b" is missing 287 nucleotides, including all of exon 3 and some of the 3' untranslated region, and the predicted RUB1 protein lacks authentic sequence after amino acid 41. A second line containing a T-DNA in *RUB1*, *rub1-2,* is in the WS ecotype, and the insert is in the first intron. No DNA fragments were visible after PCR amplification of cDNA from mRNA from homozyous *rub1-2* plants, confirming this as a null mutational allele for *RUB1* mRNA (Figure 8B, lanes 9-12, top panel).

Two T-DNA insertional lines, *rub2-1* and *rub2-2,* were identified in *UBQ7*, the locus encoding a ubiquitin-RUB2 dimer (Rao-Naik et al., 1998a); both are in the Columbia ecotype. *UBQ7* will be referred to as *RUB2* for clarity. The T-DNA inserts are located 337 and 810 nucleotides, respectively, downstream of the ATG for *RUB2* (Figure 8A, *RUB2*). Neither line produces a PCR product when cDNA was amplified with *RUB2*-specific primers (Figure 8B, lanes 1, 5, and 7, middle panel). Thus, both *rub2-1* and *rub2-2* are *RUB2* null lines.

To determine if inactivation at one locus affected expression at the other non-disrupted locus, RT-PCR was used to detect mRNA for the intact RUB-encoding gene in each single insertion line (Figure 8B). There were no changes in the level of *RUB2* mRNA in *rub1-1* and *rub1-2* lines compared to a *UBQ10* (polyubiquitin) control (Figure 8B, lanes 1, 3, 9, and 11, middle and bottom panel). Similarly, *RUB1* mRNA is unchanged in *rub2-1* and *rub2-2* homozygous plants compared to the *UBQ10* control (Figure 8B, lanes 1, 5, and 7, top and bottom panels). This indicates that loss of one RUB gene does not affect expression of the other. The growth of single homozygous lines was compared to wild-type siblings, and no phenotypic differences could be detected (Figure 9A).

To determine if RUB1 and RUB2 are functionally redundant, we crossed *rub2-1* homozygous plants to plants homozygous for one of the two insertional alleles for *RUB1* (*rub1-1* or *rub1-2*) and F2 plants were genotyped using PCR (data not shown). A wild-type phenotype was observed for all plants with a single functional *RUB1* or *RUB2* (called sesquimutant); *RUB1/rub1 rub2* and *rub1 RUB2/rub2* plants for both *rub1* alleles were indistinguishable from *RUB1 RUB2* plants in vegetative growth. This result supports the hypothesis that RUB1 and RUB2 proteins are redundant, as one wild-type allele of *RUB1* complements a homozygous *rub2* plant and one wild-type allele of *RUB2* complements a homozygous *rub1* plant.

Further support that a single *RUB* gene is sufficient for wild type growth comes from analysis of the CULLIN1 (CUL1) conjugation status in these plants. RUB in Arabidopsis (not yet determined which RUB-see below) attaches to CUL1 (del Pozo and Estelle 1999). On immunoblot blots using anti-CUL1 Ab, two electrophoretic species can been seen (Figure 9B, Col control lane on the left). In the *RUB* single and sesquimutants, two species can be detected and the ratio of unmodified CUL1 to rubylated CUL1 appears to be the same (Figure 9B). This supports the phenotypic observations that a single *RUB*1 or RUB2 gene is sufficient for wild type growth.

We sought to obtain a plant lacking all wild type *RUB1* and *RUB2* genes. From 100 F2 individuals, no plant was found homozygous for insertions at both loci, although the expectation is one in sixteen plants would have this genotype ($p < 0.01$). To better test whether double mutant plants were viable, the *RUB1* and *RUB2* genotypes of progeny from multiple F2 plants that should segregate double mutants at a higher frequency were determined. F2 plants with the genotypes *RUB1/rub1 rub2* or *rub1 RUB2/rub2* (homozygous in one and heterozygous in the other- termed sesquimutant) were subsequently allowed to self-fertilize and their progeny genotyped. For this F3 population, the expected frequency of *rub1 rub2* plants is 25%. From 40 seedlings from a *RUB1/rub1-2 rub2* parent, no *rub1-2 rub2* plants were found ($p < 0.0005$). From 71 seedlings from a *RUB1/rub1-1 rub2* parent, no *rub1-1 rub2* plants were found ($p < 0.0005$). In 34 seedlings from a *rub1-2 RUB2/rub2* parent, no *rub1-2 rub2* plants were found ($p < 0.001$). Because F2 and F3 seed appeared to have 100% viability and no seedling lethality is seen after germination (data not shown), the loss of a double mutant plant must occur early in seed development. Inspection of siliques from *RUB1/rub1-1 rub2* parent showed loss of ovules/embryos (Figure 10).

Next, additional studies on the percent inheritance of specific genotypes showed that there was reduced inheritance of the T-DNA alleles through both gametes that results from embryonic death of a proportion of heterozygous embryos. If only the *rub1 rub2* developing seeds were not viable, then the progeny of a *RUB1/rub1-2 rub2* or a *rub1-2 RUB2/rub2* plant allowed to self-fertilize would segregate 2:1 for heterozygous and homozygous wild type at the heterozygous locus of the parent. However, the observation was that the percentage of heterozygous seedlings was much less than 67%, with only 15% heterozygous at the *RUB1* locus and 44% heterozygous at the *RUB2* locus. Neither percentage supports a 2:1 segregation (*RUB2*; $p < 0.0005$) or even a 1:1 ratio (*RUB2*; $p < 0.005$). This deviation from a standard inheritance pattern implies death of more than just the double null developing seed. From theses studies we conclude that the RUB1/2 proteins are essential for embryo development and important, and often required during gamete development. This essential function makes it difficult to study the vegetative roles of the Rub pathway.

2.2. To study vegetative roles for the Rub pathway, plants down-regulated for RUB1/2 expression were isolated (called *dsrub* lines) and characterized.

An approach was taken to reduce, but not eliminate, endogenous Rub expression since the Rub pathway was essential in order to study post-embryonic roles for the Rub pathway. A transgene, called *dsrub*, designed to express an mRNA containing the RUB1 coding region in both a sense and anti-sense direction separated by an intron, was introduced into Arabidopsis (diagram in Figure 8A, *dsrub*). When expressed *in planta*, this mRNA has the potential to form a double-stranded RNA capable of eliciting post-transcriptional gene silencing (PTGS)

(Waterhouse *et al.,* 2001). *RUB1* and *RUB2* share 85% nucleotide identity in the Rub coding region, so both mRNAs are likely to be affected by *RUB1*-elicited PTGS. RUB3 with 16 amino acid substitutions from RUB1 and the corresponding nucleotide sequence has lower identity to *RUB1* (74%), and the *dsrub* construct is not expected to decrease the amount of *RUB3* mRNA. In addition, there is no stretch of nucleotide identity of greater than 21 nucleotides, the minimum required to elicit PTGS.

One hundred and fifty-six antibiotic resistant T1 seedlings, each representing an independent transformation event, were characterized phenotypically at the T1 generation. Twenty-three percent of the 156 plants died soon after transplanting before producing any seed, often before the emergence of true leaves. Fifteen percent had severe changes in their general morphology compared to wild-type plants, but grew to maturity. The remaining 62% showed little or no differences in morphology or development from the progenitor. From the 156 T1 individuals, 30 with phenotypic differences from wild type were propagated; the phenotype or antibiotic resistance of progeny of some lines was unstable. Of the twelve lines with a strong phenotype that was maintained in subsequent generations, three independent lines produced a sufficient seed to identify homozygous lines for biochemical studies: *dsrub-1*, *dsrub-2*, and *dsrub-3*. *dsrub-con*, a kanamycin-resistant line generated at the same time with the same transgene and not differing phenotypically from wild type, was propagated for use as a transgenic negative control. These four transgenic lines were used in subsequent studies and their phenotypes are representative of other lines that were analyzed less extensively.

To characterize the efficacy of induction of PTGS, the levels of mRNA and protein for RUB1 and RUB2 were analyzed in transgenic lines *dsrub-1*, *dsrub-2*, *dsrub-3*, *dsrub-con*, and Col. The mRNA levels for *RUB1* and *RUB2* were amplified from cDNA with gene-specific primers (Rao-Naik *et al.,* 1998b). Primers amplifying cDNA for the polyubiquitin gene, *UBQ10*, were used as a control for cDNA levels. Control experiments indicate that the reactions were analyzed in the linear range of amplification (data not shown). RNA from Col and *dsrub-con*, gave comparable levels of amplified DNA for all three genes (Figure 8C, lanes 1, 5). The sizes of the PCR products were smaller than that obtained using genomic DNA as a template (Figure 8C, lanes 7) and are identical to the predicted sizes of spliced mRNAs and PCR products observed previously. Two of the *dsrub* transgenic lines, *dsrub-1* and *dsrub-3*, showed about one-tenth of the level of *RUB1* mRNA and about 30% and 50%, respectively, of the level of *RUB2* mRNA compared to control lines (Figure 8C, lanes 2, 4). In *dsrub-2*, mRNA for *RUB1* was moderately reduced to 70% of the control level, whereas *RUB2* mRNA level was roughly equivalent to the controls (Figure 8C, lane 3). In conclusion, all three *dsrub* lines showed significant decreases in *RUB1* mRNA, and two lines showed significant reduction in *RUB2* mRNA levels compared to wild type.

Representative phenotypes of the lines whose molecular characterization was shown in Figures 8 (*dsrub-1*, *dsrub-2*, and *dsrub-3*), plus the phenotypes of additional independent lines that did not produce sufficient tissue for thorough molecular analyses (*dsrub-4*, *dsrub-5*, and *dsrub-6*) are shown in Figure 11. All of these *dsrub* lines grew slower as seedlings and produced smaller plants. After transplanting and 3 weeks in soil, Col seedlings had green cotyledons with one pair of fully expanded leaves and a second emergent pair (Figure 11A). In contrast, *dsrub* lines grown under the same condition had produced either smaller cotyledons with no visible true leaves (*dsrub-4*, Figure 11B) or smaller cotyledons and true leaves at a slightly slower rate (*dsrub-5*, Figure 11C). However, *dsrub* lines flowered with the same number of leaves as control lines (data not shown). Seedlings with a slight purple color were regularly seen (Figure

11C), indicating anthocyanin production, which suggests induction of a stress response. By five weeks, the difference in rosette size between Col and the *dsrub* lines was even more evident (Figure 11D-F).

During reproductive growth, Col plants extend multiple racemes with some branching (Figure 11J, left). For the three *dsrub* lines characterized molecularly, the racemes were short (Figure 11G-I). Some lines did not extend a raceme at all, producing just a few siliques right out of the rosette, such as *dsrub-3* (Figure 11G). Although with different severity, all of the transgenic partial loss-of-function RUB1/2 lines had similar attributes, suggesting disruption of the same pathways in multiple lines.

The activating enzyme for RUB1 in Arabidopsis is an AXR1/ECR1 heterodimer (del Pozo *et al.,* 1998). *axr1-13* has short inflorescences with increased branching on the primary inflorescence and a greater number of secondary inflorescences than wild type, resulting in a "bushy" appearance (Figure 11J, right). The *dsrub* lines were more severely dwarfed than *axr1-13* (Figure 11J, center and right), and in lines with elongating inflorescences there were fewer than for *axr1-13* (Figure 11H, I, and J right). These differences suggest that although *axr1-13* and the transgenic lines are both smaller than wild type, the *dsrub* lines have a dwarfed phenotype distinct from that seen in *axr1-13* lines.

2.3. *dsrub* seedlings exhibit altered growth morphology when grown in the dark, suggesting alterations in the ethylene pathway

The morphology of seedlings was also examined. Dark-grown *dsrub* seedlings had obvious morphological differences from wild type. Relative to light-grown seedlings, dark-grown Col seedlings develop an elongated hypocotyl, arrested chloroplast development, unexpanded cotyledons, and an apical hook, collectively referred to as skotomorphogenesis (Figure 12A, J). When grown in the dark, the control line, *dsrub-con*, exhibits normal skotomorphogenesis, however the *dsrub* seedlings, *dsrub-1*, *dsrub-2*, and *dsrub-3*, have shorter, thicker hypocotyls, and an exaggerated hook with slightly expanded cotyledons (Figure 12B-D, I). These differences were also observed in additional *dsrub* lines with a similar light growth phenotype as *dsrub-1*, indicating that it was characteristic of this category of *dsrub* lines (data not shown). The shorter, thicker hypocotyls and the exaggerated hook were reminiscent of the triple response that is seen in dark-grown, wild-type seedlings exposed to the gaseous hormone ethylene, or its immediate precursor ACC (1-aminocyclopropane-1-carboxylic acid). Exposure of Col seedlings to ACC (Figure 12E) resulted in a swollen hypocotyl, an exaggerated hook, and reduced hypocotyl and root growth (Schaller and Kieber 2002b; Schaller and Kieber 2002a). The *dsrub* lines had all of these characteristics, except their roots were still elongated, illustrating a partial triple response phenotype.

The constitutive triple response seen in dsrub lines could result from a lesion in the ethylene response pathway, leading to constitutive activation of the pathway, or from a lesion in regulation of ethylene production leading to increased synthesis of the hormone. To distinguish between these possibilities in the *dsrub* lines, *dsrub-1* seedlings were grown in the presence of Ag^{+}, an ethylene receptor inhibitor that blocks perception of ethylene. Growth in the presence of Ag^{+} completely abolished the triple response phenotype of *dsrub-1* seedlings (Figure 12F); the hypocotyl was long and narrow and the hook straightened. This indicated that the hypocotyls of *dsrub* seedlings have a functional ethylene response pathway and established a role for RUB1/2 upstream of the ethylene receptor.

To determine whether increased ethylene production was leading to the partial triple response in *dsrub* lines, *dsrub-1* seedlings were treated with AVG (aminoethoxyvinyl glycine hydrochloride), an inhibitor of ACS whose activity typically limits *in vivo* ethylene production (Capitani *et al.,* 2002). This treatment completely abolished the triple response (Figure 12G), strongly suggesting that the *dsrub* dark-grown phenotype resulted from increased ethylene production.

As AXR1 functions to activate RUB1 for attachment to cullins, the dark-grown phenotype of *axr1-13* seedlings was compared to that of the *dsrub* lines. Strikingly, dark-grown *axr1-13* seedlings did not exhibit the partial triple response seen in the *dsrub* lines. Their hypocotyl length was longer, identical to Col, and as previously observed, the hypocotyls were hookless (Figure 12H).

2.4. *dsrub* lines overproduce the hormone ethylene

The constitutive partial triple response phenotype and its loss in the presence of AVG strongly suggested that the *dsrub* dark-grown seedlings overproduced ethylene. To test this directly, ethylene released by dark-grown *dsrub* seedlings over 4 days was measured by GC (gas chromatography) and compared to Col. The *dsrub* lines produced 3-5 times more ethylene than Col (Figure 13). These measurements confirmed that the *dsrub* seedlings were overproducing ethylene when grown in the dark. In contrast, the amount of ethylene released from the *axr1-13* line was less than from Col (Figure 13). These results implicate AXR1 in enhancing, and RUB1/2 in the opposite, suppressing ethylene levels in dark-grown seedlings, although that may be an oversimplified model.

2.5. The mRNA levels for proteins involved in ethylene synthesis were analyzed in dsrub lines to see if they are misregulated, however, increased ethylene in *dsrub-1* is not produced by increased transcription of *ACS* or *ACO* family members.

Typically ethylene production is regulated by limiting the amount of ACS protein available for the conversion of AdoMet to ACC. This regulation has been illustrated to be mediated by regulating transcription, protein activity, or protein degradation. For this reason, it is important to test if changes in transcription are leading to increases in ethylene production seen in *dsrub* lines. RNA was extracted from four-day-old, dark-grown *dsrub-con*, *dsrub-1*, and *eto2* seedlings. cDNA was made from the RNA and transcripts from *ACS2*, *ACS5*, *ACS6*, *ACS9*, and *ACS11* were amplified by PCR with gene-specific primers (Vandenbussche *et al.,* 2003). Generally, all of the transcripts were low; *ACS4*, *ACS7*, and *ACS8* were not amplified at all (data not shown). *ACS5* had the highest transcription levels and these levels were comparable between the three plant lines (Figure 14). There were no striking differences for the levels of most *ACS* genes between *dsrub-con* and *dsrub-1* lines. This is not true for *axr1-12*, which has lower levels of ethylene produced (Figure 13). *axr1-12* has comparable levels of *ACS6* as control lines, but moderately decreased levels of *ACS9*, *ACS11* (Figure 14), and *ACS5*. These data show no evidence that the increased levels of ethylene produced by the *dsrub* lines is from increased *ACS* transcripts, but that decreased ethylene levels in *axr1-12* may be from decreased *ACS* mRNA.

The second family of enzymes required for ethylene production is the *ACO* genes. Of the six *ACO* genes present in the Arabidopsis genome, we tested the mRNA level of four of them by

semi-quantitative PCR. For the genes tested, *ACO2*, *ACO-A*, *ACO-B*, and *ACO-E* (AGI numbers At1g62380, At5g63600, At1g04350, and At2g19590, respectively), there was no obvious increase in transcript for the *dsrub-1* or *eto2* lines compared to the *dsrub-con* seedlings (Figure 14). We also tested the mRNA levels of *ACO-A* in *axr1-12*, and there was no difference from other lines, indicating that this gene is not transcribed in an AXR1-dependent manner. As no increase in transcription of the ACO genes was identified, this is not the sole site of misregulation of the ethylene production pathway in the *dsrub* lines.

2.6. Epitope-tagged versions of RUB1 and RUB2 have identical conjugation patterns and conjugate to the same cullin

In addition to genetic evidence for RUB1 and RUB2 functioning redundantly in plants, this study looked at biochemical redundancy between these two proteins through their conjugation patterns. Yeast Rubp1 conjugates to yeast cullin protein. To determine whether plant RUB proteins act similarly and to be able to visualize the two closely related proteins individually, HA (hemagglutinin) –tagged versions of RUB1 and RUB2 were expressed under a dexamethasone (dex) inducible promoter. The conjugation of the epitope-tagged RUB1 and RUB2 was observed by SDS-PAGE and immunoblotting with anti-HA antibodies extracts from dex-induced plants. The conjugation patterns for 3HA-RUB1 and 3HA-RUB2 under the same induction condition were indistinguishable (Figure 15A, lanes 3 and 5), and the two strongest bands were in the area of the cullin proteins, around 100 kDa, and the monomer, around 15 kDa. Arabidopsis cullins are similar in size, between 75 and 92 kDa, and therefore, are difficult to distinguish on this gel. Some bands of lighter intensity were also observed, although their identity is still unknown. In addition, the conjugation pattern for 3HA-RUB1 and 3HA-RUB2 was unchanged by the addition of the plant hormone, auxin (Figure 15A, lanes 2 and 4).

Previously, it was shown that RUB1 attaches to CULLIN1 (CUL1) in Arabidopsis (del Pozo and Estelle 1999). To confirm that both 3HA-RUB1 and 3HA-RUB2 conjugate to the same cullin, the proteins were expressed for seventeen hours. This allowed for visualization of a triplet when extracts were reacted with anti-CUL1 antibodies, where the fastest-migrating band was unconjugated CUL1 and the middle band was the endogenous RUBx-CUL1 (Figure 15B, lanes 1 and 2). The slowest-migrating band was present after only extended dex treatment (compare 15B and 3C, lanes 1 and 2). Immunoprecipitations of the 3HA-RUBx-CUL1 complex were performed with antibodies against the epitope-tagged Rub proteins and were visualized with anti-CUL1 antibodies. This confirmed that the slowest migrating CUL1 immunoreactive band was indeed 3HA-RUBx-CUL1 (Figure 15B, lanes 3 and 4). This blot confirmed that both RUB1 and RUB2 conjugate to CUL1 when over-expressed and allowed for a marker to identify where this protein complex migrated in an SDS-PAGE.

Once the migration of the 3HA-RUBx-CUL1 complex was established, it was important to see if the conjugation of 3HA-RUB1 and 3HA-RUB2 occurred after short term induction. Immuno-precipitations were performed with extracts from seedlings only dex-treated for two hours, as well as with extracts from seedlings that were mock-treated. The slowest migrating CUL1 band is no longer visible from total seedling extracts (Figure 15C, lanes 1 and 2), but is present in immunoprecipitations and present in a dex-dependent fashion (Figure 15C, lanes 3-6). These data confirm that in addition to 3HA-RUB1, 3HA-RUB2 attaches to CUL1 in plant extracts.

To determine whether RUB proteins attach to other cullins in Arabidopsis, we tested whether 3HA-RUB1 or 3HA-RUB2 attached to members of the CUL3 family, of which there are two closely related members in Arabidopsis, CUL3A and CUL3B. Using an *in vitro* reaction, it has been shown that GST-RUB1 attaches to AtCUL3A synthesized *in vitro* (Weber *et al.,* 2005). Through collaboration with the Xing-Wang Deng laboratory (Yale University), who produced anti-CUL3 antibodies (cross-reactive to both 3A and 3B), we tested if 3HA-RUB1 and 3HA-RUB2 attach to CUL3 in plants (Figure 16). Expression of the 3HA-RUB1 and 3HA-RUB2 proteins was done using the dexamethasome-inducible construct stably transformed into wild-type plants. Immunoblot blotting of extracts prior to anti-HA immuno-precipitation clearly shows that AtCUL3 is present in two species with an approximate 8 kDa difference in migration on SDS-PAGE, consistent with an unmodified and modified form, both with and without dex treatment (Figure 16, lanes 1-2, 5-6). Anti-HA immuno-precipitations were performed on seedlings dex-treated or mock-treated for two hours, and the eluents were visualized with anti-CUL3 antibodies. An anti-CUL3 reactive band, migrating more slowly than the slower band visible in the anti-Cul3 blot from extracts, is visible in the CUL3 blots from the eluent from the immunoprecipitation for both 3HA-RUB2 (Figure 16, lane 3) and 3HA-RUB1 (Figure 16, lane 7) in a dex dependent manner (compare to Figure 16, lanes 4 and 8, respectively). Their slower migration is consistent with the slower migration seen for 3HA-RUB1 and 2 proteins attached to CUL1. Although it is clearer for RUB2, this experiment confirms that both RUB1 and RUB2 attach to CUL3.

2.7. RUB-specific antibody demonstrates that dsrub lines have reduced RUB1/2 protein level and decreased amount of conjugated CUL1

To determine if the RUB1 and RUB2 protein levels were decreased in the *dsrub* lines, RUB1/2-specific antibodies were developed and utilized. Because RUB1 and RUB2 only differ by 1 amino acid, it is extremely difficult to create antibodies that distinguish between these two Rub family members. Instead, antibodies were raised and affinity-purified against a peptide sequence identical between RUB1 and RUB2, but sufficiently diverged from RUB3 and ubiquitin to prevent cross-reactivity. The specificity of the affinity-purified antibodies was tested on purified GST fusion proteins using immunoblots. The antibodies reacted specifically with GST-RUB1 and not GST alone, GST-RUB3, or GST-ubiquitin even when the latter was present at 200X higher concentration (Figure 17A, lower panel).

These antibodies were also tested for their ability to specifically recognize endogenous RUB1 and RUB2 in plant protein extracts. The anti-RUB1/2 antibodies reacted with purified recombinant RUB1 and a co-migrating band in Col extracts, but did not recognize purified ubiquitin (Figure 17B, top panel). To confirm that the anti-RUB1/2 immunoreactive band visualized in Col extracts was RUB1/2, Col extract was enriched with purified ubiquitin prior to electrophoresis, and the intensity of the band was unchanged (Figure 17B, lanes 3, 4). The same extracts were probed with anti-ubiquitin antibodies to demonstrate the inclusion of ubiquitin in this sample (Figure 17B, bottom panel). This result demonstrates that the RUB1/2 antibodies are visualizing endogenous RUB1/2 and not ubiquitin.

Anti-RUB1/2 antibodies were used in immunoblots against protein extracts from the *dsrub* transgenic lines. Protein extracts from Col and *dsrub-con* had detectable levels of RUB1/2 (Figure 17C, lanes 2, 3, and 7), while *dsrub-1* and *dsrub-3* had RUB1/2 levels below the level of detection (Figure 17C, lanes 8, 4). RUB1/2 protein was faintly visible in some immunoblots

containing extracts from *dsrub-2*, suggesting higher levels of RUB1/2 protein in this line compared to *dsrub-1* and *-3* (data not shown). *axr1-13*, an *AXR1* null line, extracts contained unconjugated RUB1/2 levels equivalent to that seen in Col (Figure 17C, lane 5). These data indicated that the reduction in *RUB1* and *RUB2* mRNAs resulted in a significant decrease in the total amount of RUB1 and/or RUB2 proteins in *dsrub* lines.

As described above, CUL1 exists as a doublet, with the slower-migrating band identified as a RUBx-CUL1 complex. This doublet was visible with both Col and *dsrub-con* extract (Figure 17D, lanes 3 and 2). It has previously been shown that the conjugation state of CUL1 is changed in the *axr1-12* line, such that there is an increase in the total amount of unmodified CUL1 and no change in modified form, decreasing the ratio (del Pozo and Estelle 1999) This decrease in the proportion of conjugated form of CUL1 also found in *axr1-13* and in the three *dsrub* lines (Figure 17D, lane 6 compared to lanes 1, 4, and 5). These data correlate the phenotype of the *dsrub* lines with a decrease in the ratio of Rub-conjugated CUL1 to unconjugated CUL1.

2.8. *dsrub* lines have smaller cell size in the hypocotyl.

The decrease in inflorescence height of full-grown partial loss-of-function plants led us to look at the height of 4-day-old seedlings to determine whether differences can be seen early in development. The *dsrub*, *axr1-13*, and wild-type lines were grown for four days in the light or in the dark, and the length of the hypocotyls was measured. In both the light and dark, all three of the *dsrub* lines were not different from each other, but their hypocotyls were 65% of the two control lines, Col and *dsrub-con* (Figure 18). These data indicate a measurable decrease in plant height even after only 4 days of growth in the light or dark in the *dsrub* lines. To determine if a lack of cell elongation or a reduction in the number of hypocotyl cells was responsible for the observed height difference, 4-day-old seedling hypocotyls were visualized and cell length observed under a microscope. The cells of *dsrub-1* were shorter in length than Col in both in dark and light-grown seedlings. This indicates that the shorter hypocotyl in *dsrub* plants results from reduced cell elongation.

In summary, these studies discovered that the RUB1/2 proteins are redundant and together are essential for early development. Down-regulation rather than elimination, allowed us to discover the pleiotropic phenotypes of plants with insufficient RUB proteins. These plants are dwarfed. Unexpectedly, dsrub plants over-produce ethylene in the dark, indicating misregulation of the ethylene synthesis pathway. This phenotype is in marked contrast to the phenotype of reduction in the enzyme that attaches RUB to substrates; these plants produce less ethylene. In conclusion, the RUB1/2 proteins are essential and play multiple diverse roles in plant development. Like yeast Rubp1, plant RUB1/2 attach to multiple cullin proteins.

3. Identification and biochemical characterization of RUB pathway components

3.1. AXL1 catalyzes thioester formation between ECR1 and RUB1 *in vitro.*

Sequence similarity between AXR1 and AXL1 suggests that AXL1 has the same, or similar, biochemical activity to AXR1 (Dharmasari *et al.,* 2007). Previous *in vitro* assays show AXR1 able to catalyze formation of a thioester linkage between the C-terminus of RUB1 and the catalytic cysteine, C215, of ECR1 (del Pozo et al., 1998). However, the biochemical activity of the AXR1-like protein AXL1 had not been demonstrated directly. Utilizing an *in vitro* thioester assay, we show there that RUB1-ECR1 thioester formation is also catalyzed by AXL1 (Figure 19). Recombinant GST-ECR1 and 6HIS-3HA-RUB1 were incubated with 6HIS-AXL1 or 6HIS-AXR1, in the presence of ATP. Each reaction was then split: one-half was added to stop buffer lacking dithiothreitol (Figure 19, upper panel), and the other half was added to stop buffer containing DTT (Figure 19, lower panel). Thioester linkages are reduced by DTT, while oxyester and amide linkages are resistant to DTT-mediated cleavage. After separation by SDS-PAGE, conjugated 6HIS-3HA-RUB1 was visualized by anti-HA immunoblot analysis. In these experiments unconjugated 6HIS-3HA-RUB1 is 17 kDa in size and is not present on the blots. GST-ECR1 alone migrates at 72 kDa (Figure 19, left panel, αGST). An anti-HA band migrating approximately 20 kDa larger than GST-ECR1 was visible in complete reactions containing either 6HIS-AXR1 or 6HIS-AXL1 and stopped in the absence of DTT (Figure 19, lanes 1 and 2, compare top and bottom panels), indicative of a RUB1-ECR1 thioester conjugate. GST-ECR1 and 6HIS-3HA-RUB1, in reactions lacking 6HIS-AXR1 and 6HIS-AXL1, were insufficient to support RUB1-ECR1 thioester formation (Figure 19, lane 3). No slow-migrating HA-immunoreactive protein was visible when either GST-ECR1 or 6HIS-3HA-RUB1 was omitted from reactions containing 6HIS-AXR1 or 6HIS-AXL1 (Figure 19, lanes 4-7). Thus, AXL1 is required for conjugation of RUB1 to ECR1 in an in vitro thioester reaction, as seen for AXR1 under the same conditions.

Additionally, enzyme specificity for RUB1 over UBQ was examined for AXL1 in comparison to AXR1. 6HIS-AXR1 and 6HIS-AXL1 again supported 6HIS-3HA-RUB1 thioester formation to GST-ECR1, but neither was able to support HA-UBQ attachment to GST-ECR1, while the same HA-UBQ formed an UBQ-E1 thioester conjugate. In conclusion, AXL1 and AXR1 support RUB1, but not UBQ, thioester formation, demonstrating that AXL1 has biochemical activity and specificity similar to AXR1.

3.2. AXL1 and AXR1 have similar biochemical activities *in vitro.*

While having the same selectivity for RUB1, it is possible that AXR1 and AXL1 differ subtly in ability to catalyze RUB1-ECR1 thioester formation. To further examine the biochemical activities of AXR1 and AXL1 we set up an *in vitro* time course assay to compare the ability of each enzyme to catalyze covalent attachment of RUB1 to ECR1. Here we utilized $ECR1^{C215S}$ [described in (del Pozo et al., 1998)] that carries a cysteine to serine mutation at the active site, in order to stabilize the bond for visualization purposes. Recombinant 6HIS-FLAG-$ECR1^{C215S}$ and GST-3HA-RUB1 were incubated with either 6HIS-AXL1 or 6HIS-AXR1 for one, two, or four hours. At each time point, reaction aliquots were split and both halves were subjected to anti-HA-agarose immunoprecipitation to capture GST-3HA-RUB1 and interacting proteins.

One-half of each reaction was kept under neutral conditions to maintain the RUB1-$ECR1^{C215S}$ oxyester bond (Figure 20a, αHA IP, even-numbered lanes), while the other half reaction was treated with base to destroy the oxyester bond (data not shown) to demonstrate the nature of the RUB1-ECR1 linkage. In addition, parallel reactions were done with $ECR1^{C215A}$

that carries a cysteine to alanine mutation at the active site (Figure 20a, αHA IP, odd-numbered lanes). This protein should not support covalent RUB attachment, and it serves to verify the specificity of the reaction. Presence of 6HIS-AXL1, 6HIS-AXR1, 6HIS-FLAG-ECR1^{C215S}, and 6HIS-FLAG-ECR1^{C215A} in the reactions was verified by anti-HIS immunoblot analysis (Figure 20a, Input). To visualize the RUB1-ECR1 oxyester bond, anti-FLAG immunoblots were done (Figure 20a, αHA IP). Only reactions that included 6HIS-FLAG-ECR1^{C215S}, not 6HIS-FLAG-ECR1^{C215A}, supported RUB1-ECR1 oxyester bond formation.

To compare relative activities of 6HIS-AXL1 and 6HIS-AXR1, immunoblots were quantified and RUB1- ECR1^{C215S} bond formation was plotted against time (Figure 20b). Regression line slopes for ECR1^{C215S} reactions containing 6HIS-AXR1 or 6HIS-AXL were not statistically different (factorial ANOVA, $p = 0.0755$). The marginal p-value does not exclude the possibility that a subtle difference in catalytic abilities might exist between AXR1 and AXL1, but a more precise assay would be required to discern such a difference. In this assay, we could not detect a difference between AXR1 and AXL1 in ability to support RUB1-ECR1^{C215S} bond formation over time.

3.3. AXR1-ECR1 and AXL1-ECR1 transfer activated RUB1 to RCE1 and RCE2.

After determining that AXR1 and AXL1 have similar ability to function with ECR1 in catalyzing RUB1-ECR1 conjugation (Figures 19, 20), we investigated the ability of both RUB-activating enzyme to transfer activated RUB to each RUB-conjugating enzyme, RCE1 and RCE2. First, GST-HA-RUB1-6HIS-ECR1 thioester was made by incubation of reaction components with either 6HIS-AXR1 or 6HIS-AXL1. Then, the reactions were split in three and GST-HA-RUB1 was immunoprecipitated (utilizing the HA epitope) from each reaction, along with any co-precipitate. Subsequently, one aliquot was incubated with buffer (negative reaction), one with 6HIS-FLAG-RCE1, and one with 6HIS-FLAG-RCE2. After elution (with 8M urea), reactions were again split and either treated with non-reducing or reducing loading buffer. Proteins were then resolved by SDS-PAGE and analyzed by anti-FLAG immunoblot analysis.

An initial comparison of E2 loading capacity was made between 6HIS-AXL1-6HIS-ECR1 and 6HIS-ECR1 (negative control) to establish whether 6HIS-AXL1-6HIS-ECR1 is able to transfer activated GST-3HA-RUB1 to both 6HIS-FLAG-RCE1 and 6HIS-FLAG-RCE2 and to determine where GST-3HA-RUB1-6HIS-FLAG-RCE1/2 conjugate migrated on an SDS-PAGE gel. Only 6HIS-AXL1-6HIS-ECR1 is able to catalyze GST-3HA-RUB1-6HIS-FLAG-RCE1/2 conjugation (Figure 21a, lanes 4 and 5), where 6HIS-ECR1 cannot (Figure 21a, lanes 2 and 3). Conjugate is formed with both 6HIS-FLAG-RCE1 and 6HIS-FLAG-RCE2, at the expected size of ~70 kDa, and is sensitive to reducing agents (Figure 21a, lanes 11 and 12, compared to lanes 4 and 5). Additionally, the conjugate is dependent on the presence of 6HIS-FLAG-RCE1/2 (Figure 21a, lanes 1 and 6).

Next we compared E2 loading capacity of 6HIS-AXR1-6HIS-ECR1 and 6HIS-AXL1-6HIS-ECR1 (Figure 21b). Both RUB activating enzymes are able to transfer activated RUB to both 6HIS-FLAG-RCE1 and 6HIS-FLAG-RCE2 (Figure 21b, compare lanes 2 and 3 to lanes 5 and 6). In the absence of 6HIS-FLAG-RCE1 or 6HIS-FLAG-RCE2, no conjugate formed (Figure 21b, lanes 1 and 4). All conjugates are sensitive to reducing agents (Figure 21b, lanes 7-12). In conclusion, both AXR1-ECR1 and AXL1-ECR1 are able to catalyze transfer of activated RUB1 to both RCE1 and RCE2 *in vitro*.

3.4. AXR1 and AXL1 interact with RUB1 *in vivo.*

To assess whether AXL1 functions in native RUB E1 complexes, we used a mass spectrometry (MS) approach. Transgenic plant lines that express 3HA-RUB1 under control of an inducible promoter were utilized [described in section 2] and protein extracts were made from seedlings induced for 3HA-RUB1 expression. Proteins that interact with 3HA-RUB1 were immunoprecipitated with anti-HA-agarose beads, digested with trypsin, and analyzed by high-accuracy MS. Results were compiled from five biological replicates; recovered peptides were compared between Columbia expressing 3HA-RUB1 and wild-type Columbia, prepared in parallel. Table 1 combines data from replicates where peptide and protein standards were met, specifically a minimum 95% peptide probability, using the Peptide Prophet algorithm, and protein probability of minimally 95% with 2 unique peptides, using the Protein Prophet algorithm (Keller *et al.,* 2002; Nesvizhskii *et al.,* 2003). Peptides were identified from AXR1, AXL1, and other known RUB-conjugation components, including RUB1, ECR1, RCE1, CUL1, and CUL4. These results suggest that AXL1, as found naturally in cells, interacts with 3HA-RUB1, despite the presence of AXR1, suggesting that AXL1 forms functional E1 complexes in vivo and is active concurrent with AXR1.

Additionally, single peptide-based protein identifications were made for CUL1, CUL3a, CUL4, and RCE2, as individual peptides met MS criteria, but within a particular biological replicate, protein criteria were not met (lack of 2 unique peptides and/or below 95% protein probability threshold- Table 2). Of interest, peptides are recovered for both RCE2 and RCE1, suggesting both are functional RUB E2s.

3.5. Neither AXR1, nor AXL1, is rapidly degraded.

Previously, it was reported that the HECT-type E3 ligase TRIP12 ubiquitylates APP-BP1, the sole mammalian homolog of AXR1 and AXL1, thus targeting it for degradation (Park *et al.,* 2008)We hypothesized that a functionally homologous E3 might ubiquitylate either AXR1 or AXL1, or both proteins, in *Arabidopsis,* rendering one or both short-lived *in vivo*. To this end, we performed cycloheximide (CHX) time-courses on AXR1 and AXL transgenic lines, to determine the stability of 10MYC-AXR1 and 10MYC-AXL1. The level of each protein at various times after CHX addition was determined by immunoblot analysis (Figure 22a).

Eight-day-old seedlings from two AXL lines (lines 1 and 3 from in vivo phenotypic analyses) and two AXR1 lines (from phenotypic analyses, see below) are treated with 0.2 mg ml^{-1} cycloheximide for a six-hour time-course. Equal protein amounts from aqueous protein extracts were run on SDS-PAGE. Results were then analyzed by anti-MYC immunoblot analysis. 10MYC-AXL1 and 10MYC-AXR1 levels were unchanged over the six-hour cycloheximide time-course, suggesting neither protein is rapidly degraded (Figure 22a). Furthermore, there is no apparent difference in protein stability between 10MYC-AXR1 and 10MYC-AXL1. As an experimental control, we included a cycloheximide chase on 3HA-ARF1 transgenic lines (characterized in (Salmon *et al.,* 2008)) and found it to be largely degraded over the six-hour time-course (Figure 22b), indicating that the protein synthesis inhibitor was active. In conclusion, AXR1 and AXL1 are long-lived *in vivo*.

3.6. *AXR1* corrects *axr1-30* phenotypic defects more than *AXL1* throughout development.

We wanted to test whether AXR1 and AXL1 have equivalent biological activities *in vivo*. We failed to detect a difference *in vitro*, however, loss of AXL1 does not have affect plants while loss of AXR1 does. One reason that AXL1 cannot mask the loss of AXR1 in axr1 plants could be because AXL1 is not expressed at a sufficiently high enough level or not expressed in the same cells as AXR1, or both. Therefore, we sought to determine if there are differences *in vivo*. We asked whether AXL1 could complement the growth defects seen in *axr1* plants. If AXR1 and AXL1 have the same biochemical function *in vivo*, but are expressed in different cells or at different amounts, then we would expect AXL1 to convert *axr1* plants to wild type if it is expressed under control of the *AXR1* promoter. We generated transgenic lines expressing either AXR1 or AXL1 under control of the *AXR1* promoter in the *axr1-30* mutant background that is null for *AXR1*. We obtained homozygous *axr1-30* lines that are also homozygous for either the *AXR1p:10MYC-AXR1* (AXR1 lines) or *AXR1p:10MYC-AXL1* (AXL lines) expression cassette. We measured the protein levels in these lines (Figure 23a). Lines had comparable levels of AXL1 or AXR1 expression.

Next, we measured the effect of transgene expression by comparing growth of transgenic lines to *axr1-30* and to wild-type Columbia. Surprisingly, *AXR1p:10MYC-AXR1* and *AXR1p:10MYC-AXL1* expression cassettes differentially corrected *axr1-30* phenotypic defects. Of five AXR1 lines analyzed, all showed moderate to strong complementation of *axr1-30* phenotypic defects in adult plants. In contrast, of nine AXL lines analyzed, none showed strong complementation of *axr1-30* phenotypic defects. Four AXL lines were then characterized in detail and compared to two AXR1 lines. For each set of phenotypic observations (i.e. root length, rosette diameter, and inflorescence height), Student's t-tests with Bonferroni correction for multiple comparisons were performed to compare all lines to *axr1-30* and wild type (Columbia). Additional statistical tests were then done to make comparisons among those lines that had phenotypes intermediate between *axr1-30* and Columbia.

First, root length was measured in nine-day-old seedlings. *axr1-30* roots, averaging 20.3 mm in length, are significantly longer than Columbia roots, which average 11.8 mm (Figure 23b). Most lines are not significantly different from *axr1-30*, with only AXR1 line 1 that averages 16.8 mm showing a phenotype intermediate between *axr1-30* and Columbia (Figure 23b). Of the two AXR1 lines, line 1 expresses more 10MYC-AXR1 (Figure 23a). Unexpectedly, AXL line 4 with average length of 23.3 mm is significantly longer than *axr1-30*, suggesting a potential ectopic phenotype, resulting from transgene over-expression or site of transgene insertion (Figure 23b).

Next, rosette diameter at four weeks was measured and statistical analyses were performed. *axr1-30* plants are dwarfed with small leaves; their rosette diameter is 45% that of Columbia at the same age (Figure 24a). At this point in development, correction of the *axr1-30* phenotype is readily apparent for AXR1 lines, but is not for AXL lines. The average rosette diameters for AXL line 1 and AXR1 lines 1 and 2 are 4.0 cm, 5.9 cm, and 4.0 cm, respectively, statistically larger than for *axr1-30*, which averages 3.4 cm in diameter. However, none are equivalent to Columbia, which averages 7.5 cm in diameter (Figure 24a). Of these three lines that are significantly larger than *axr1-30*, AXR1 line 1 is significantly larger than the other two ($p < 0.0001$), and AXL line 1 and AXR1 line 2 are indistinguishable ($p = 0.7165$), utilizing a Student's t-test with Bonferroni correction and $\alpha = 0.00313$. At four weeks, AXL line 1 is the only AXL line that is significantly larger than *axr1-30*, whereas both AXR1 lines are distinguishable from *axr1-30*.

Finally, inflorescence height at ten weeks was measured for all lines. Here the difference in ability to restore the phenotype to Columbia between AXR1 and AXL1 expression is most apparent. Both AXR1 lines show good restoration of height, averaging 45.8 cm and 37.3 cm, compared to *axr1-30* and Columbia, which average 25.2 cm and 52.1 cm, respectively (Figure 24b). Of the AXL lines, only line 1 that averages 29.3 cm in height shows a moderate correction of *axr1-30* height. Statistical analyses confirm that AXL line 1, AXR1 line 1, and AXR1 line 2 are significantly taller than *axr1-30*, though none are the same height as Columbia (Figure 24b). Both AXR1 lines ($p < 0.0001$) are significantly taller than AXL line 1, and AXR line 1 is taller than AXR1 line 2 ($p < 0.0001$), using a Student's t-test with Bonferroni correction and $\alpha = 0.00313$. These differences in height can be readily seen from pictures of the plants (Figure 25).

In summary, we show that the *in vivo* functions of *AXR1* and *AXL1* are not equal. When AXL1 is expressed at a similar or higher level than AXR1, AXL1 does not have equivalent ability to correct *axr1-30* phenotypic defects, suggesting that the two proteins differ in function at either the biochemical level, or with preference for downstream interacting partners.

Why two functional RUB E1s exist remains a question, but as seen with the ubiquitin E1s, UBE1 and UBA6, or the mammalian Nedd8/Rub E2s, UBE2M and UBE2F, the purpose of two *Arabidopsis* RUB E1s could be to preferentially interact with different downstream proteins (Jin *et al.,* 2007; Huang *et al.,* 2009). However, data suggests that, at least *in vitro*, both RUB E1s are capable of transferring RUB1 to RCE1 and RCE2. Alternatively, subtle differences in enzyme activity, not detected by our methods of analysis, could exist and AXL1 could function in RUB E1 complexes during certain developmental stages or cellular conditions, as also observed for UBE2M and UBE2F (Huang *et al.,* 2004).

4. Identification of additional RUB interacting proteins using mass spectrometry approach.

4.1. Mass spectrometry of rubylated proteins

One important goal of our DOE funded work is to determine whether there are additional proteins covalently modified with RUB. This method utilized transgenic *Arabidopsis* lines that express 3HA-RUB1 under control of an inducible promoter (RUB lines, see section 2, above). Protein extracts were made from seedlings induced for 3HA-RUB1 expression or from mock-induced wild-type *Arabidopsis* seedlings. To recover 3HA-RUB1-interacting proteins, soluble protein fractions from RUB and control lines were immunoprecipitated with anti-HA-agarose beads, digested with trypsin, and analyzed by LC-MS/MS. Proteins present in RUB and control lines were identified using two programs- X! Tandem (www.thegpm.org) and INSPECT (www.proteomics.ucsd.edu)- with further validation steps. In total, results were compiled from seven MS replicates comparing RUB and control lines; data were also compared to one additional control replicate. A low threshold was set for selection of candidate RUB-interacting proteins- for either search algorithm. If two spectra were recovered in one RUB replicate, or a combination of replicates, and no spectra were recovered in control replicates for that protein, it was considered as a candidate RUB-interacting protein. Proteins unique to RUB samples were compiled from both searches and the datasets were compared. Proteins found in the control samples by reciprocal search algorithms were eliminated as candidate RUB-interacting proteins. If candidate RUB-interacting proteins were found in an additional LC-MS/MS control experiment, or if a related protein was found in the control replicates, the candidate protein was

also eliminated. Thus we narrowed the list of potential RUB-interacting proteins to 12 new candidates to validate by further experimental methods (Table 3).

4.2. RUB1 interacts with proteins from MS screen in tobacco transient assays.

Of 12 candidate proteins identified in the MS screen, 10 were successfully cloned (Table 3) and tested in a tobacco transient assay to visualize in planta RUB modification. The tobacco transient assay involves co-infiltration of *Nicotiana benthamiana* (tobacco) leaves with two *Agrobacterium* cultures, one containing a plasmid engineered for expression of the putative RUB-interacting protein (candidate protein) with an N-terminal MYC epitope and the other containing a plasmid for expression of 6HIS-3HA-RUB1. As a negative control for the subsequent anti-MYC immunoprecipitation (IP), we use tobacco leaves infiltrated with only *Agrobacterium* carrying the 6HIS-3HA-RUB1 expression construct (i.e. the "RUB1 only" control) to indicate the level of background in the anti-MYC IP. Equal amounts of infiltrated tissue are collected three days post-infiltration, and soluble protein is extracted in equal volumes of aqueous buffer. A fraction (1/10 of total volume) of the total soluble protein is examined by anti-HA immunoblot analysis to confirm that 6HIS-3HA-RUB1 is expressed in all reactions. The remaining extract (9/10 of total volume) is subjected to anti-MYC-agarose IP to capture MYC-tagged candidate proteins and interacting proteins. IP samples are then split and resolved by SDS-PAGE. After transfer to membranes, IP samples are analyzed by anti-MYC and anti-HA immunoblot analyses to assess whether IP of the MYC-tagged candidate protein has been successful and whether 6HIS-3HA-RUB1 is present in the anti-MYC IP, respectively.

Several outcomes are possible. If 6HIS-3HA-RUB1 covalently attaches to the co-expressed MYC-tagged candidate protein, then an anti-HA immunoreactive band will be present in the anti-MYC IP with slower migration than the unmodified candidate protein on the anti-MYC immunoblot (~15 kDa larger in size). The RUB-modified form might also be visible on the anti-MYC immunoblot as a slower-migrating form than the unmodified protein, if sufficiently abundant. If 6HIS-3HA-RUB1 non-covalently interacts with the candidate protein, then 6HIS-3HA-RUB1 will be recovered, migrating at its expected mass of ~15 kDa; non-covalent interaction with 6HIS-3HA-RUB1 was not assessed in this assay, as we were primarily interested in the identification of novel covalently RUB-modified proteins. Finally, 6HIS-3HA-RUB1 could covalently attach, not to the MYC-tagged candidate protein, but to an endogenous tobacco protein that non-covalently interacts with the candidate protein. In this case, the RUB-modified endogenous protein could be visualized by anti-HA immunoblot analysis, but the size would not correspond with the predicted size of the modified candidate protein.

As a demonstration of assay specificity, we tested a known substrate, CUL1, to assess whether we could visualize RUB modification and whether mutation of its verified rubylation site (K682) would eliminate co-IP of RUB1. CULLIN 1 is a subunit of a combinatorial ubiquitin E3 ligase that ubiquitinates substrates, and thus targets many proteins for degradation. CUL1 is a well-known RUB substrate (section 2). We compared 6HIS-3HA-RUB1 modification of MYC-CUL1 to the rubylation site mutant MYC-CUL1^{K682R} in the above-described assay, which should not be RUB-modified. Total aliquots of soluble protein extracts were examined by anti-HA immunoblot analysis to verify that 6HIS-3HA-RUB1 expressed in all samples and that its expression was highest in the negative control (Figure 26, Totals, αHA). Anti-MYC IPs on the remaining soluble protein fractions, demonstrated that while both MYC-CUL1 and MYC-CUL1^{K682R} were successfully immunoprecipitated (Figure 26b**,** αMYC IP, αMYC blot) only

MYC-CUL1 readily interacted with slow-migrating anti-HA immunoreactive bands (Figure 26**b,** αMYC IP, αHA), indicative of its RUB modification. Background was low on both anti-HA and anti-MYC immunoblots for the "RUB1 only" negative control (Figure 26b, αMYC IP). For some infiltrations, MYC-CUL1^{K682R} showed slight RUB-modification on long exposures. The highly expressed bacterial protein GUS (encoded by *uidA*) also shows a slight level of interaction with slow-migrating 6HIS-3HA-RUB1 forms, suggesting a low level of modification. These results indicate that despite over-expression of the MYC-tagged candidate protein and 6HIS-3HA-RUB1, our in planta rubylation assay has a high degree of specificity, suggesting that this assay could identify authentic rubylation substrates.

After establishment of assay specificity, RUB modification of the 10 candidate proteins (in Table 3) was investigated. Prior to anti-MYC IP, total soluble protein aliquots were examined by anti-HA immunoblot analysis to verify that 6HIS-3HA-RUB1 expressed in all samples and that its expression was highest in the negative control. Expression for 6HIS-3HA-RUB1 was sometimes considerably higher in the negative control than in the total extracts from co-infiltrated samples.

Anti-MYC IP of MYC-tagged candidate proteins was successful for all 10 tested constructs (Figure 27a-g, αMYC), though expression was quite variable. Four of the ten candidate proteins, specifically proteins encoded by At1g50250, At4g26110, At5g22610 and At4g05420 (Figure 27c,d,f, αMYC), interacted with slow-migrating anti-HA immunoreactive proteins (Figure 27c,d,f, αHA), suggesting a covalent interaction between 6HIS-3HA-RUB1 and these candidate proteins. Alternatively, this could indicate interaction of a candidate protein with an endogenous tobacco protein that is covalently modified by 6HIS-3HA-RUB1. Although MYC-tagged candidate proteins were immunoprecipitated for the products of At1g06410, At3g44110, At5g23060, At2g31800, At5g23820, and At3g09310 (Figure 27a,b,e,f,g, αMYC), no slow-migrating anti-HA immunoreactive bands were detected (Figure 27a,b,e,f,g, αHA) for these candidate proteins, suggesting that they are not authentic RUB-modified proteins. These six proteins were not further examined and we focused on one of the potential RUB targets, DDB1a.

4.3. Dissection of an identified RUB target, MYC-DDB1a

At4g05420 encodes DDB1a (DAMAGED DNA BINDING PROTEIN1a), an adaptor subunit of CUL4-type CRLs. DDB1 proteins bring CUL4 and substrate recognition subunits into close proximity to make functional ubiquitin E3 ligases and can interact with additional proteins like DEETIOLATED1 (DET1) in alternative protein complexes (Smalle and Vierstra 2004) Thus when expressed in tobacco, *Arabidopsis* MYC-DDB1a could interact with 6HIS-3HA-RUB1-modified tobacco CUL4 in an active CUL4-type CRL, and tobacco CUL4 could be rubylated by HA-RUB1. Based on the size of the anti-HA immunoreactive band that co-immunoprecipitated with MYC-DDB1a (Figure 27F, compare αHA to αMYC), it appeared that MYC-DDB1a was itself modified by 6HIS-3HA-RUB1, but tobacco CUL4 was not, or its modification was below the level of detection on the anti-HA immunoblot.

The crystal structure of the human DDB1 protein has been solved; DDB1 is composed of three β-propeller (βPa-c) domains with βPb interacting with the N terminus of CUL4 and βPa-βPc interacting with the substrate specificity subunit of CUL4-type CRLs (Angers *et al.,* 2006). Using this information, we decided to test if βPb and/or βPa-βPc were modified by RUB1 in our

in planta rubylation assay. Expression constructs for MYC-tagged βPb or βPa-βPc were co-infiltrated with 6HIS-3HA-RUB1 by *Agrobacterium*-mediated transformation, utilizing the same protocol as described above. Soluble protein extracts were prepared and a fraction of the total soluble protein extract was kept for anti-HA immunoblot analysis, while the rest was subjected to anti-MYC IP. After IP, samples were split and run on SDS-PAGE, followed anti-MYC and anti-HA immunoblot analysis. As above, 6HIS-3HA-RUB1 expressed alone served as the negative control. Anti-HA analysis of total protein aliquots showed that all samples expressed 6HIS-3HA-RUB1 to similar levels (Figure 28a, Totals, αHA). IPs of MYC-tagged βPb and βPa-βPc were successful (Figure 28b, αMYC IP, αMYC) and similar amounts of MYC-tagged protein were immunoprecipitated. However, there was a strong preference for 6HIS-3HA-RUB1 modification of the βPb subunit (Figure 28b, αMYC IP, compare αHA short and long exposures). In conclusion, DDB1a is RUB-modified and the preferred RUB-modification site is housed in its βPb domain.

In summary, using a mass spectrometry approach, we identified a number of potential RUB substrates, and developed a transient assay to test whether these could be visualized as RUB conjugates *in vivo*. We studied one protein in more detail- DDB1a. We demonstrated that DDB1a is RUB-modified, preferentially on one of its subdomains.

5. Characterization of a novel mutant form of CULLIN 1 that disrupts interaction with RBX1, a subunit of the SCF complex.

5.1. A screen for mutants defective in IAA1-LUC degradation identifies a new allele of *CUL1*.

To identify genes important for regulating Aux/IAA protein degradation, a genetic screen based on an increase in LUC activity from plants expressing an Aux/IAA-LUC fusion protein from a transgene in *Arabidopsis thaliana* was performed. *In vivo* LUC activity from individual seven-to-ten day old M_2 seedlings expressing full length IAA1-LUC was measured. The substrate luciferin was added to intact seedlings, and light emission, a product of LUC activity, from each seedling was measured. Seedlings emitting >50% more light than the progenitor line were propagated. To determine if increases in light emission result from slowed IAA-LUC degradation, an assay to measure protein degradation directly in intact single seedlings was designed. Single M_4 or control seeds were sown directly into individual wells of a 96 well plate and after seven days, luciferin and cycloheximide, a protein synthesis inhibitor, were added. The amount of light emitted was monitored over a 60 min time-course.

Using this assay, we identified one line that exhibited slower IAA1-LUC degradation (Figure 29A). The half-life of IAA1-LUC in the mutant line (designated *cul1-7*, see below) was ~50 min, ~3.5 times slower than the ~15 min half-life for IAA1-LUC in the non-mutagenized seedlings. (Figure 29A, designated *CUL1*). The half-life of IAA1-LUC in *cul1-7* was similar to that of LUC (~70 min), which lacks the IAA1 degron (Figure 29A). This measurable loss of activity from plants expressing LUC alone has been observed previously and ascribed to increased degradation when luciferin is added to intact cells (unpublished data). The increased rate of loss of LUC alone from *in vivo* addition of its substrate prevents using this specific *in vivo*

degradation assay to measure the half-lives of LUC fusion proteins if the fusion protein half-life is slower than that observed for LUC alone, which is about 70 min.

To confirm the half-life differences observed using the screening method and single seedling degradation assay and to more accurately measure the IAA1-LUC degradation rate in *cul1-7*, we determined degradation rates in these same lines using our traditional pooled-seedling degradation assay (Zenser *et al.,* 2003; Dreher *et al.,* 2006) (Figure 29B). In this case, only cycloheximide is added to the intact seedlings and LUC activity is determined in extracts prepared at various times after addition. In these assays, LUC alone shows no loss of activity in the time course (Figure 29B), consistent with previous results. The half-life of IAA1-LUC was ~80 and 21 min in mutant and wild type seedlings, respectively, confirming that the mutant shows altered rates of IAA1-LUC degradation (Figure 29B). This ~80 min half-life was consistent between generations and in homozygous seedlings after several back-crosses to the non-mutagenized transgenic line.

We wanted to identify the lesion in this line. We mapped the site of the mutation using bulked segregant analysis (Michelmore *et al.,* 1991), which placed the mutation on the short arm of chromosome IV. Using a series of SSLP and CAPS markers spanning the short arm of chromosome IV, the mutation was located within a genetic interval that included the *CULLIN1* (*CUL1*) gene, which encodes the cullin subunit of SCF-type ubiquitin ligases (Gray *et al.,* 1999). We sequenced the *CUL1* coding region from the mutant line and found one difference from wild type – a C to T transition in exon 16 of *CUL1* resulting in a T510I substitution. We called this allele *cul1-7*. The threonine residue in wild type CUL1 is conserved among other cullin family members; AtCUL1, AtCUL2, AtCUL3a, AtCUL3b, and AtCUL4. Additionally, amino acid sequence alignment revealed that Thr510 of AtCUL1 aligns with Ser541 of HsCUL1, suggesting a functional conservation of this residue between the species.

We modeled the sequence of AtCUL1 with the known crystal structure of human CUL1 (HsCUL1) in complex with HsRBX1 (Zheng *et al.,* 2002) and Thr510 of AtCUL1 overlapped with Ser541 of HsCUL1 as suggested by the primary sequence alignment. Ser541 is at the end of HsCUL1 beta-strand near the beginning of a loop in HsCUL1. This HsCUL1 beta-strand interacts with a beta-strand of HsRBX1. While the hydroxyl group of HsCUL1 Ser541 does not participate in hydrogen bonding with any residues of HsRBX1, it is within hydrogen bonding distance of Asp510 of HsCUL1, which is conserved as Asp477 in AtCUL1. Moreover, the backbone nitrogen of Leu540 is within hydrogen bonding distance of the backbone carbonyl of Ala31 of HsRBX1, and these residues are conserved in the corresponding *Arabidopsis* homologs. There is insufficient room for the side group of isoleucine (the amino acid in cul1-7) in the crystal structure when substituted for Ser541 *in silico*, and such a substitution could potentially affect the described interaction with RBX1 in this region.

5.2. *cul1-7* is recessive and plants display pleiotropic developmental defects similar to other *CUL1* alleles.

In order to assess the recessivity of the *cul1-7* allele, we performed single-seedling degradation assays on a segregating F_2 population derived from the self of a backcross of *cul1-7* with the progenitor transgenic line. The defect in IAA1-LUC degradation segregated 3:1 (χ^2 = 0.68, p= 0.410, df = 1, n= 49) indicating that the trait was recessive. The *cul1-7* allele co-segregated with the mutant phenotype after three back-crosses, suggesting that the mutation in

cul1-7 is responsible for the observed phenotypic differences and that the cul1-7 protein has impaired function.

cul1-7 plants display pleiotropic phenotypes at almost all stages of development (Figure 30). Adult *cul1-7* plants are dwarfed, exhibit a reduction in apical dominance, and have numerous curly leaves (Figure 30A). We more directly determined that the lesion in *cul1-7* was responsible for the observed phenotypes by performing an allelism test with *axr6-3*, a recessive, temperature-sensitive allele of *CUL1* that contains a missense mutation near the N-terminus (Quint *et al.,* 2005). We used a dCAPS-based method to distinguish the mutant alleles from wild type to verify the genotypes of individuals from crosses. The phenotypes of the *cul1-7*/*axr6-3* heteroallelic F_1 plants are equivalent to *cul1-7* homozygotes (Figure 30C), indicating that the lesion in *cul1-7* is likely responsible for the observed phenotypes. Finally, we complemented the mutant phenotype with expression of CUL1 on a transgene. Altogether, these experiments prove that the mutation in CUL1 is responsible for the mutant phenotype.

5.3. Cul1-7 protein is affected in its interaction with the subunit RBX1

A modification that is important for full SCF activity is the attachment of RUB to one lysyl residue of CUL1. To determine whether the mutation in *cul1-7* affects the ability of the protein to be RUB-modified, we performed an immunoblot blot analysis on total protein prepared from 9-day-old seedlings grown on GM plates. The amount of RUB-modified CUL1 appears unaffected by the mutation, as *cul1-7* has the same amount of modified protein as wild type. Surprisingly, the amount of unmodified protein in *cul1-7* is drastically reduced compared to wild type, accounting for a 43% reduction of total CUL1 protein in the mutant. This reduction increases the ratio of modified to unmodified CUL1 from ~0.2-0.27 in wild type to ~1.0 in *cul1-7*. In contrast, in *axr1-30,* where the RUB-conjugation pathway is compromised, the total amount of CUL1 increases about 45% from wild type levels. Thus, the modified to unmodified ratio is reduced further than wild type, strikingly different from *cul1-7*.

Based on the location of the amino acid change in cul1-7, cul1-7 could have impaired interaction with RBX1, a subunit that interacts with CUL1 at CUL1's C-terminus. To determine whether cul1-7 is affected in RBX1 binding, we synthesized epitope tagged versions of wild type and mutant CUL1, HIS_{6x}-EXP-CUL1, and HIS_{6x}-EXP-cul1-7, respectively, in a rabbit reticulocyte lysate system, which has the ability to conjugate NEDD8 to CUL1 (Furukawa *et al.,* 2000). In plants over-expressing RBX1, the majority of CUL1 is in the RUB-modified form (Gray *et al.,* 2002), suggesting that RBX1 interaction is limiting CUL1 modification. The RUB protein in mammals is called Nedd8 and that is the form present in rabbit *in vitro* translations, so we will refer to CUL1 modification in rabbit reticulocyte lysates as neddylation. We hypothesized that the addition of recombinant RBX1 (here as GST-RBX1) to the *in vitro* translation reaction could increase production of Nedd8-modified CUL1, but not increase equivalently NEDD8-modified cul1-7 if the substitution in cul1-7 impairs RBX1 interaction. GST-RBX1 and GST were added at the initiation of translation so that the proteins are translated in the presence of RBX1, which gives maximal neddylation. Addition of GST-RBX1 resulted in increased levels of Nedd8-modified CUL1, more easily visualized in a long exposure (bottom panel), compared to addition of GST alone (Figure 31A, lane 3). Addition of GST-RBX1 to the translation reaction synthesizing cul1-7 did not promote equivalent neddylation (Figure 31A, lane 4). These results are consistent with cul1-7 having reduced RBX1 interaction.

To demonstrate more directly a difference in RBX1 interaction between CUL1 and cul1-7, we pulled down GST-RBX1 or GST from *in vitro* translation reactions with glutathione sepharose and determined the amount of the HIS_{6x}-EXP-CUL1 or HIS_{6x}-EXP-cul1-7 present in the pull-down fraction (Figure 31B). GST and GST-RBX1 translation master mixes were prepared and added to HIS_{6x}-EXP-CUL1 and HIS_{6x}-EXP-cul1-7 DNA templates. The amounts of CUL1 and cul1-7 produced in these reactions are nearly identical (Figure 31B, INPUT lanes and quantified below). As observed before, CUL1 translation reactions with added GST-RBX had increased levels of a slower migrating band, $CUL1^{Nedd8}$ compared to GST-containing reactions. After the pull-down with glutathione beads from the GST-RBX containing reactions, much more CUL1 was present than cul1-7, ~3-fold after normalization to respective input (Figure 31B, compare lane 6 to 8). The enhancement of NEDD8 modification by RBX1, together with the reduced recovery of cul1-7 in RBX1 pull-down assays, indicate that cul1-7 has impaired interaction with RBX1.

Based on the results of Figure 31A and evidence that RBX1 abundance affects total CUL1 protein levels (Gray et al., 2002), we hypothesized that unmodified cul1-7 is less stable *in vivo* than CUL1. We performed a cycloheximide degradation assay over a 12-hour time-course for *CUL1* and *cul1-7*, and determined CUL1 levels as described above. Because there is approximately twice as much CUL1 in wild type as in *cul1-7*, twice the amount of total protein was loaded in *cul1-7* lanes. The amount of total CUL1 does not significantly change over this time-course; however, half of the total cul1-7 protein is degraded in 12 hours (Figure 9E). We did not analyze the stability of either CUL1 or $CUL1^{RUB}$ singly in these experiments, but rather total CUL1, because CUL1 could enter the $CUL1^{RUB}$ pool and vice versa during the course of the experiment thereby confounding the interpretation.

In summary, we designed and successfully used a genetic screen to identify mutants with a defect in CUL1, a rubylated protein in plants. We show that the amino acid substitution in cul1-7 reduces the stability of the protein, likely because it does not associate well with RBX1. This mutation affected *in vitro* rubylation, but we do not know if it affects the rate of *in vivo* rubylation. This mutant line is an extremely valuable reagent because it impairs the function of the SCF-type ubiquitin ligase, yet is a viable plant. This line can be used to determine whether a ubiquitin pathway substrate is modified by an SCF-type ubiquitin ligase. It has been requested by other laboratories for that very reason.

6. Analysis of degradation of Auxin Response Factor 1 (ARF1), a transcription factor important in auxin responses in plants.

We were interested in identifying additional target proteins of the ubiquitin pathway and with DOE support have analyzed the degradation of Auxin Response Factor 1 (ARF1), and member of an important transcription factor in auxin signaling. We utilized our luciferase fusion approach (generated in section 5) to measure the degradation rate of ARF1:LUC fusions in transgenic seedlings. We generated transgenic lines expressing LUC-tagged forms of ARF1 and measured their degradation rates. Three independent lines expressing ARF1:LUC proteins had the same 3-hour half-life (Figure 33). Expressing ARF1 with the HA epitope tag gave the same results. Using deletion derivatives of ARF1 fused to LUC, we were able to identify a region of ARF1 required for its observed degradation (Figure 34). The middle region of the protein is required for the degradation. Finally, we demonstrated that ARF1 degradation required the

proteasome, but did not appear to require CUL1 (Figure 35). This suggests that ARF degradation is not mediated by ubiquitylation by a CUL1 type E3 ligase. The ligase responsible for AFR1 degradation remains unknown.

In summary, we demonstrated that LUC fusions can be used to measure the degradation of proteins, using ARF1 as our model. We show that ARF1 degradation requires the variable middle region and does not require CUL1.

Experimental Methods

Many of the methods are standard biochemical and molecular biology methods, published by others. Included here are methods either developed in our laboratory or extensively modified by our laboratory.

Thioester reactions to measure activity of activating enzymes.
Arabidopsis ECR1 (At5g19180.1) coding sequence (del Pozo et al., 2002) was used to create pDEST15-ECR1 (Gateway, Invitrogen, www.invitrogen.com all pDEST and pDONR plasmids are from this source) for production and purification of recombinant GST-ECR1 using glutathione-sepharose (GE Healthcare, *www.gehealthcare.com*). *Arabidopsis AXL1* (At2g32410.1) coding sequence was isolated from mRNA, recombined into pDONR201, sequence verified (to TAIR v7), expressed as 6HIS-AXL1 from the pDEST17 vector and used from a bacterial extract. A bacterial extract expressing recombinant 6HIS-AXR1 (derived from At1g05180.1) from pQE30-AXR1 was used. 3HA-RUB1 (derived from At1g31340.1) coding sequence was used to create pDEST17-3HA-RUB1 for production and purification of 6HIS-3HA-RUB1 using Ni-NTA-sepharose (GE Healthcare). Recombinant 6HIS-HA-ubiquitin was expressed from pDEST17-HA-UBQ, derived from HA-UBQ [described in (Nishikawa *et al.,* 2004)]. Recombinant ubiquitin E1 (from yeast) was cloned into pTYB2 (NEB, www.neb.com), then expressed and purified using the IMPACT-CN (NEB) system.

For thioester reactions, proteins were incubated in 2 mM ATP, 0.1 mM DTT, 10 mM $MgCl_2$, and 100 mM TRIS (pH 7.5) buffer at 37°C for 5 min. Reactions were then split in half and stopped in the presence or absence of DTT (5.3% SDS, 13.3% glycerol, 5.3 M urea, ± 133 mM DTT) for 15 min at RT. The proteins were separated on a non-reducing 8% tris-glycine gel at 4°C, transferred to Immobilon-P membrane (Millipore, www.millipore.com), and analyzed by anti-HA (monoclonal rat anti-HA-HRP; Roche, www.roche.com) and anti-GST (polyclonal rabbit anti GST(Z-5); Santa Cruz Biotech., www.scbt.com) immunoblot analysis.

Oxyester reactions

Vectors used in this assay include: pDEST17-AXR1, pDEST17-AXL1, pDEST17-FLAG-ECR1^{C215S}, pDEST17-FLAG-ECR1^{C215A}, and pDEST15-3HARUB1. All vectors were cloned using Gateway cloning technology; sources for original sequences are as described above. In brief, all coding sequences were first cloned into pDONR201 and sequenced, then moved into appropriate expression vectors. pDEST17-FLAG has been modified to have a FLAG sequence 3' to 6HIS and 5' to att1 sequences. All proteins were induced in BL21(DE3)pLysS cells and the soluble protein fraction was recovered by centrifugation after cells were lysed by sonication. Anti-HIS (monoclonal mouse anti-HIS; GE Healthcare) immunoblot analysis and/or Coomassie blue staining were used to establish relative protein concentrations.

For oxyester assays, proteins were incubated in 2 mM ATP, 0.1 mM DTT, 10 mM $MgCl_2$, 0.6 U ml^{-1} inorganic pyrophosphatase, and 100 mM TRIS (pH 7.5) buffer (with one replicate containing 0.3 U ml^{-1} creatine kinase and 5 mM creatine kinase in addition, with negligible effect) at 30°C for the duration of the time course (1 h, 2 h, 4 h). At each time point, 10 µl of sample were removed from a 25 µl reaction for base and neutral conditions and mixed with 10 µl EZ-view anti-HA-agarose beads (Sigma-Aldrich, www.sigmaaldrich.com) and 90 µl of 50 mM TRIS (pH 7.5). Immunoprecipitation proceeded for 45 minutes, then beads were washed 3x 5 min in 50 mM TRIS (pH 7.5). Finally, beads were mixed with 10 µl of 50 mM TRIS (pH 7.5) and were subjected to base or neutral conditions. For base conditions, 20 µl TRIS/beads were incubated with 10 µl 0.4 M NaOH for 20 min at 30°C, then 25 µl of 5x loading buffer [125 mM TRIS (pH 6.8), 20% glycerol, 5% SDS, 5% BME] were added, followed by 1 µl concentrated HCl (to acidify the reaction). Reactions were then titrated back to neutral pH with 1 M NaOH. For neutral conditions, 20 µl TRIS/beads were mixed with 25 µl 5x loading buffer and water was added to make volume equivalent with base treatment. Samples were then boiled for 5 min and run on reducing 8% tris-glycine gels at RT, transferred to Immobilon-P membrane, and analyzed by anti-FLAG-HRP (monoclonal mouse anti-FLAG M2-HRP; Sigma-Aldrich). Loading was checked by analysis of inputs (fraction of total for each sample), which were not subjected to immunoprecipitation, using anti-HA-HRP (monoclonal rat anti-HA-HRP; Roche) and anti-HIS (monoclonal mouse anti-HIS; GE Healthcare) immunoblot analysis. Time course experiments were done in quadruplicate.

Immunoblots were scanned using a flatbed scanner at 600 dpi, with no auto-correction. Blots were then analyzed in ImageJ (version 1.43u, National Institutes of Health, http://rsb.info.nih.gov/ij), using the Gel Analyzer program. In brief, all bands on a blot were boxed in uniform rectangles, then intensity peaks were plotted, and the absolute intensity of each band was calculated as the area under each peak. These values were then plotted against time and analyzed using the JMP (version 8.0.1, SAS Institute Inc., http://www.jmp.com) statistical package.

RUB E2 thioester loading assay

Vectors used in this assay include: pDEST17-AXR1, pDEST17-AXL1, pDEST17-ECR1, pDEST17-FLAG-RCE1 (derived from At4g36800.1), pDEST17-FLAG-RCE2 (derived from At2g18600.1), and pDEST15-3HARUB1. All vectors were cloned using Gateway cloning technology; sources for original sequences are as described above. All proteins were induced in BL21(DE3)pLysS cells and the soluble protein fraction was recovered by centrifugation after cells were lysed by sonication. Anti-HIS (monoclonal mouse anti-HIS; GE Healthcare) immunoblot analysis and/or Coomassie blue staining were used to establish relative protein concentrations.

For E2 thioester assays, proteins (in bacterial lysates) are incubated in 120uL reactions, buffered in 1.67 mM ATP, 0.083 mM DTT, 8.3 mM $MgCl_2$, 0.5 U ml^{-1} inorganic pyrophosphatase, 0.25 U ml^{-1} creatine kinase, 4.2 mM creatine phosphate, and 83 mM TRIS (pH 7.5), at 37°C for 15 min. Next, 3 x 30 µl reaction aliquots (for negative control, + 6HIS-FLAG-RCE1, and + 6HIS-FLAG-RCE2) are moved to new tubes and mixed with 90 µl 50 mM TRIS (pH 7.5) and 20 µl (1:1) slurry anti-HA-agarose beads (Sigma-Aldrich). Immunoprecipitations then proceed for 45 min at 4°C. Following immunoprecipitation, beads are washed 3x 5 min in 50 mM TRIS (pH 7.5) at 4°C. Next, 120 µl 50 mM TRIS (pH 7.5) and 30 µl bacterial lysate, containing 6HIS-FLAG-RCE1 or 6HIS-FLAG-RCE2, or for the negative control, 150 µl 50 mM

TRIS (pH 7.5), is mixed with beads, and samples are agitated for 15 min at RT. Beads are again washed 3x 5 min in 50 mM TRIS (pH 7.5) at 4°C.

After final wash, beads are eluted in 40 µl 8 M Urea for 15 min at RT (with agitation). Then for each reaction, 15 µl eluate is mixed with 30 µl reducing loading buffer [112.5 mM TRIS (pH 6.8), 18% glycerol, 4.5% SDS, 100 mM DTT], and 15 µl eluate is mixed with 30uL non-reducing loading buffer [112.5 mM TRIS (pH 6.8), 18% glycerol, 4.5% SDS]. Reactions are incubated 15 min at RT (with mixing), then heated 1-3 min at 42°C and run on a 4-12 % bis-tris gradient gel (Invitrogen), first at RT (for samples to enter gel) and then at 4°C. After SDS-PAGE, resolved proteins are transferred to Immobilon-P membrane, and analyzed by anti-FLAG-HRP (monoclonal mouse anti-FLAG M2-HRP; Sigma-Aldrich). Flow-through aliquots, from both immunoprecipitation steps, are kept and analyzed for the presence of all proteins carrying the 6HIS epitope (all proteins except GST-3HA-RUB1); immunoblot analysis is done using anti-HIS (monoclonal mouse anti-HIS; GE Healthcare).
One experiment was done comparing 6HIS-AXL1-6HIS-ECR1 to 6HIS-ECR1 alone allowing for the determination that GST-3HA-RUB1-6HIS-RCE1/2 conjugates run at ~70 kDa and that numerous bands, sensitive to reducing agents, are also present on anti-FLAG immunoblots that are independent of an active E1 (i.e. present in ECR1 alone samples). Additional experiments were done comparing 6HIS-AXR1-6HIS-ECR1 to 6HIS-AXL1-6HIS-ECR1, which allowed for the determination that both AXR1 and AXL1, in conjunction with ECR1, transfer activated RUB1 to both RCE1 and RCE2. AXR1-ECR1 and AXL1-ECR1 transferred activated RUB to both RUB-conjugating enzymes minimally twice.

Mass spectrometry of 3HA-RUB1-interacting proteins
We developed a protocol in our laboratory for the identification of Rub interacting proteins. In preparation for mass spectrometric (MS) analysis, a minimum of 0.25 g seeds dexamethasone (DEX)-inducible *6xUAS$_{gal4}$:3HA-RUB1* in Columbia and Columbia (control) were bleach-sterilized and then cold-treated minimally overnight before plating. For each line, seeds were evenly distributed over 4-section culture plates and 1 ml of germination media (GM; 1x MS salts, 1% sucrose, 1x B-vitamins, 0.05% MES) was added to each quadrant. Plates were then grown under continuous light for 7 days. Plates were then removed from lights, excess GM was removed and 1 ml of fresh GM + 30 µM dexamethasone (DEX) was added. Plates were returned to lights and seedlings were DEX-treated overnight, before seedlings were collected and flash-frozen in liquid N_2.

Protein was extracted in aqueous buffer [50 mM TRIS (pH 8), 150 mM NaCl, 20 mM EDTA, 10% glycerol, 0.15% NP-40, 1 mM PMSF, 0.5 mM 1,10-phenanthroline, 1x protease inhibitors (Roche)] with 1.5% PVPP (w/w) by grinding with mortar and pestle in liquid N_2. Samples were then clarified at 4^{o}C by centrifugation at 16060 x ***g*** and 17369 x ***g***. Between each centrifugation step, the soluble fractions were moved to new collection tubes. We then proceeded with analysis of the soluble fraction and determined protein concentration by Bradford assay. Samples were brought to equal concentration, and anti-HA immunoprecipitation proceeded overnight at 4^{o}C from minimally 65 mg soluble protein with minimally 0.25 ml equilibrated EZ-view anti-HA-agarose beads (Sigma-Aldrich).

Method 1 for Recovery of Trypsin-digested Peptides
All washes were carried out at 4°C. Anti-HA-agarose beads were washed with 450x bead volume of various buffers [60x bead volume buffer 1 (50 mM TRIS (pH 8), 150 mM NaCl,

0.15% NP-40, 0.5x protease inhibitors); 60x bead volume buffer 2 (50 mM MES (pH 6), 150 mM NaCl, 0.5x protease inhibitors); 150x bead volume buffer 3 (50 mM TRIS (pH 8), 150 mM NaCl); 180x bead volume buffer 4 (100 mM ammonium bicarbonate (pH 8)]. Then (next day) samples were trypsin digested, using minimally 1.6 µg trypsin (Promega, www.promega.com) in 100 mM ammonium bicarbonate, for 6-8 h at 37°C. We recovered minimally 5 µg digested peptides per sample by A_{280} measurement. Samples were dried nearly to completion by vacuum centrifugation at RT, and digested peptides were then stored at -80°C, until LC-MS/MS analysis.

Method 2 for Recovery of Trypsin-digested Peptides

Anti-HA-agarose beads were washed at 4°C with 150x bead volume of various buffers [60x bead volume buffer 1 (50 mM TRIS (pH 8), 150 mM NaCl, 0.15% NP-40, 0.5x protease inhibitors); 90x bead volume buffer 5 (50 mM TRIS (pH 8), 150 mM NaCl, 0.5x protease inhibitors)] before proceeding with elution. Proteins were eluted with 20x bead volume 200 mM Ammonium hydroxide (pH 12.3). Elution proceeded two hours at RT, then eluates were moved to new collection tubes and neutralized with 10x bead volume 1 M TRIS (pH 6.8). Then eluted proteins were TCA precipitated in 13% TCA overnight at 4°C.

Next day, protein pellets were collected by centrifugation at 16060 x ***g*** for 20 min at 4°C. Then protein pellets were washed twice in 2 ml acetone; pellets were collected by centrifugation at 16060 x ***g*** for 20 min at 4°C after each wash. Then samples were briefly dried in a vacuum centrifuge and resuspended in 50 µl 1M TRIS (pH 6.8). Protein concentrations were determined by A_{280} measurement, then 15 µl loading buffer **(**125 mM TRIS (pH 6.8), 20% glycerol, 5% SDS, 1% BME**)** was added to each sample and BME was brought to 1% (v/v). Samples were neutralized with NaOH, as needed. Approximately 75% of each sample was run briefly into a NuPAGE 10% (1.5 mm x 10-well) Bis-TRIS gel (Invitrogen, www.invitrogen.com) in 1x MES running buffer (50 mM MES, 50 mM TRIS, 0.1% SDS, 1 mM EDTA, pH 7.3), before proceeding with in-gel trypsin digest, modified from (Jensen *et al.,* 1999).

Approximately 400 µl 1-cubic-mm gel pieces were washed 3 x 5 min at RT in 1 ml 100 mM ammonium bicarbonate. Gel pieces were then dried by washing 3 x 5 min at RT in 250 µl 100% acetonitrile. To allow for further drying of samples, samples were vacuum centrifuged at RT for 20 min. Gel pieces were rehydrated in 1 ml 10 mM DTT (in 100 mM ammonium bicarbonate) for 30 min at 56°C. Then excess liquid was decanted and gel pieces were washed 3 x 5 min in 200 µl 100% acetonitrile, before 5-10 min vacuum centrifugation at RT. Gel pieces were then incubated in 200 µl 55 mM iodoacetamide (in 100 mM ammonium bicarbonate) for 20 min in the dark at RT. Samples were washed briefly in 1ml 100mM ammonium bicarbonate, twice. Then, samples were washed 2 x 5 min in 250 µl 100% acetonitrile and dried to completion (15 min at RT) by vacuum centrifugation.

Proteins were then subjected to in-gel trypsin digestion overnight at 37ºC with 0.5 µg Trypsin (Promega) in 350 µl 100 mM ammonium bicarbonate. Digested peptides in solution were recovered next day and a final extraction of peptides from gel pieces was performed in 200 µl 60% acetocitrile-1% TFA with 10 min sonication. Peptides were then vacuum-centrifuged until nearly dry and a final estimation of recovered peptides was performed by A_{280} measurement. Minimally 16 µg digested peptides were recovered.

LC-MS/MS Run

The peptides from approximately 50% of each sample were separated by reverse phase chromatography using a Waters nanoACQUITY UPLC system (www.waters.com) and a Waters

BEH C_{18} 1.7 µm, 100 µm x 10 cm column, using a gradient of 1% to 80% acetonitrile with 0.1% formic acid maintained throughout the gradient. Peptides were directly eluted into a ThermoElectron LTQ-FT mass spectrometer (www.thermo.com) with a nano-electrospray ionization source at a flow rate of 1 µl min^{-1} for detection of the intact peptides' mass to charge (*m/z*) ratios. Data-dependent software parameters allowed the top four most abundant ions to be selected with a 30 sec exclusion list time and repeat count of 2. Singly-charged ions were disallowed for collision-induced dissociation.

Tandem mass spectra were extracted with ReADW (version 4.0.2, Seattle Proteome Center, www.proteomecenter.org), with centroiding (-c) enabled prior to MS/MS program searches.

X! Tandem Analysis and Scaffold 2 Validation of LC-MS/MS Data

All LC-MS/MS samples were analyzed using X! Tandem [version TORNADO (2009.04.01.1)] from the Global Proteome Machine (www.thegpm.org). X! Tandem was set up to search the *Arabidopsis thaliana* TAIR7 protein database (www.thegpm.org, ath1.fasta.pro, 30791 entries), along with common contaminants (crap.fasta.pro from www.thegpm.org, 101 entries), assuming the digestion enzyme trypsin. X! Tandem was searched with a fragment ion mass tolerance of 0.40 Da and a precursor ion tolerance of 10.0 p.p.m. Deamidation of asparagine and glutamine, variable oxidation of methionine and tryptophan, acetylation of the N-terminus, and diglycine (+114.042927 Da at K) and 1964 Da (+1964.04795966 Da at K) modification of lysine (rubylation footprint) were specified as variable modifications in X! Tandem. For trypsin-digested peptides prepared by method 2, carbamidomethylated cysteine and propionamide-modified cysteine were searched as additional variable modifications in X! Tandem. One missed trypsin cleavage per peptide was allowed.

Scaffold (version Scaffold_2_03_01, Proteome Software Inc., www.proteomesoftware.com) was used to validate LC-MS/MS based peptide and protein identifications. Peptide identifications were accepted if they could be established at greater than 80.0% probability as specified by the Peptide Prophet algorithm (Keller et al., 2002)Protein identifications were accepted if they could be established at greater than 80.0% probability and contained at least 1 identified unique peptide. Protein probabilities were assigned by the Protein Prophet algorithm (Nesvizhskii et al., 2003). Proteins for which peptides were found in the control sample were excluded from the list of potential RUB-interacting proteins.

Analysis of LC-MS/MS Data Using INSPECT

All LC-MS/MS samples were analyzed using INSPECT Live Search [version alpha] from University of California-San Diego (www.proteomics.ucsd.edu). INSPECT was set up to search the *Arabidopsis thaliana* International Protein Index database (www.proteomics.ucsd.edu, ipi.ARATH.v3.29), along with common contaminants, assuming the digestion enzyme trypsin. INSPECT was searched under the FT-HYBRID scoring model with a fragment ion mass tolerance of 0.50 Da and a precursor ion tolerance of 2 Da, which was then narrowed to 100 p.p.m during post-analysis. Deamidation of asparagine and glutamine, oxidation and dioxidation of methionine and tryptophan, and diglycine modification (+114.042927 Da at K) of lysine (rubylation footprint) were specified in INSPECT as optional modifications, and 1 post-translational modification was allowed. For samples prepared by method 2, carbamidomethylated cysteine and propionamide-modified cysteine were also specified as optional modifications in INSPECT.

In INSPECT, results were filtered at a spectrum-level p-value of 0.05, measured by hits to a decoy database. Proteins for which peptides were found in the control sample were excluded from the list of potential RUB-interacting proteins. Data were manually cleaned, and peptides unique to RUB samples were kept only if the following criteria were met: 1) precursor ion tolerance of 100 p.p.m. as this is the default for FT-HYBRID in the INSPECT commandline program; 2) normal cleavage after R or K on both tryptic peptide ends; 3) no more than 1 missed cleavage site within the peptide; 4) modification of lysine could not occur at a tryptic peptide end of a peptide.

Compiling Data Analyses from MS Screen

Data were combined from 7 LC-MS/MS experiments comparing DEX-inducible *6xUAS$_{gal4}$:3HA-RUB1* in *Arabidopsis* (RUB) and wild-type *Arabidopsis* (control) lines. After putative RUB-interacting proteins were identified with X! Tandem/Scaffold and INSPECT, the two datasets were compared. Putative RUB-interacting proteins were eliminated if found in the control sample by the reciprocal search method (e.g. INSPECT candidate RUB-interacting protein was identified in X! Tandem search of control lines or X! Tandem/Scaffold candidate protein was identified in INSPECT search of control lines). Additionally, candidate proteins were eliminated if a related protein (e.g. from a protein family) was found in a control sample, or if the protein was identified in an additional LC-MS/MS experiment done on control tissue only (trypsin-digested peptides prepared as described in method 2, data analysis with X! Tandem/Scaffold); proteins with 2 spectra [minimum 1 unique spectra w/ 2 hits] in one or a combination of RUB replicates that never appeared in control replicates were considered as candidate proteins. LC-MS/MS data on known RUB-interacting proteins confirmed the protocol was generally appropriate for recovery of RUB-interacting proteins. As new RUB-interacting proteins were not present above background (based on a significant presence of peptides in RUB samples as compared to control samples), the above described low stringency MS screen was implemented to generate a list of potential RUB-interacting proteins to be confirmed by additional analyses.

Cloning Putative RUB-interacting Proteins and 6HIS-3HA-RUB1

Gene sequences for putative RUB-interacting proteins [listed in (Table 3)] were cloned from mRNA, or from genomic DNA if recovery of the coding sequence proved unsuccessful. Cloning primers included gene-specific sequences and additional sequences for attB1/attB2, for Gateway-compatible cloning. After PCR amplification, gene sequences were recombined into pDONR201 and verified by sequencing. Subsequently, gene sequences were recombined into pEarleygate203 (Earley *et al.,* 2006). Expression vectors were then moved into *Agrobacterium tumefacians* strain AGL1 by electroporation.

For the split DDB1a vectors (βPb and βPa-βPc), pDONR-DDB1a (p7438) was used as a template for PCR amplification of the βP domains, additional attB1/attB2 sequences were included at 5' and 3' ends, respectively, for Gateway-compatible cloning. βPa-βPc was cloned in two PCR steps: first the separate βP domains were PCR amplified, then the βPa-βPc combined fragment was PCR amplified using a modified overlap PCR protocol (Choi and Schweizer 2005) After PCR amplification, the gene sequences were recombined into pDONR201 and verified by sequencing. Subsequently, gene sequences were recombined into pEarleygate203 (Earley et al., 2006) with the final vectors designated p7498 (βPb) and p7499 (βPa-βPc).

For 6HIS-3HA-RUB1, cloning primers include gene-specific sequences, sequence for N-terminal 6HIS-tev-3HA epitopes (forward primer) and additional sequences for attB1/attB2, for

Gateway-compatible cloning. After PCR amplification, the gene sequence was recombined into pDONR201 and verified by sequencing. Subsequently, sequence encoding 6HIS-tev-3HA-RUB1 was recombined into pEarleygate100 (Earley et al., 2006) with the final vector designated p7361.

Transient Expression in tobacco and Anti-MYC IP of MYC-tagged Protein and 6HIS-3HA-RUB1

Four- to six-week-old *N. benthamiana* (tobacco) leaves were infiltrated by *Agrobacterium*-mediated transformation [modified from (Vinatzer *et al.,* 2006)] with bacterial cultures containing constructs that express 6HIS-3HA-RUB1 or MYC-tagged candidate protein. 6HIS-3HA-RUB1 was infiltrated alone as a negative control. Glycerol stocks of bacterial cells were streaked out on Luria Broth (LB)-agar (50 μg ml^{-1} kanamycin/250 μg ml^{-1} carbomycin) and inoculated into 5 ml LB plus antibiotics. Cultures were then grown overnight at 30°C. On the next day, culture ODs were measured, then cells were collected by centrifugation and brought to a final OD ~1 in infiltration media (IM: 10mM MES (pH 5.6), 10mM $MgCl_2$, 150uM acetosyringone). A blunt syringe was used to infiltrate leaves with a 3:1 mixture of bacterial cultures for MYC-tagged candidate protein and 6HIS-3HA-RUB1, respectively, to have sufficient area for 10 leaf punches per experimental replicate. For 6HIS-3HA-RUB1 only (negative control), infiltration buffer was used in lieu of MYC-tagged candidate protein culture. Three days after infiltration, equal amounts of infiltrated tissue (10 leaf punches made with a 1.5 ml centrifuge tube cap per sample) were collected from all samples and flash frozen in liquid N_2.

Tissue in 1.5 ml centrifuge tubes was removed from liquid N_2 and briefly powdered using a hand pestle; soluble protein was then extracted in 500 μl immunoprecipitation (IP) buffer [IP buffer: 50 mM TRIS (pH 8), 150 mM NaCl, 20 mM EDTA, 0.15% NP-40, 1x protease inhibitor cocktail (Roche), 50 μM MG132, 0.1 mg ml^{-1} DEXTRAN 500,000, 1 mg ml^{-1} BSA, Cohn fraction 5, pH 7] by additional homogenization with pestle. Samples were then clarified at 4°C by centrifugation at 17369 x ***g*** twice. Between each centrifugation step, the soluble fractions were moved to new collection tubes. For each sample, total volume was measured, then one-tenth of total was saved for total protein analysis and nine-tenths of total were subjected to anti-MYC IP, using 25 μl EZ-view anti-MYC-agarose beads (Sigma-Aldrich); for both total and IP fractions, all samples were brought to the same volume. IPs were mixed 45 min at 4°C, then anti-MYC agarose beads were washed 3 x 15 min at 4°C in wash buffer [wash buffer: 50 mM TRIS (pH 8), 150 mM NaCl, 0.15% NP-40, 0.1 mg ml^{-1} DEXTRAN 500,000, 1 mg ml^{-1} BSA], then protein was eluted from beads by boiling 5 min in loading buffer [125 mM TRIS (pH 6.8), 20% glycerol, 5% SDS, 1% BME]**.**

Total fractions were run on SDS-PAGE gels, transferred to PDVF membrane (Immobilon-P, Millipore, www.millipore.com), and visualized by anti-HA-HRP (Roche) to gauge the expression of 6HIS-HA-RUB1. Experiments were continued when expression of 6HIS-3HA-RUB1 in all samples was detected and highest expression of 6HIS-3HA-RUB1 was present in the negative samples (expressing 6HIS-3HA-RUB1 only). IP fractions were split with the two aliquots run on a single gel; one-half of which was subjected to anti-MYC-HRP (Roche) immunoblot analysis and the other half was subjected to anti-HA-HRP (Roche) immunoblot analysis. Experiments were repeated minimally two times for non-interacting proteins and three times for MYC-substrate proteins that appeared to interact with 6HIS-3HA-RUB1.

Denaturing immunoprecipitations to identify covalently linked proteins

As above, four- to six-week-old *N. benthamiana* leaves were infiltrated by *Agrobacterium*-mediated transformation with constructs that express 6HIS-3HA-RUB1 and MYC-substrate protein or with the 6HIS-3HA-RUB1 construct alone as a negative control.

Protein from 10 leaf punches per sample was then extracted under denaturing conditions in 350 µl denaturing immunoprecipitation (dIP) buffer [dIP buffer: 50 mM TRIS (pH 8), 150 mM NaCl, 1% SDS, 1x protease inhibitor cocktail (Roche)]. For each sample, total volume was measured, and then one-tenth of total was saved for total protein analysis. The remaining nine-tenths of total was diluted in RIPA buffer [RIPA buffer: 50 mM TRIS (pH 8), 150 mM NaCl, 1% NP-40 (v/v), 0.5% sodium deoxycholate (w/v), 1x protease inhibitor cocktail (Roche), 0.1 mg ml^{-1} DEXTRAN 500,000, 1 mg ml^{-1} BSA, Cohn fraction 5, pH 7] and subjected to anti-MYC IP, using 25 µl EZ-view anti-MYC-agarose beads (Sigma-Aldrich). For both total and IP fractions, all samples were brought to the same volume with dIP buffer. IPs were mixed 45 min at 4°C, then anti-MYC-agarose beads were washed 3 x 15 min at 4°C in RIPA wash buffer [RIPA wash buffer: 50 mM TRIS (pH 8), 150 mM NaCl, 1% NP-40, 0.5% sodium deoxycholate (w/v), 0.1 mg ml^{-1} DEXTRAN, 1 mg ml^{-1} BSA], then protein was eluted from beads by boiling 5 min in loading buffer [125 mM TRIS (pH 6.8), 20% glycerol, 5% SDS, 1% BME]**.**

Total fractions were run on SDS-PAGE gels, transferred to Immobilon-P PDVF membrane (Millipore), and visualized by anti-HA-HRP (Roche) to gauge the expression of 6HIS-HA-RUB1 with the goal being two-fold, expression of 6HIS-3HA-RUB1 in all samples and highest expression of 6HIS-3HA-RUB1 in the negative samples (expressing 6HIS-3HA-RUB1 only). IP fractions were split with two aliquots being run on a single gel; one-half of which was subjected to anti-MYC-HRP (Roche) immunoblot analysis and the other half was subjected to anti-HA-HRP (Roche) immunoblot analysis. Experiments were repeated minimally two times.

Production of *axr1-30* complementation lines

The intergenic region (called "AXR1 promoter") 5' to the ATG start codon of *AXR1* (At1g05180.1) was amplified from genomic DNA by PCR that added *Hind*III and *Xba*I restriction sites to 5' and 3' ends, respectively. This sequence was ligated into pGWB21 replacing its 35S CaMV promoter; the construct was designated pGWB21-AXR1p. The vector was sequenced to confirm sequence and orientation of the inserted promoter. The pGWB21 vector confers an N-terminal 10xMYC epitope and is compatible with Gateway cloning technology (Nakagawa *et al.,* 2007). *AXR1* (At1g05180.1) and *AXL1* (At2g32410.1) coding sequences were first amplified by PCR and moved into pDONR201, as described above, before being moved into pGWB21-AXR1p, using Gateway cloning technology. The cloned constructs were designated *AXR1p:10MYC-AXR1* and *AXR1p:10MYC-AXL1*.

AXR1p:10MYC-AXR1 and *AXR1p:10MYC-AXL1* constructs, which carry genes for resistance to kanamycin and hygromycin, were introduced into plants heterozygous for *AXR1/axr1-30* (carrying a gene for glufosinate resistance), using the floral dip method with Agrobacterium strain AGL1 (Clough and Bent 1998). In this experiment, we utilized *axr1-30* mutants in preference to other severe *axr1* alleles because *axr1-30* carries a selectable marker and is thus readily followed when screening for complementation. T1 transformants were selected on kanamycin plates and then sprayed with Finale (1% glufosinate-ammonium; Bayer CropScience, www.bayercropscience.com) to eliminate plants with the *AXR1/AXR1* genotype. T2 seedlings were then analyzed to recover lines that carried a single *AXR1p:10MYC-AXR1* or

AXR1p:10MYC-AXL1 transgene. Individuals homozygous for *axr1-30/axr1-30* and the respective transgene were recovered in T3 and later generations.

Starting at the T2 generation, plant lines were screened for complementation of *axr1-30* phenotypic defects in adult plants; 10MYC-AXR1 and 10MYC-AXL1 protein levels were also evaluated. Nine AXL lines were recovered where 10MYC-AXL1 protein accumulated to levels equivalent to or higher than 10MYC-AXR1 protein; however complementation of *axr1-30* phenotypic defects was not obvious in these lines. Though 10MYC-AXL1 largely failed to correct *axr1-30* phenotypic defects in adult plants, screening for additional AXL lines was not pursued as 10MYC-AXL1 protein was readily expressed. Five AXR1 lines were recovered where 10MYC-AXR1 protein was visible and complementation of *axr1-30* phenotypic defects was readily apparent.

Cycloheximide chase

Seedlings were grown in continuous light for 8 days, prior to treatment with cycloheximide (0.2 mg ml^{-1}) for 0, 2, or 6 hours. On day 7, excess GM was removed and 950 μl fresh GM was added. On day 8, 50 μl of 4 mg ml^{-1} cycloheximide was added for cycloheximide time-course. After collection of tissue in liquid N_2, protein extraction in aqueous buffer [50 mM Tris (pH 8), 150mM NaCl, 20 mM EDTA, 10% glycerol, 0.15% NP-40, 1x PI (Roche)] is done. Protein is then quantified by Bradford analysis and diluted to 4 mg ml^{-1}. Then equal protein (150 μg) is run on SDS-PAGE. Anti-MYC and anti-HA immunoblot analyses are then done to determine protein stability.

Phenotypic analyses of *axr1-30* complementation lines

For seedling analyses, seeds were surface-sterilized with 30% bleach and cold-treated for a minimum of 24 h, then plated on GM (0.8% agar added). Seedlings were grown for nine days, with germination (radicle emergence noted on dissecting scope) marked on day two, in continuous light (average = 43 μmol sec^{-1} m^{-2}) at 20°C. Seedlings were then removed from GM plates and roots were photographed. Root length was then determined using the segmented line tool in ImageJ, for minimally n = 41 individuals per line per treatment. Three experimental replicates were combined and statistical analyses were done using the JMP statistical package with a log-transformation applied to correct for heterogeneity of variance, as needed.

For analyses of adult plants, seeds were surface-sterilized with 30% bleach and cold-treated for a minimum of 48 h. Seeds were then plated on GM and grown for seven days in continuous light (average = 46 μmol sec^{-1} m^{-2}) at 22°C, before transplanting seedlings to soil and continued growth in 16 h light/8 h dark (average = 116 μmol sec^{-1} m^{-2}) at 18°C and minimally 50% humidity. Plants were photographed for rosette diameter measurements at 28 days post-plating. Diameter measurements were then made in ImageJ, using the ellipse function to draw the smallest circle that would encompass the whole rosette, for minimally n = 29 individuals per line. The circle's diameter was then taken as a measure of the rosette's broadest diameter. Measurements of inflorescence height were made 70 days post-plating. The longest measurement from rosette base to inflorescence tip was used as a measure of height. Measurements were made with a ruler, for minimally n = 24 individuals per line. Plants representative of average height were also photographed. Two experimental replicates were combined and statistical analyses were done using the JMP statistical package with a log-transformation applied to correct for heterogeneity of variance, as needed.

Technology Transfer Efforts
Publications supported by this grant:

Laplaza, J.M., Bostick, M., Scholes, D.T., Curcio, M.J. and Callis, J. 2004. *Saccharomyces cerevisiae* ubiquitin-like protein Rub1 conjugates to cullin proteins Rtt101 and Cul3 *in vivo.* Biochemical J. 377: 459-467

Bostick, M. Lochhead, S., Honda, A., Palmer, S. and Callis, J. 2004. RUB1 and RUB2 (Related to Ubiquitin) are redundant, essential, and regulate vegetative growth, auxin signaling, and ethylene production in Arabidopsis. Plant Cell 16: 2418-2432

Figueroa, P., Gusmaroli, G., Serino, G., Habashi, J., Ma, L., Shen, Y., Feng, S., Bostick, M., Callis, J., Hellmann, H., and Deng, X-W. 2005. Arabidopsis has two redundant cullin3 proteins that are essential for embryo development and that interact with RBX1 and BTB proteins to form multi-subunit E3 ubiquitin ligase complexes *in vivo*. Plant Cell 17: 1180-1195.

Stone, S.L. and Callis, J 2007. Ubiquitin ligases mediate growth and development by promoting protein death. Current. Op. Plant Biol. 10: 624-632.

Hotton, S and Callis, J. 2008. Regulation of Cullin-based E3 ligases. Annual Review of Plant Biology 59: 467-489.

Gilkerson, J. Hui, J, Brown, J., Jones, A., Sun, T-P. and Callis, J. 2009. Isolation and Characterization of *cul1-7*, a Recessive Allele of *CULLIN1* that Disrupts SCF Function at the Cterminus of CUL1 in *Arabidopsis thaliana*, GENETICS 181:945-963.

Salmon, J., Ramos, J. and Callis, J. 2008. Degradation of the auxin response factor ARF1. Plant J, 54, 118-128

Hotton S.K., Eigenheer R.A., Castro M.F., Bostick M. and Callis J. 2011. AXR1-ECR1 and AXL1-ECR1 heterodimeric RUB-activating enzymes diverge in function in Arabidopsis thaliana. Plant Mol Biol, 75: 515-26.

Hotton, S.K., Castro M.F., Eigenheer, R.A., Callis, J, 2012. Recovery of DDB1a (DAMAGED DNA BINDING PROTEIN1a) in a Screen to Identify Novel RUB-Modified Proteins in *Arabidopsis thaliana*. Molecular Plant 5: 1163-1166.

Conclusions

This DOE supported project has advanced our understanding of an essential regulatory mechanism in higher eukaryotes, using both yeast and a model plant species as experimental organisms. The ubiquitin pathway regulates the stability of many proteins by the covalent modification of targets with the protein ubiquitin. RUB (Rub1p in yeast and Nedd8 in mammals) is a ubiquiitn-like protein similarly conserved in eukaryotes and is another protein modifier of proteins. When the work was initiated, only one RUB/Nedd8/Rub1p substrate was known. Interestingly, this protein is Cullin (Cdc53p in yeast), a subunit of a ubiquitin modification E3 called SCF. Thus, one protein modification system regulates another. This work reveraled new information on the scope and roles of the Rub pathway in both yeast and plants. We discovered that the other cullin-like proteins in yeast, Cul3p and Rtt101p, are substrates of the Rub pathway. Nothing had yet linked these proteins to the ubiquitin pathway, but given their identity to cullin and our demonsration that they are modified by Rub1p, this has led others to determine their roles in the ubiquitin pathway. We discovered that Rtt101p is regulated by another Rub-independent modfiication. The plant protein RUB1 can be conjugated in yeast to Cdc53p, indicating conservation of the pathways. However, some specificity is lost, since plant RUB1 attaches to additional proteins in yeast.

In plants, we made major advances in our understanding of the RUB pathway. We showed that that RUB1/2 proteins are functionally equivalent and redundant, but loss of both leads to inviability of many gametes and of all embryos. To study the vegtative effects of loss of Rub fapthway, we developed lines with reduced RUB1/2 expression and carefully characterized these lines. They are affected in many aspects of growth. Most strikingly, they over-produce ethylene as dark-grown seedlings. This is likely due to misregulation of the genes responsible for ethylene synthesis.

Attachment of RUB to its substrates requires a RUB activating enzyme, a heteromeric protein consisting of AXR1 and ECR proteins. Another AXR1-like protein exists in plants. We functionally characterized the second protein, called AXL1, for AXR1-like. We showed that it has specificity for activating RUB proteins in a manner similar to AXR1. In addition, it will transfer RUB1 to the Rub E2 enzymes, similar to AXR1. However is does not appear to function equivalently to AXR1 when expressed at equivalent levels in plants. It may interact in a distinct manner with as yet unknown proteins.

Our mass spectrometry approach to isolate novel Rub conjugates is a relatively novel one for plants; hence we have provided advise to others interested in using our approach. We have identified a new possible RUB1 target in plants, DDB1a, a subunit of a CUL4-based ubiqutin ligase. The biological consequences of this modification remain unknown.

Through isolation of a mutation in Arabidosis CUL1 in a genertic screen, we show here that the interaction of CUL1 with RBX1 is important for the stability of CUL1. This viable line with impaired CUL1 function is a useful reagent to identify its potential substrates. Finally, we utilize our knowledge of monitoring proten degradation with LUC protein fusions to measure the degradation rate od AFR1, a transcription factor.

References Cited

Angers, S., Li, T., Yi, X., MacCoss, M.J., Moon, R.T. and Zheng, N. (2006) Molecular architecture and assembly of the DDB1-CUL4A ubiquitin ligase machinery. *Nature*, **443**, 590-593.

Capitani, G., McCarthy, D.L., Gut, H., Grutter, M.G. and Kirsch, J.F. (2002) Apple 1-Aminocyclopropane-1-carboxylate Synthase in Complex with the Inhibitor L-Aminoethoxyvinylglycine. *J. Biol. Chem.*, **277**, 49735-49742.

Choi, K.H. and Schweizer, H.P. (2005) An improved method for rapid generation of unmarked *Pseudomonas aeruginosa* deletion mutants. *BMC Microbiol.*, **5**, 30.

Clough, S.J. and Bent, A.F. (1998) Floral dip: a simplified method for *Agrobacterium*-mediated transformation of *Arabidopsis thaliana*. *Plant J.*, **16**, 735-743.

del Pozo, J.C., Dharmasiri, S., Hellmann, H., Walker, L., Gray, W.M. and Estelle, M. (2002) AXR1-ECR1-dependent conjugation of RUB1 to the Arabidopsis cullin AtCUL1 is required for auxin response. *Plant Cell*, **14**, 421-433.

del Pozo, J.C. and Estelle, M. (1999) The *Arabidopsis* cullin AtCUL1 is modified by the ubiquitin-related protein RUB1. *Proc. Natl. Acad. Sci. USA*, **96**, 15342-15347.

del Pozo, J.C., Timpte, C., Tan, S., Callis, J. and Estelle, M. (1998) The ubiquitin-related protein RUB1 and auxin response in Arabidopsis. *Science*, **280**, 1760-1763.

Dharmasari, N., Dharmasari, S., Weijers, D., Karunarathna, N., Jurgens, G. and Estelle, M. (2007) AXL and AXR1 have redundant functions in RUB conjugation and growth and development in Arabidopsis. *Plant J.*, **PMID: 17655650**

Dreher, K.A., Brown, J., Saw, R.E. and Callis, J. (2006) The Arabidopsis Aux/IAA protein family has diversified in degradation and auxin responsiveness. *Plant Cell*, **18**, 699-714.

Earley, K.W., Haag, J.R., Pontes, O., Opper, K., Juehne, T., Song, K. and Pikaard, C.S. (2006) Gateway-compatible vectors for plant functional genomics and proteomics. *Plant J.*, **45**, 616-629.

Feldman, R.M., Correll, C.C., Kaplan, K.B. and Deshaies, R.J. (1997) A complex of Cdc4p, Skp1p, and Cdc53p/cullin catalyzes ubiquitination of the phosphorylated CDK inhibitor Sic1p. *Cell*, **91**, 221-230.

Furukawa, M., Zhang, Y., McCarville, J., Ohta, T. and Xiong, Y. (2000) The CUL1 C-Terminal Sequence and ROC1 are Required for Efficient Nuclear Accumulation, NEDD8 Modification, and Ubiquitin Ligase Activity of CUL1. *Mol. Cell. Biol.*, **20**, 8185-8197.

Gray, W.M., del Pozo, J.C., Walker, L., Hobbie, L., Risseeuw, E., Banks, T., Crosby, W.L., Yang, M., Ma, H. and Estelle, M. (1999) Identification of an SCF ubiquitin-ligase complex required for auxin response in *Arabidopsis thaliana*. *Genes Dev.*, **13**, 1678-1691.

Gray, W.M., Hellmann, H., Dharmasiri, S. and Estelle, M. (2002) Role of the Arabidopsis RING-H2 protein RBX1 in RUB modification and SCF function. *Plant Cell*, **14**, 2137-2144.

Huang, D.T., Ayrault, O., Hunt, H.W., Taherbhoy, A.M., Duda, D.M., Scott, D.C., Borg, L.A., Neale, G., Murray, P.J., Roussel, M.F. and Schulman, B.A. (2009) E2-RING expansion of the NEDD8 cascade confers specificity to cullin modification. *Mol. Cell*, **33**, 483-495.

Huang, D.T., Walden, H., Duda, D. and Schulman, B.A. (2004) Ubiquitin-like protein activation. *Oncogene*, **23**, 1958-1971.

Jensen, O., Wilm, M., Shevchenko, A. and Mann, M. (1999) Sample preparation methods for mass spectrometric peptide mapping directly from 2-D gels. *Methods Mol Biol*, **112**, 513-530.

Jin, J., Li, X., Gygi, S.P. and Harper, J.W. (2007) Dual E1 activation systems for ubiquitin differentially regulate E2 enzyme charging. *Nature*, **447**, 1135-1138.

Keller, A., Nesvizhskii, A., Kolker, E. and Aebersold, R. (2002) Empirical statistical model to estimate the accuracy of peptide identifications made by MS/MS and database search. *Anal Chem*, **74**, 5383–5392.

Lammer, D., Mathias, N., Laplaza, J.M., Jiang, W., Lui, Y., Callis, J., Goebl, M. and Estelle, M. (1998) Modification of yeast Cdc53p by the ubiquitin-related protein Rub1p affects function of the SCF^{Cdc4} complex. *Genes Dev.*, **12**, 914-926.

Leyser, H.M.O., Lincoln, C.A., Timpte, C., Lammer, D., Turner, J. and Estelle, M. (1993) *Arabidopsis* auxin-resistance gene AXR1 encodes a protein related to ubiquitin-activating enzyme E1. *Nature*, **364**, 161-164.

Michelmore, R., Paran, I. and Kesseli, R. (1991) Identification of markers linked to disease-resistance genes by bulked segregant analysis: A rapid method to detect markers in specific genomic regions by using segregating populations. *Proc. Natl. Acad. Sci. USA*, **88**, 9828-9832.

Nakagawa, T., Kurose, T., Hino, T., Tanaka, K., Kawamukai, M., Niwa, Y., Toyooka, K., Matsuoka, K., Jinbo, T. and Kimura, T. (2007) Development of series of gateway binary vectors, pGWBs, for realizing efficient construction of fusion genes for plant transformation. *J Biosci Bioeng*, **104**, 34-41.

Nesvizhskii, A., Keller, A., Kolker, E. and Aebersold, R. (2003) A statistical model for identifying proteins by tandem mass spectrometry. *Anal Chem*, **75**, 4646-4658.

Nishikawa, H., Ooka, S., Sato, K., Arima, K., Okamoto, J., Klevit, R.E., Fukuda, M. and Ohta, T. (2004) Mass spectrometric and mutational analyses reveal Lys-6-linked polyubiquitin chains catalyzed by BRCA1-BARD1 ubiquitin ligase. *J Biol Chem*, **279**, 3916-3924.

Park, Y., Yoon, S.K. and Yoon, J.B. (2008) TRIP12 functions as an E3 ubiquitin ligase of APP-BP1. *Biochem Biophys Res Commun*, **374**, 294-298.

Quint, M., Ito, H., Zhang, W. and Gray, W.M. (2005) Characterization of a novel temperature-sensitive allele of the *CUL1/AXR6* subunit of the SCF ubiquitin ligase. *Plant J.*, **43**, 371-383.

Rao-Naik, C., Delacruz, W., Laplaza, J.M., Tan, S., Callis, J. and Fisher, A.J. (1998a) The Rub family of proteins: crystal structure of Arabidopsis RUB1 and expression of multiple RUBs in Arabidopsis. *J Biol Chem*, **273**, 34976-34982.

Rao-Naik, C., delaCruz, W., Laplaza, J.M., Tan, S., Callis, J. and Fisher, A.J. (1998b) The Rub Family of Ubiquitin-like Proteins. *J. Biol. Chem.*, **273**, 34976-34982.

Salmon, J., Ramos, J. and Callis, J. (2008) Degradation of the auxin response factor ARF1. *Plant J*, **54**, 118-128.

Schaller, G.E. and Kieber, J.J. (2002a) Ethylene. *The Arabidopsis Book*, 1-18.

Schaller, G.E. and Kieber, J.J., Eds. (2002b). Ethylene (September 30, 2002). The Arabidopsis Book. Rockville, MD, doi/10.1199/tab.0071, http://www.aspb.org/publications/arabidopsis/, American Society of Plant Biologists.

Scholes, D.T., Banerjeea, M., Bowena, B. and Curcio, M.J. (2001) Multiple Regulators of Ty1 Transposition in Saccharomyces cerevisiae Have Conserved Roles in Genome Maintenance. *Genetics*, **159**, 1449-1465.

Smalle, J. and Vierstra, R.D. (2004) The ubiquitin 26S proteasome proteolytic pathway. *Annu. Rev. Plant Biol.*, **55**, 555-590.

Vandenbussche, F., Vriezen, W.H., Smalle, J., Laarhoven, L.J., Harren, F.J. and Van Der Straeten, D. (2003) Ethylene and auxin control the Arabidopsis response to decreased light intensity. *Plant Physiol.*, **133**, 517-527.

Vinatzer, B.A., Teitzel, G.M., Lee, M.W., Jelenska, J., Hotton, S., Fairfax, K., Jenrette, J. and Greenberg, J.T. (2006) The type III effector repertoire of Pseudomonas syringae pv. syringae B728a and its role in survival and disease on host and non-host plants. *Molecular Microbiology*, **62**, 26-44.

Wada, H., Yeh, E.T. and Kamitani, T. (1999) Identification of NEDD8-conjugation site in human cullin-2. *Biochem. Biophy. Res. Comm.*, **257**, 100-105.

Waterhouse, P.M., Wang, M.-B. and Lough, T. (2001) Gene silencing as an adaptive defense against viruses. *Nature*, **411**, 834-842.

Weber, H., Bernhardt, A., Dieterle, M., Hano, P., Mutlu, A., Estelle, M., Genschik, P. and Hellmann, H. (2005) Arabidopsis AtCUL3a and AtCUL3b form complexes with members of the BTB/POZ-MATH protein family. *Plant Physiol.*, **137**, 83-93.

Zenser, N., Dreher, K.A., Edwards, S.R. and Callis, J. (2003) Acceleration of Aux/IAA proteolysis is specific for auxin and independent of AXR1. *Plant J.*, **35**, 285-294.

Zheng, N., Schulman, B.A., Song, L.Z., Miller, J.J., Jeffrey, P.D., Wang, P., Chu, C., Koepp, D.M., Elledge, S.J., Pagano, M., Conaway, R.C., Conaway, J.W., Harper, J.W. and Pavletich, N.P. (2002) Structure of the Cul1-Rbx1-Skp1-F box^{Skp2} SCF ubiquitin ligase complex. *Nature*, **416**, 703-709.

List of Acronyms and Abbreviations

ACC 1-aminocyclopropane-1-carboxylic acid
ACO ACC-oxidase
ACS ACC SYNTHASE
ARF AUXIN RESPONSE FACTOR
AVG Aminoethoxyvinylglycine
AXL AXR1-LIKE
AXR AUXIN RESISTANT
Cdc Cell Division Cycle
CUL CULLIN
Dex dexamethasone
DDB DNA DAMAGE BINDING
ECR E1-like C-terminal Related
ENR E1 N-terminus Related
GG Glycine-glycine
HA hemaglutinin peptide sequences from human influenza hemagglutinin protein (YPYDVPDYA)
K lysine residue of protein
LC liquid chromatography
LUC luciferase
MS mass spectrometry
PAGE polyacrylamide gel electrophoresis
R arginine residue of protein
RBX RING BOX
RCE RUB Conjugating Enzyme
RUB RELATED TO UBIQUITIN
Nedd8 Neuronally Expressed Developmentally Down-regulated 8
Rtt101 Regulator of Ty1 Transposition
SDS sodium dodecyl sulfate
UBA ubiquitin activating enzyme
UBE ubiquitin E2 enzyme

List of Figures and Tables. Each Figure and Table is on a single page that follows this list.

Tables

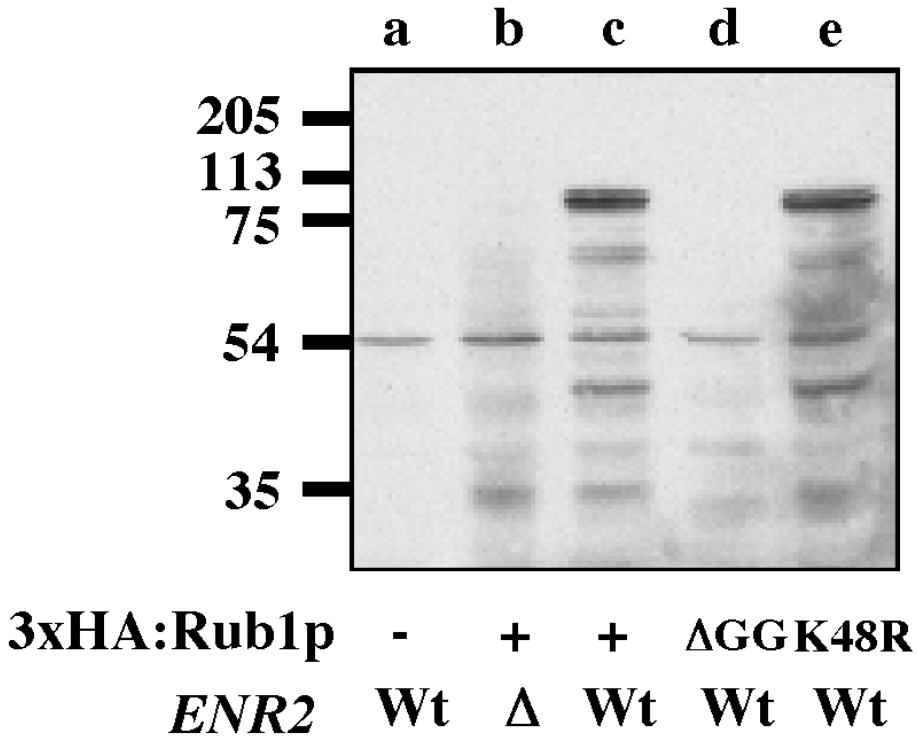

Figure 1. Multiple proteins covalently attached to 3xHA:Rub1p can be detected by SDS-PAGE and western blotting with anti-HA Ab, and require Enr2p, the Rub1p activating enzyme.

Protein extracts from yeast strains (a) *rubΔ*; (b) *enr2Δ rubΔ* expressing 3xHA:Rub1p; (c) *rubΔ* expressing 3xHA:Rub1p; (d) *rubΔ* expressing 3xHA:Rub1pΔGG, lacking the 2 C-terminal Rub1p amino acids; and *rubΔ* expressing 3xHA:Rub1pK48R, with lysine-48 substituted with arginine.

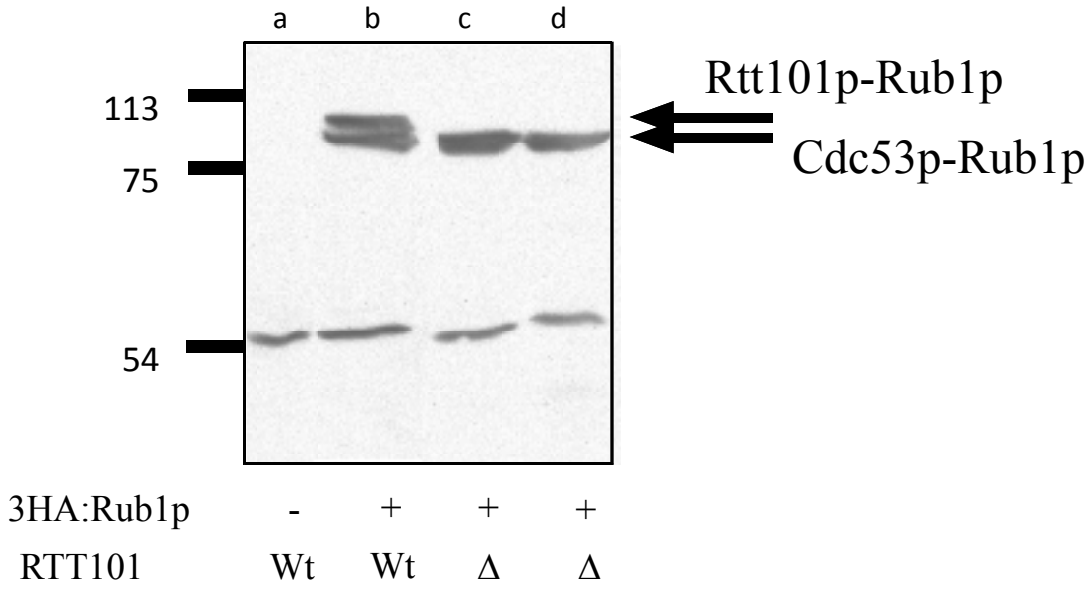

Figure 2. Deletion of Rtt101p loses a Rub1p conjugate.

3xHA:Rub1p was expressed in a wt strain or a strain deleted for Rtt101p. Extracts were Fractionated by SDS-PAGE and HA-tagged Rub1p visualized with anti-HA western blot analysis.

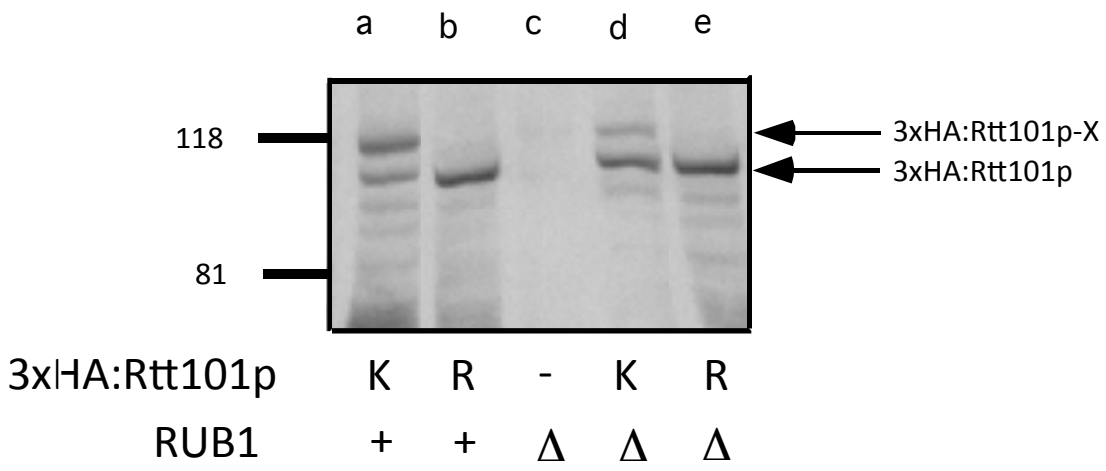

Figure 3. Rtt101p exists as two electrophoretic forms, the slower migrating form is reduced in rub deletion srain and lost when the K791 was changed to arginine, an amino acid that cannot be rubylated or ubiquitinated.

3xHA:Rtt101p was expressed in wt (+, lane a) or in a strain deleted for Rubp1 (lane d). A form of Rtt101p with arginine substituted for lysine 791 was expressed in the same two strains; in wt (+, lane b) or in a strain deleted for Rubp1 (lane e). Lane c is the rub deletion strain alone, lacking the expression plasmid.

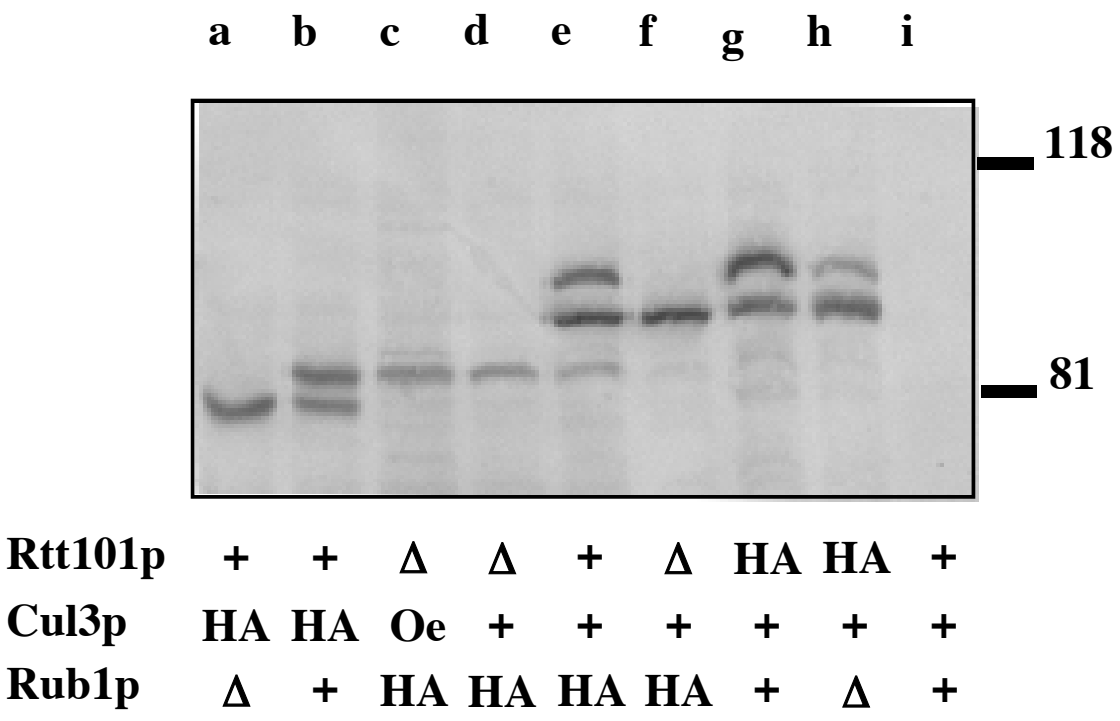

Figure 4. Cul3p and Rtt101p are Rub1p conjugates in yeast.

These experiments were conducted in a yeast strains disrupted in specific genes. s was also deleted (lane a and h) or Rtt101p (lanes c,d and f) background expressing Cdc53K760Rp, a form of Cdc53 that cannot be rubylated. In this strain were introduced plasmids expressing epitope-tagged forms of Cul3p (lanes a,b), Rub1p (lanes c-f) or Rtt101p (lanes g-h). Proteins were extracts, separated by SDS-PAGE, and visualized with anti-HA Ab. In this background, RUB.

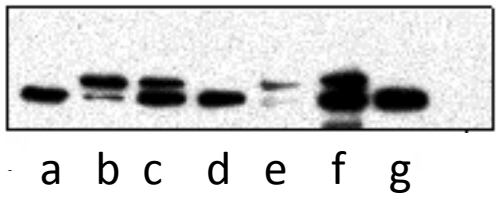

Figure 5. Plant RUB1, but not RUB3, covalently attach to yeast Cdc53p *in vivo* in yeast.

A *rub* deletion strain expressing HA-tagged Cdc53p was transformed with a plasmid expressing either (a) no protein; (b) yeast Rub1p; (c) plant RUB1 (cDNA from *Brassica napus* identical to AtRUB1; (d) AtRUB3; (e) HA:Rub1p; (f) HA:RUB1; (g) HA:RUB3.

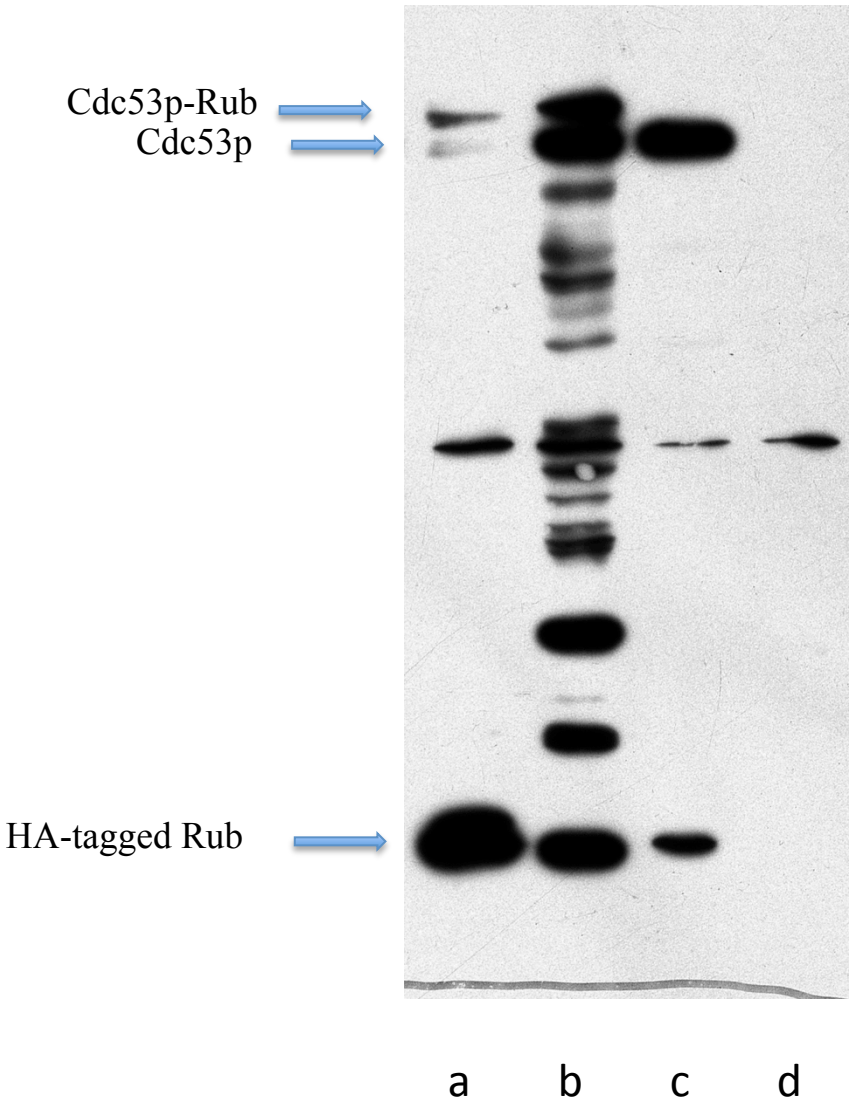

Figure 6. Expression of plant RUB1, but not plant RUB3, in yeast results in RUB1 conjugation to a large number of proteins.

A *rub* deletion strain expressing HA-tagged Cdc53p was transformed with a plasmid expressing either (a) yeast Rub1p; (b) plant HA:RUB1 (cDNA from *Brassica napus* identical to AtRUB1; (c) AtHA:RUB3; (d) no protein

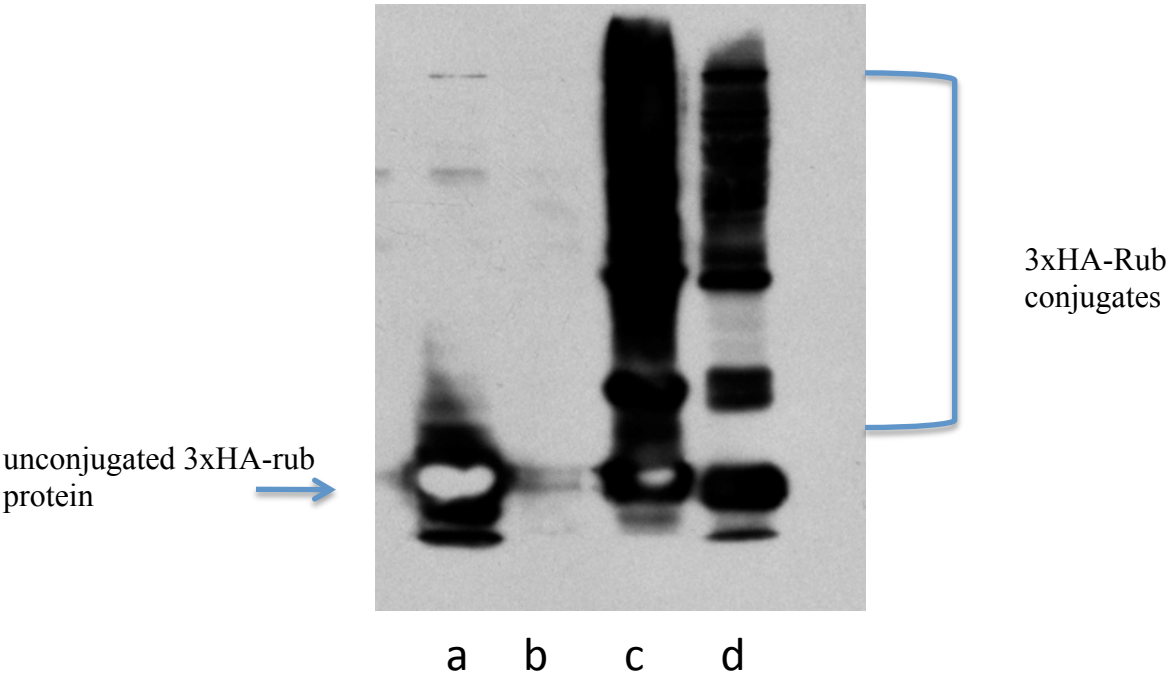

Figure 7. The C-terminal half of Plant RUB is sufficient for conjugation via both the ubiquitin pathway and the RUB pathway.

Yeast strains over-expressing (a) yeast 3xHA:Rub1p; (b)plant 3xHA:AtRUB1; (b) chimera of 3xHA:NAtRUB1-CScRub1p; (c) opposite chimera of 3xHA:NRubp1-CAtRUB1; and (d) plant 3xHA:AtRUB1.

Protein extracts were separated by SDS-PAGE and anti-HA proteins visualized by western blotting.

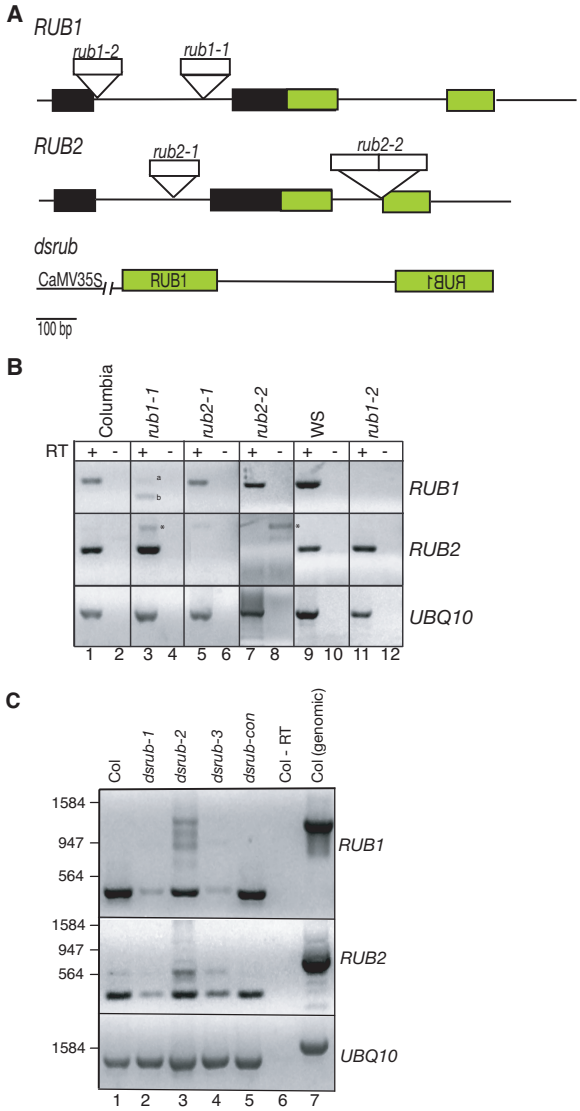

Figure 8. Authentic *RUB1* and *RUB2* mRNAs are eliminated in T-DNA insertional lines and reduced in *dsrub* lines.

(A) Genomic representations of *RUB1* and *RUB2* and the *dsrub construct*. Introns are lines and exons are boxes; shaded boxes are RUB1 or RUB2 protein, black boxes are ubiquitin, and open boxes are T-DNA (not to scale). *dsrub* lines were created with a construct containing the RUB1 ORF in opposite directions, separated by an intron, under transcriptional control of the CaMV (Cauliflower Mosaic Virus) 35S promoter. **(B)** RT-PCR for *RUB1*, *RUB2*, and *UBQ10* (polyubiquitin) with cDNA from Col (lanes 1, 2), *rub1-1* (lanes 3, 4), *rub2-1* (lanes 5, 6), *rub2-2* (lanes 7, 8), WS (lanes 9, 10), and *rub1-2* (lanes 11, 12) seedlings. Asterisks (*) indicate genomic PCR band for *RUB2*. "a" and "b" are splice variants. Odd numbered lanes contain PCR reactions from cDNA using reverse transcriptase, while even numbered lanes contain PCR reactions with no reverse transcriptase. **(C)** RT-PCR with total RNA from Col (lane 1), *dsrub-1* (lane 2), *dsrub-2* (lane 3), *dsrub-3* (lane 4), and the transgenic control line, *dsrub-con*, (lane 5) using primers for *RUB1* (top panel), *RUB2* (middle panel), and *UBQ10* (bottom panel). Lane 6 is identical to lane 1, except reverse transcriptase was not included. PCR using the same primers on Col genomic DNA is shown in lane 7. The numbers indicate size markers in basepairs.

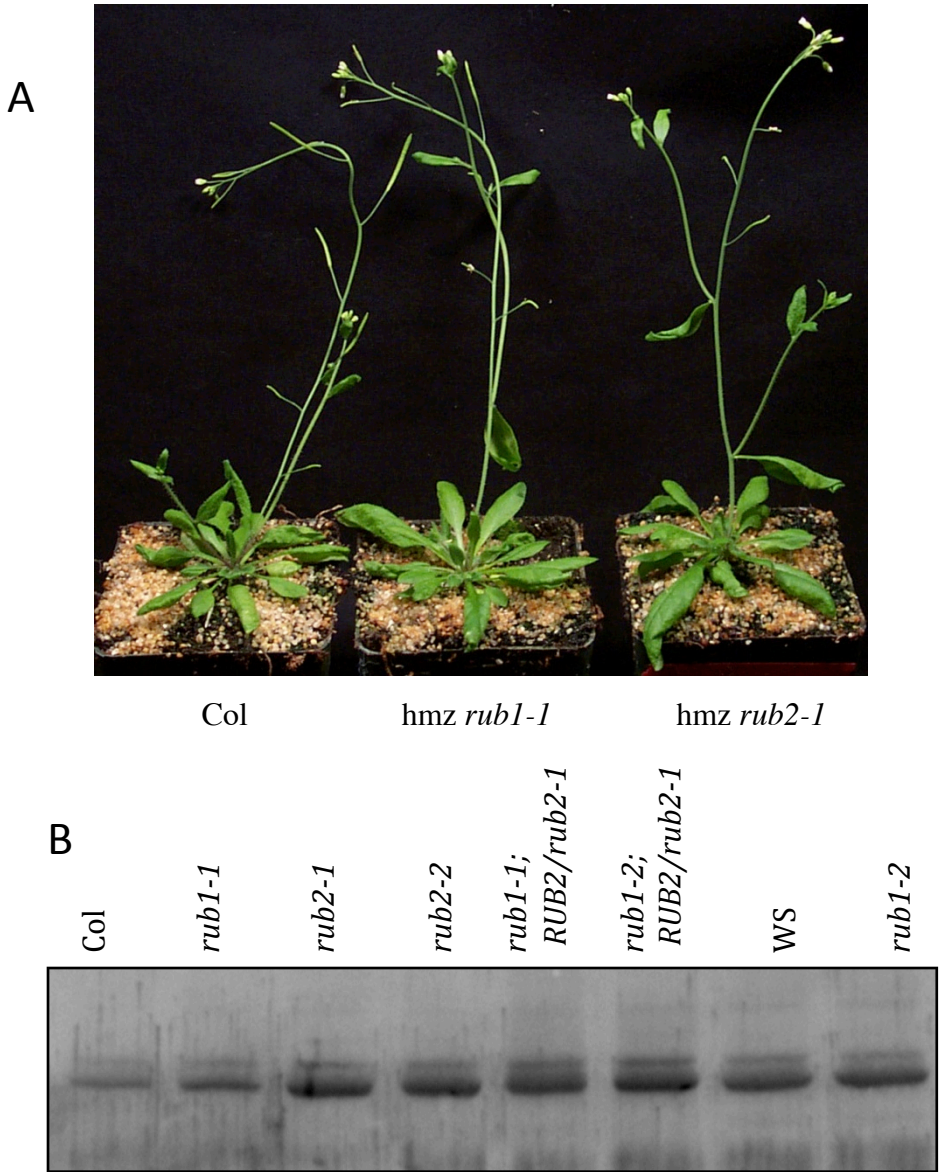

Figure 9. The single *RUB1* and *RUB2* null lines have a wild-type phenotype.

(A) The *rub1* and *rub2* lines have a wild-type phenotype. Col, *rub1-1*, and *rub2-1* lines after four backcrosses at 6 weeks old (left to right). **(B)** The conjugation pattern of AtCUL1 is not affected by disruptions in RUB1 or RUB2. An anti-AtCUL1 western blot with 50 mg of total plant extracts from wild type Col (lane 1) or WS (lane 7); single mutants *rub1-1* (lane 2), *rub1-2* (lane 8), *rub2-1* (lane 3) and *rub2-2* (lane 4); and sesquimutants *rub1-1RUB2/rub2-1* (lane 5) and *rub1-2 RUB2/rub2-1* (lane 6).

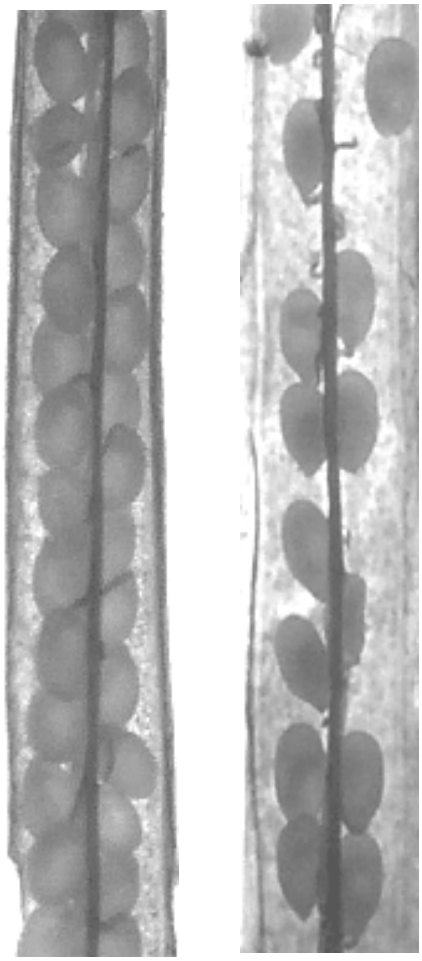

Figure 10. Embryos do not develop in *rub1 rub2* background.

Fully developed siliques from *RUB1 rub2* (left), and *RUB1/rub1-1 rub2* (right) parent that naturally self.

Empty spaces indicate embryo death. A single *RUB1* or *RUB2* gene is sufficient, but loss of both leads to embryo death.

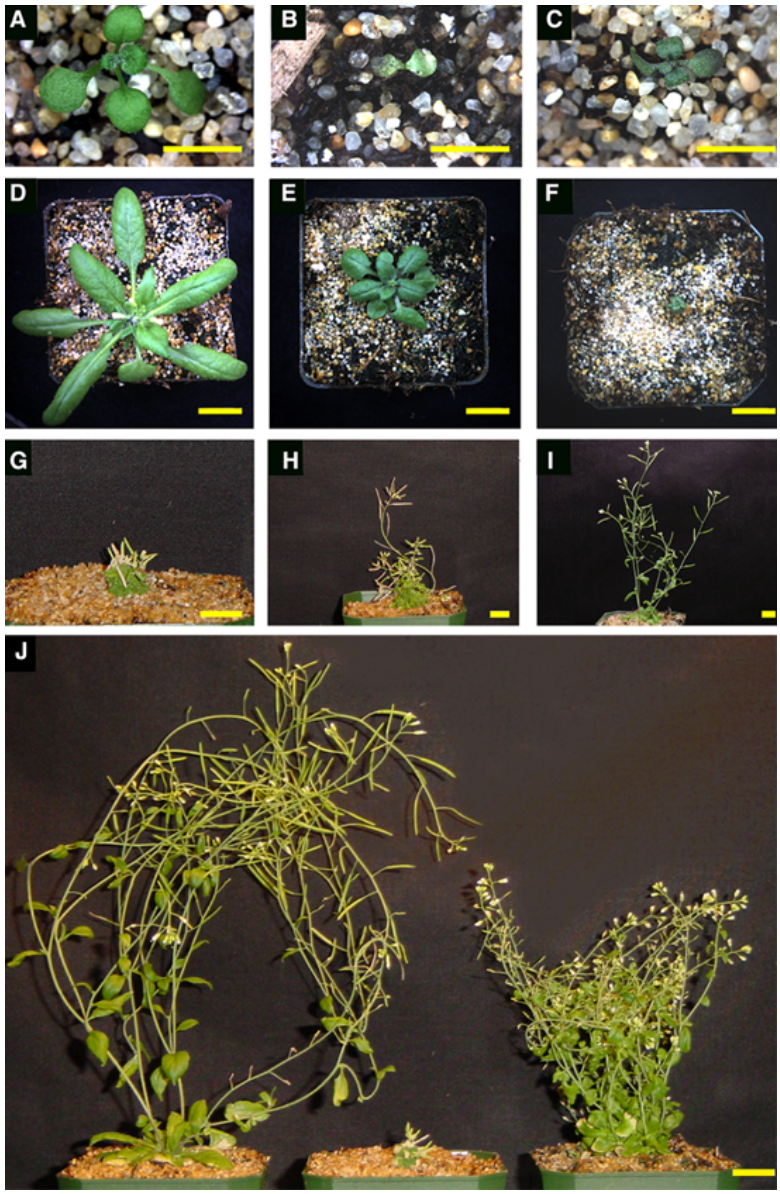

Figure 11. Growth of *dsrub* plants is slower and overall size is severely reduced.

(A-C) Seedlings at 3 weeks: **(A)** Col; **(B)** *dsrub-4*; and **(C)** *dsrub-5*. Scale Bar = 0.5 cm.
(D-E) Plants at 5 weeks: **(D)** Col; **(E)** *dsrub-6*; and **(F)** *dsrub-5*. Scale Bar = 1.0 cm.
(G-I) Plants at 8 weeks: **(G)** *dsrub-3*; **(H)** *dsrub-1*; and **(I)** *dsrub-2*. Scale Bar = 1.0 cm.
(J) Col (left), *dsrub-3* (middle), and *axr1-13* (right) at 8 weeks. Scale Bar = 2.0 cm.

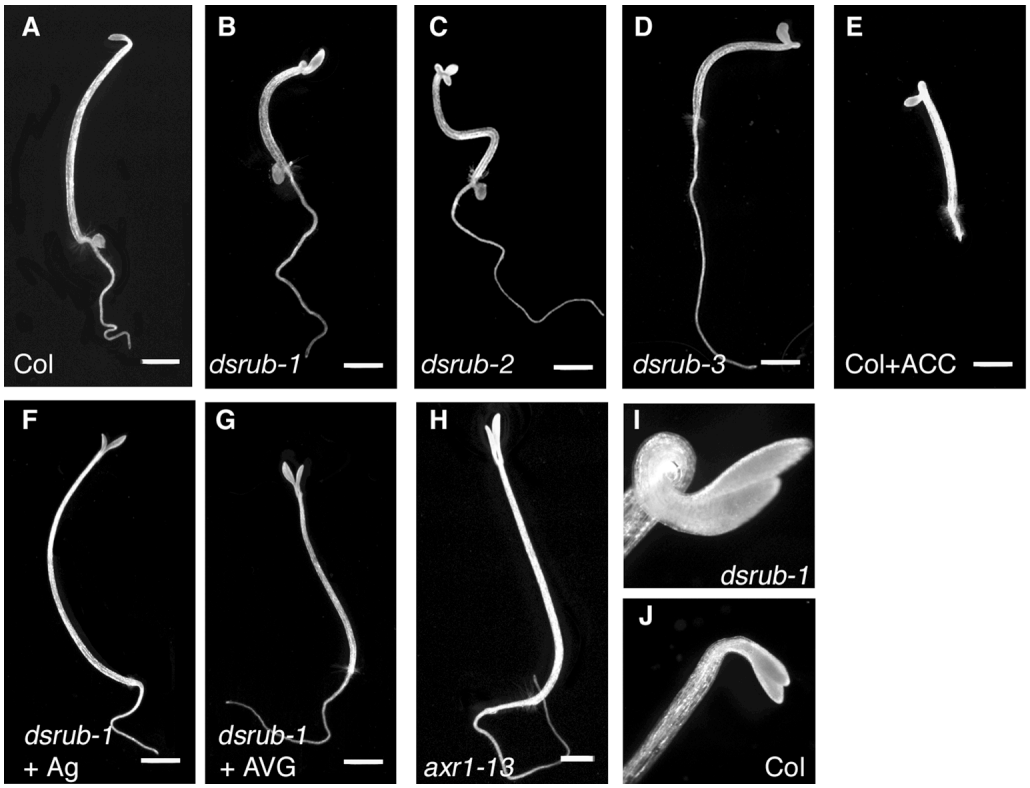

Figure 12. 4-day-old, dark-grown *dsrub* seedlings exhibit a partial triple response that is reversed by inhibitors of the ethylene pathway.

Seedlings after germination on GM plates **(A)** Col, **(B)** *dsrub-1*, **(C)** *dsrub-2*, **(D)** *dsrub-3*, and **(H)** *axr1-13*; **(E)** Col on GM with 50 mM ACC; **(F)** *dsrub-1* on GM with 100 mM $AgNO_3$; **(G)** *dsrub-1* on GM with 5 mM AVG. Scale Bar = 1 mm. The apical hook of **(I)** *dsrub-1* and **(J)** Col is magnified.

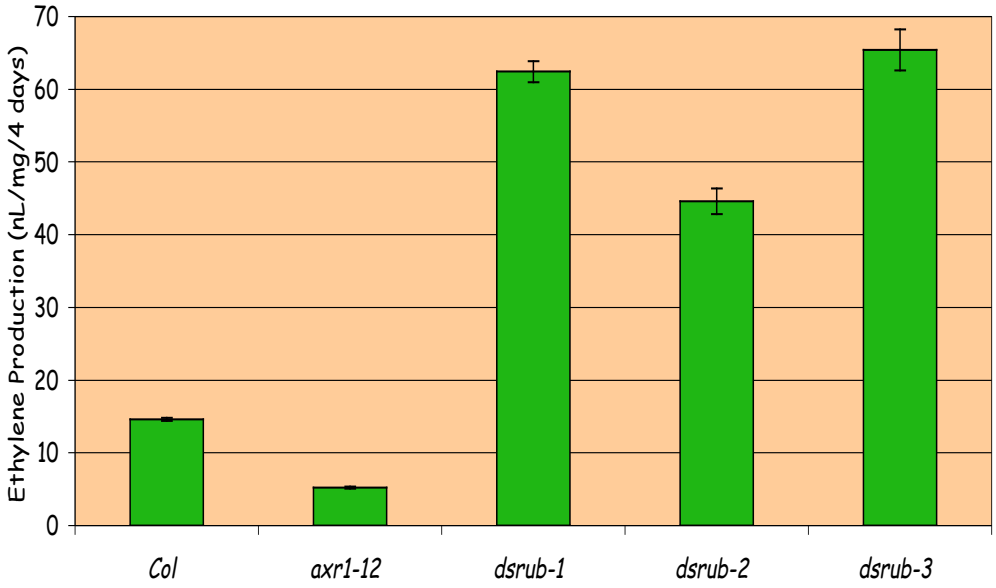

Figure 13. Dark-grown *dsrub* seedlings overproduce ethylene.

Col, *axr1-13*, *dsrub-1*, *dsrub-2*, and *dsrub-3* seedlings were germinated and grown in gas chromatography vials for four days. The amount of ethylene (nL) produced per fresh weight of seedlings (mg) is indicated as the mean +/- SE of triplicate injections from at least three experiments. All lines are statistically different from Col (student's t-test; $P < 0.001$).

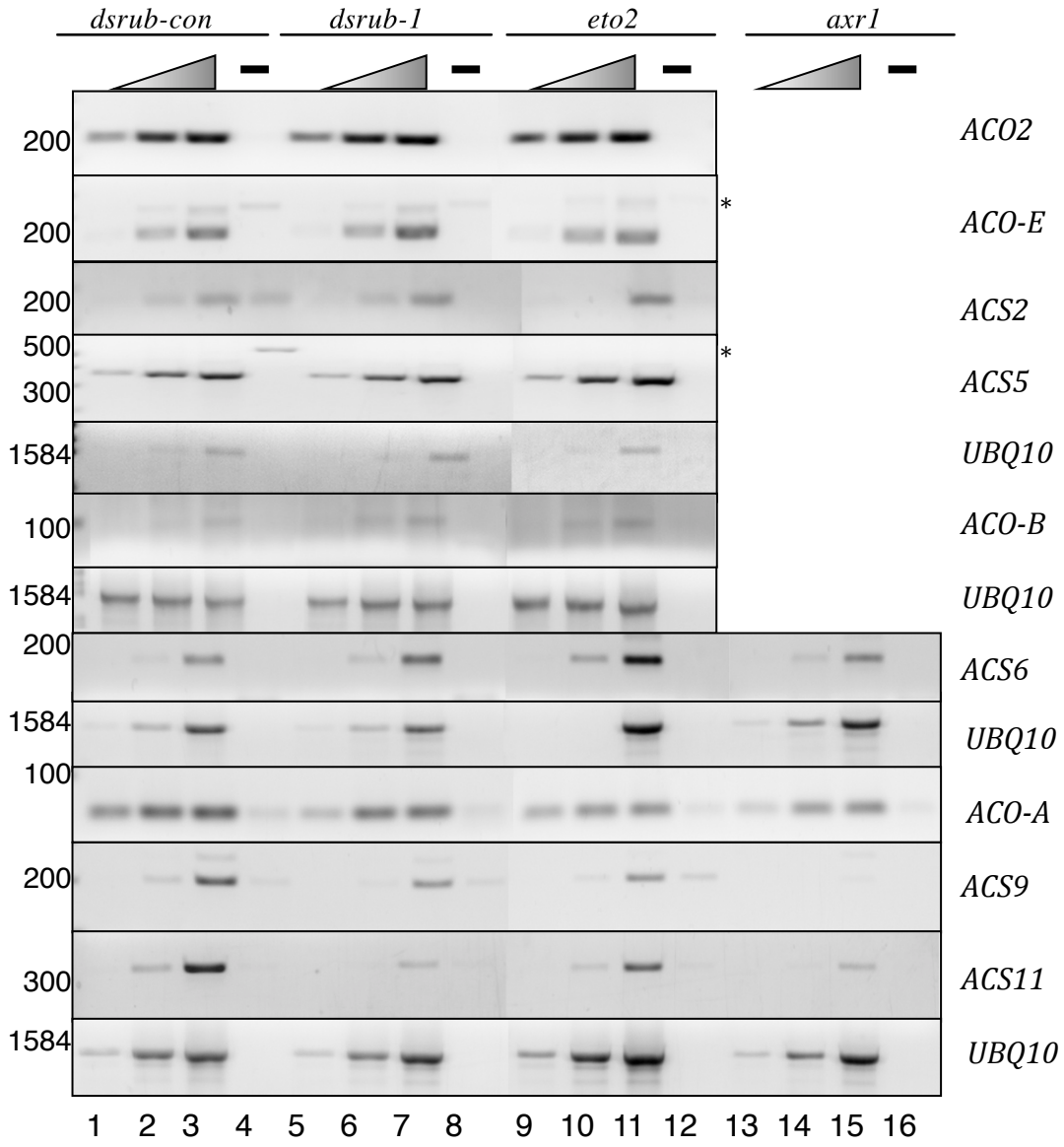

Figure 14. Small changes in *ACS* and *ACO* transcripts are observed in *dsrub-1*, *eto2*, and *axr1-12* lines.

PCRs using primers specific for the genes indicated on the right. Increasing numbers of cycles for the PCR using cDNA made from dark-grown seedlings of the indicated genotype: *dsrub-con* (lanes 1-4), *dsrub-1* (lanes 5-8), *eto2* (lanes 9-12), and *axr1-12* (lanes 13-16). The dashed line represents samples without RT added (lanes 4, 8, 12, and 16). Markers are indicated on the left in base pairs. Genomic bands are represented by asterisks. Different preparations of RNA and cDNA were used and a *UBQ10* PCR is below each unique set of cDNA preparations for loading controls.

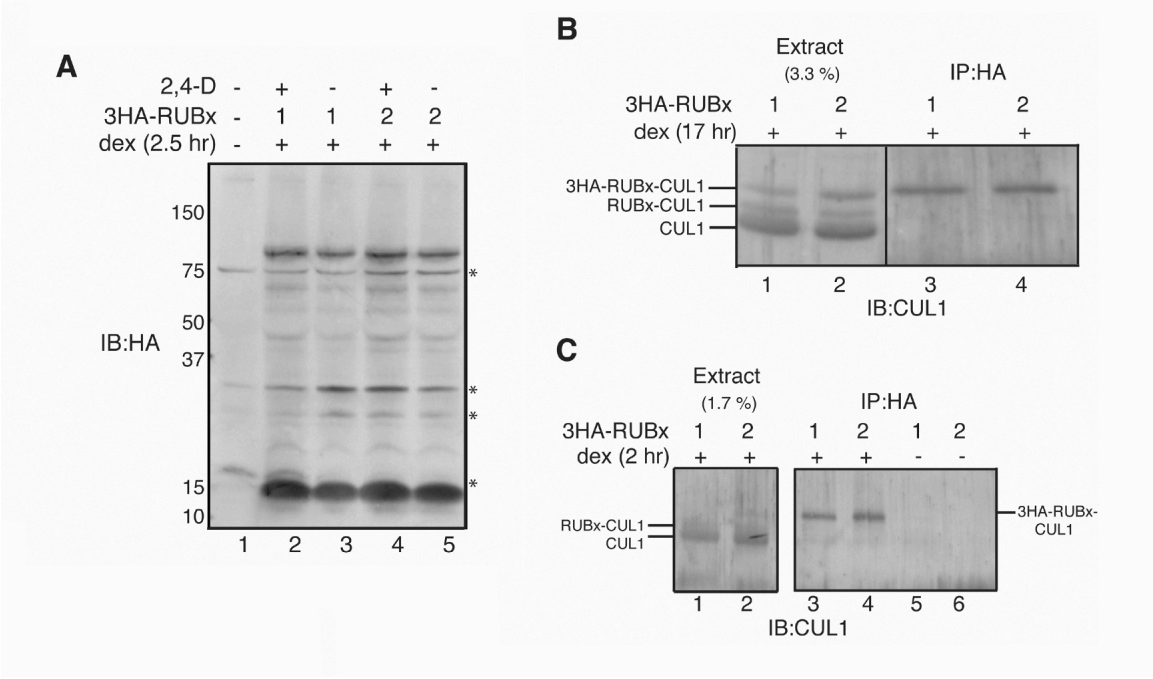

Figure 15. 3HA-RUB1 and 3HA-RUB2 attach to the same proteins.

(A) Dex-induced expression of 3HA-RUB1 and 3HA-RUB2 in seedlings has the same conjugation pattern and is unchanged by auxin treatment. Total plant extract (80 mg) from seedlings expressing 3HA-RUB1 (lanes 2, 3) or 3HA-RUB2 (lanes 4, 5) treated with 10 mM 2,4-D (lanes 2, 4) or mock-treated (lanes 3, 5) for 30 minutes was reacted with anti-HA antibodies. Background bands (marked with an asterisks) are determined by electrophoresis of extract from untreated, Col seedlings (lane 1). The numbers indicate size markers in kiloDaltons. **(B)** Expression of 3HA-RUB1 and 3HA-RUB2 at high levels leads to CUL1 existing in three forms. Immunoblot (IB) with anti-CUL1 antibodies of extracts from seedlings treated with dex to express 3HA-RUB1 (lane 1) or 3HA-RUB2 (lane 2) for seventeen hours illustrates the unmodified, (fastest band), RUBx-modified (middle band), and 3HA-RUBx-modified (slowest band) forms of CUL1. Samples eluted from anti-HA antibody conjugated beads after incubation in extracts from seedlings dex treated to express 3HA-RUB1 (lane 3) or 3HA-RUB2 (lane 4) for seventeen hours immuno-reacted with anti-CUL1 antibodies creating a band that co-migrated with the slowest band from extracts (lanes 1 and 2). **(C)** 3HA-RUB1 and 3HA-RUB2 attach to CUL1 in a dex-dependent manner. Samples eluted from anti-HA antibody-conjugated beads after incubation in extracts from seedlings dex- or mock-treated for 2 hours to express 3HA-RUB1 (lanes 3 and 5) or 3HA-RUB2 (lanes 4 and 6) seedlings still maintain a CUL1 band, in a dex-dependent manner. The conjugate pattern of CUL1 in the lines expressing the 3HA-RUBx dex-induced for two hours is limited to only two bands (lanes 1 and 2).

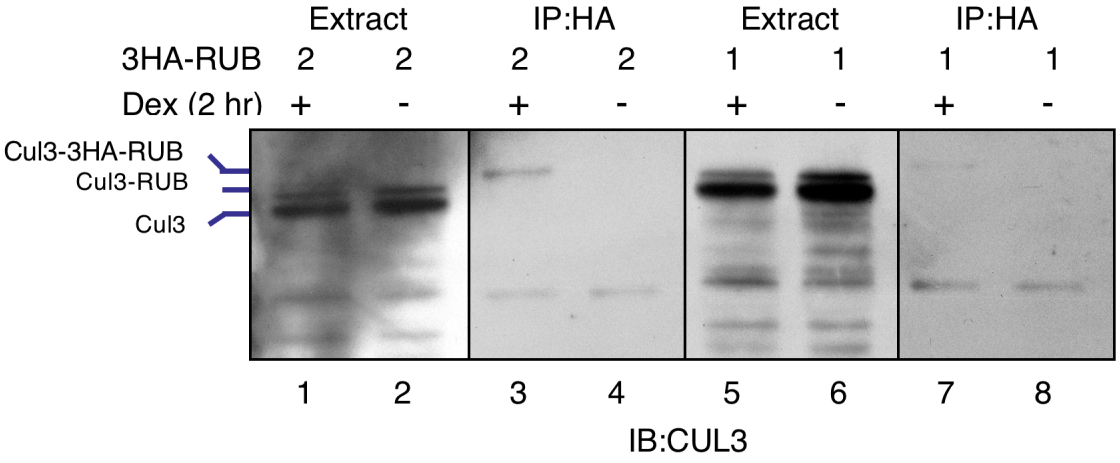

Figure 16. 3HA-RUB1 and 3HA-RUB2 attach to Arabidopsis CULLIN 3, CUL3.

An anti-CUL3 immunoblot was used to visualize the conjugation state of CUL3 in extracts (lanes 1-2, 5-6), and it was unchanged by a two hour induction of 3HA-RUB2 (lane 1) or 3HA-RUB1 (lane 5) with an unconjugated form and a modified form visible. A CUL3 immunoblot was also used to confirm that CUL3 is immunoprecipitated by 3HA-RUB2 (lanes 3, 4) and 3HA-RUB1 (lanes 7, 8) in a dex-dependent manner.

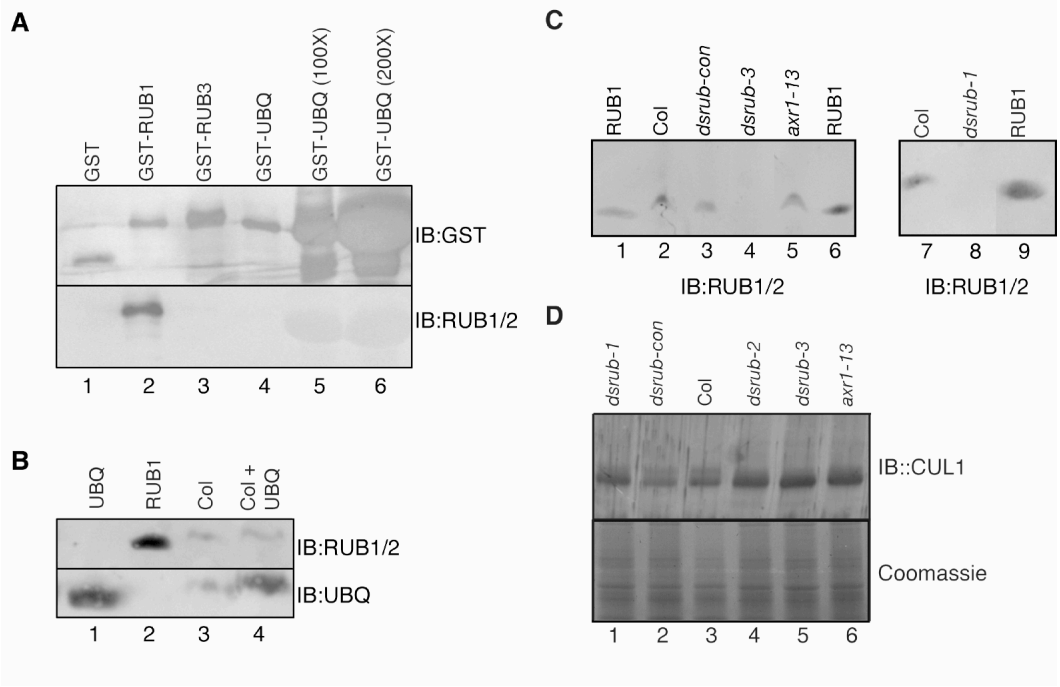

Figure 17. RUB1/2 affinity-purified antibodies specifically react with GST-RUB1.

Immunoblot (IB) of purified GST (lane 1) and GST fusion proteins: GST-RUB1 (lane 2), GST-RUB3 (lane 3), and GST-UBQ (lane 4) probed with affinity-purified anti-RUB1/2 antibodies (lower panel). The antibodies were also tested on 100X (lane 5) and 200X (lane 6) GST-UBQ. An anti-GST IB (upper panel) verifies protein levels (lane 6 has 400X GST-UBQ). (B) Affinity-purified anti-RUB1/2 antibodies show specificity against whole plant extract. Immunoblot analysis of purified ubiquitin (UBQ) (lane 1), purified RUB1 (lane 2), Col protein extract (lane 3), and Col protein extract enriched with purified ubiquitin (lane 4). The anti-RUB1/2 antibodies (upper panel) detect endogenous RUB1/2 protein and the anti-ubiquitin antibodies (lower panel) verify the presence of purified ubiquitin, as well as visualizing endogenous ubiquitin in Col extract (lane 3). (C) Immunoblot with anti-RUB1/2 antibodies on 200 mg of total protein extracted from Col (lane 2, 7), *dsrub-con* (lane 3), *dsrub-3* (lane 4), *axr1-13* (lane 5), and *dsrub-1* (lane 8). Purified RUB1 is used as a positive control (lanes 1, 6, 9). Lane 7 contains half the protein as lane 8. (D) The *dsrub* lines have a decreased level of CUL1-RUBx conjugate. Immunoblot with anti-CUL1 antibodies of extracts from seedlings of control lines, Col (lane 3) and *dsrub-con* (lane 2), *dsrub-1* (lane 1), *dsrub-2* (lane 4), *dsrub-3* (lane 5), and *axr-13* (lane 6). Coomassie stain of identically loaded samples serves as a loading control (lower panel).

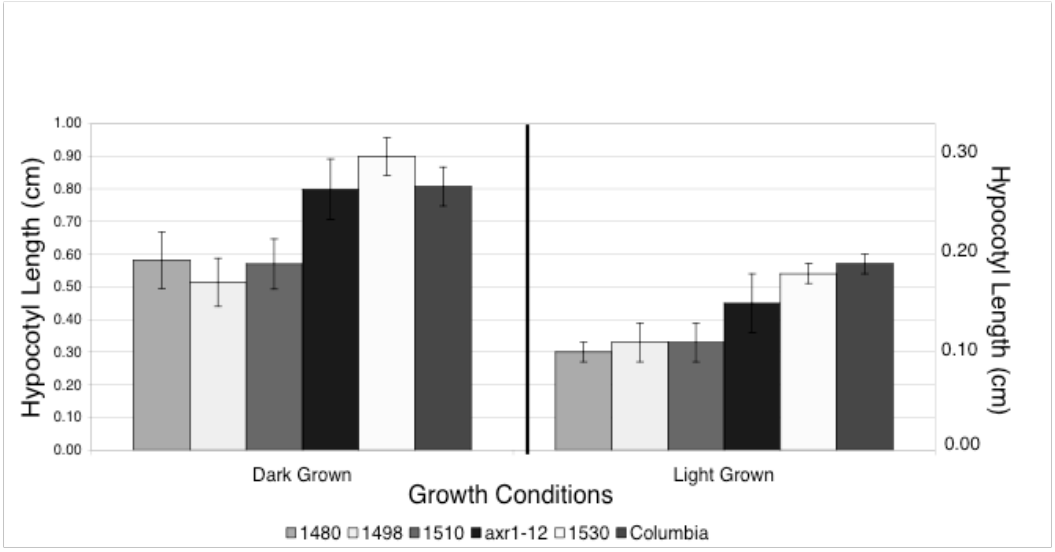

Figure 18. Hypocotyl length is reduced in *dsrub* plants from reduced cell expansion.

The height of dark (left) and light (right) grown 4-day-old seedlings from three *dsrub* lines (*dsrub-2*, *dsrub-3*, and *dsrub-1*) is compared to *axr1-13*, *dsrub-con*, and Col. Bars are mean + sd. Line 1530 is the *dsrub-con* control line.

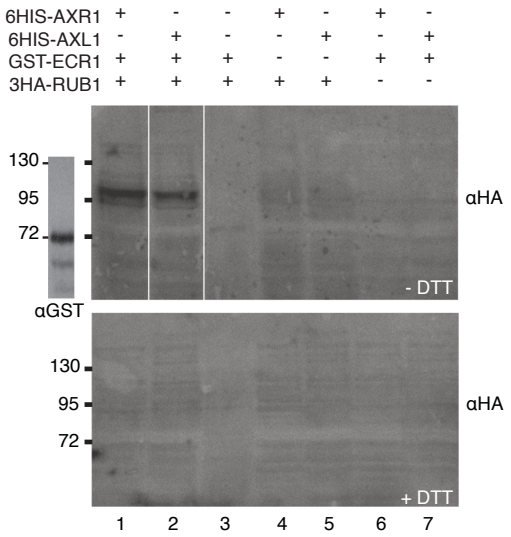

Figure 19. AXL1 catalyzes RUB1-ECR1 thioester formation like AXR1.

In vitro thioester assays with recombinant 6HIS-AXR1, 6HIS-AXL1, GST-ECR1, and 6HIS-3HA-RUB1 are shown. An anti-GST blot of purified GST-ECR1 at 72 kDa is included for reference. Anti-HA immunoblot analysis detected 3HA-RUB1--GST-ECR1 thioester formation under non-reducing conditions (-DTT) only, catalyzed by AXR1 (lane 1), or by AXL1 (lane 2). Lanes 3-7 for both upper and lower panels show reactions lacking AXL1 and AXR1 (lane 3), ECR1 (lanes 4 and 5), or RUB1 (lanes 6 and 7), as negative controls. All reactions were stopped under non-reducing (-DTT, upper panel) or reducing (+DTT, lower panel) conditions and separated by non-reducing SDS-PAGE. White spaces represent positions where unnecessary lanes were removed, or where lanes were moved for alignment purposes. Size markers are in kDa.

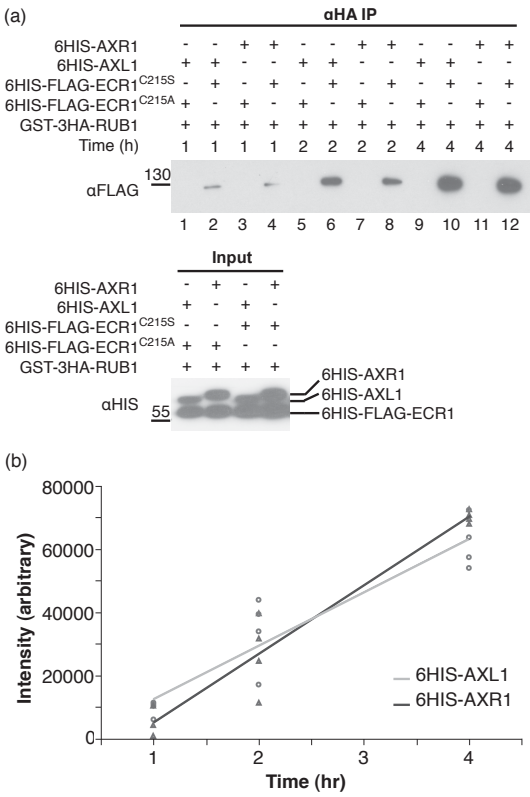

Figure 20. AXL1 and AXR1 have similar biochemical activities in vitro.

(a) Time course for various oxyester assays with recombinant 6HIS-AXR1, 6HIS-AXL1, 6HIS-FLAG-ECR1^{C215S}, 6HIS-FLAG-ECR1^{C215A}, and GST-3HA-RUB1. After anti-HA immunoprecipitation, anti-FLAG immunoblot analysis was used to detect GST-3HA-RUB1--6HIS-FLAG-ECR1^{C215S} oxyester formation, catalyzed by AXL1 (lanes 2, 6, 10), or by AXR1 (lanes 4, 8, 12), for various lengths of time. As a negative control, parallel reactions were done with the catalytic mutant ECR1^{C215A} and AXL1 (lanes 1, 5, 9) or AXR1 (lanes 3, 7, 11). Input (fraction of total for each sample, removed prior to start of time course) was checked with anti-HIS immunoblot to verify addition of 6HIS-AXL1, 6HIS-AXR1, 6HIS-FLAG-ECR1^{C215S}, and 6HIS-FLAG-ECR1^{C215A}. Size markers are in kDa. (b) GST-3HA-RUB1--6HIS-FLAG-ECR1^{C215S} band intensity plotted against time, comparing catalytic activity of AXL1 (circles) and AXR1 (triangles) for n = 4 replicates. Regression lines for AXL1 (light gray) and AXR1 (dark gray) are included. At $\alpha = 0.05$, testing for an E1*time interaction is not significant (factorial ANOVA, $p = 0.0755$).

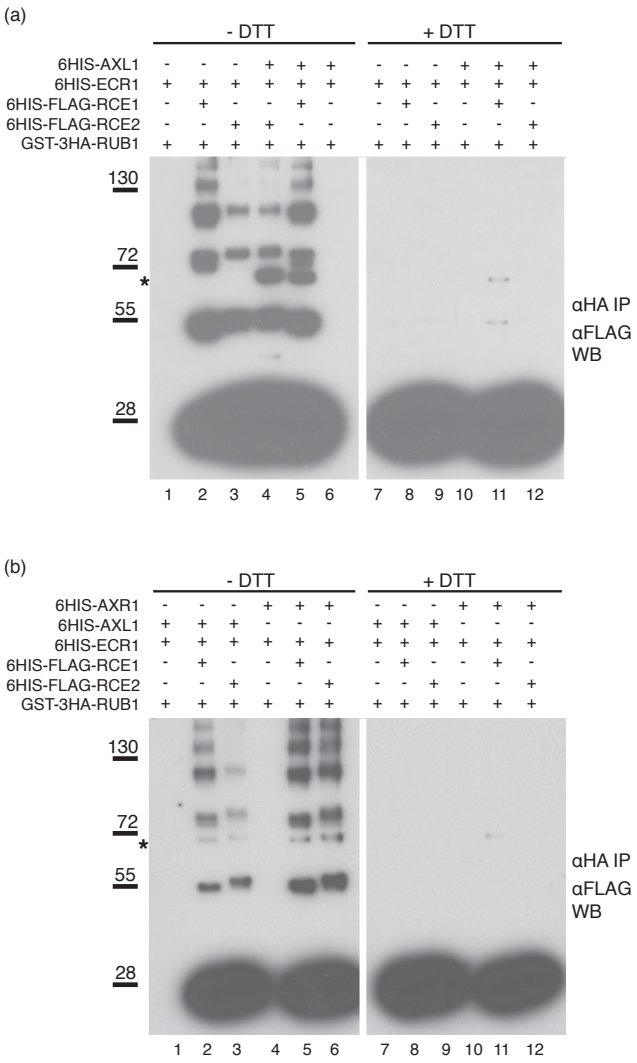

Figure 21. AXR1/ECR1 and AXL1/ECR1 both transfer activated RUB1 to RCE1 and RCE2 by a trans-thioesterfication reaction.

In vitro thioester assays with 6HIS-AXR1, 6HIS-AXL1, 6HIS-ECR1, and GST-3HA-RUB1, followed by anti-HA IP of GST-3HA-RUB1 and incubation with 6HIS-FLAG-RCE1 or 6HIS-FLAG-RCE2. (a) Ability of AXL1/ECR1 or ECR1 (negative control) to transfer RUB1 to RCE1 and RCE2. Anti-FLAG immunoblot analysis detected GST-3HA-RUB1--6HIS-FLAG-RCE1/2 thioester formation, under non-reducing conditions (-DTT), catalyzed by AXL1/ECR1 (lanes 4 and 5), but not ECR1 (lanes 2 and 3). Asterisk is GST-3HA-RUB1--6HIS-FLAG-RCE1/2. Lanes 1 and 6 are negative controls, no RCE1/2. 6HIS-FLAG-RCE1/2 monomer runs at 28 kDa with RCE2 migrating slower than RCE1. Reactions stopped under non-reducing (-DTT, lanes 1-6) or reducing (+DTT, lanes 7-12) conditions and separated by SDS-PAGE. (b) Ability of AXL1/ECR1 or AXR1/ECR1 to transfer RUB1 to RCE1 and RCE2. Anti-FLAG immunoblot analysis detected GST-3HA-RUB1--6HIS-FLAG-RCE1/2 thioester formation, under non-reducing conditions (-DTT), catalyzed by both AXL1/ECR1 (lanes 2 and 3) and AXR1/ECR1 (lanes 5 and 6). Asterisk indicates GST-3HA-RUB1--6HIS-FLAG-RCE1/2 conjugate. Lanes 1 and 4, negative controls lacking RCE1/2. Reactions were stopped under non-reducing (-DTT, lanes 1-6) or reducing (+DTT, lanes 7-12)conditions, separated by SDS-PAGE.

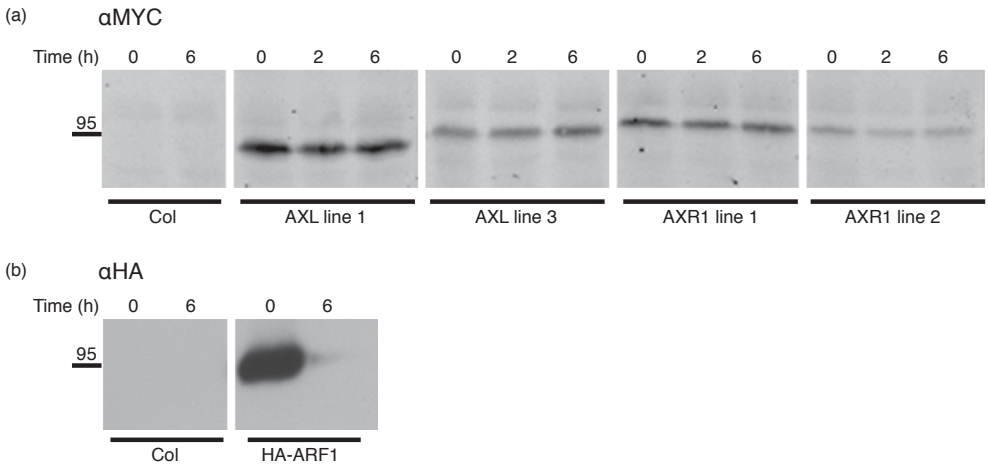

Figure 22. Protein levels for AXR1 and AXL1 are stable.

(a) Protein levels in eight-day-old seedlings treated for 0, 2, or 6 hours with 0.2 mg ml-1 cycloheximide. Based on anti-MYC immunoblot analyses, 10MYC-AXL1 and 10MYC-AXR1 accumulate protein to similar levels above background (Col). For both 10MYC-AXL1 and 10MYC-AXR1, protein is stable over 6 hours cycloheximide (0.2 mg ml-1) treatment. 150 µg total protein is loaded for all samples. 95 kDa protein marker is added for reference. (b) Protein levels in eight-day-old seedlings treated for 0 or 6 hours with 0.2 mg ml-1 cycloheximide. Based on anti-HA immunoblot analysis, 3HA-ARF1 accumulates protein above background (Col). 3HA-ARF1 protein levels are diminished over 6 hours cycloheximide (0.2 mg ml-1) treatment. 150 µg total protein was loaded for all samples. 95 kDa protein marker is added for reference.

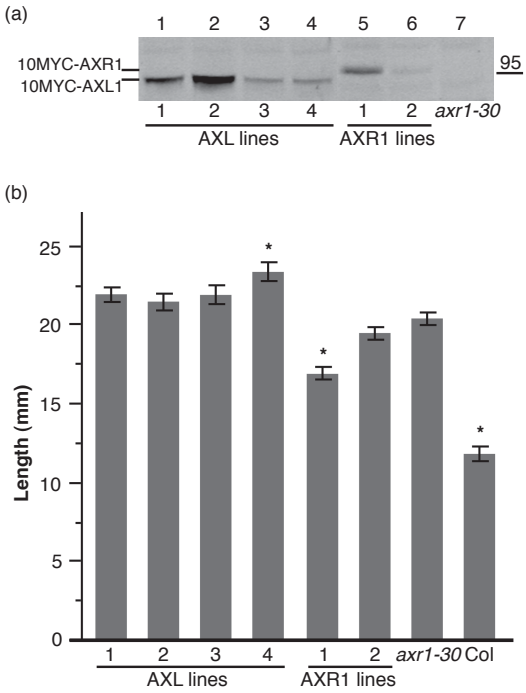

Figure 23. Protein levels for AXR1 and AXL1 are similar in *axr1-30* transgenic lines, but only AXR1 line 1 shows moderate correction of *axr1-30* phenotype in seedlings.

(a) Protein levels in eight-day-old seedlings. Based on anti-MYC immunoblot analyses, 10MYC-AXL1 (lanes 1-4) and 10MYC-AXR1 (lanes 5 and 6) accumulate protein to similar levels above background (lane 7), in characterized *axr1-30* transgenic lines. 150 µg total protein was loaded for all samples. b Root length in nine-day-old seedlings. Transgenic lines were plated on GM agar and grown for nine days with germination marked on day two. On day nine, seedlings were removed from plates, photographed, and root length was measured. Student's t-tests with Bonferroni adjustment ($\alpha = 0.00385$) were performed on combined data from three replicates. Plant lines marked with an asterisk are significantly different from *axr1-30*. Error bars represent SE with minimally n = 41 measurements per line.

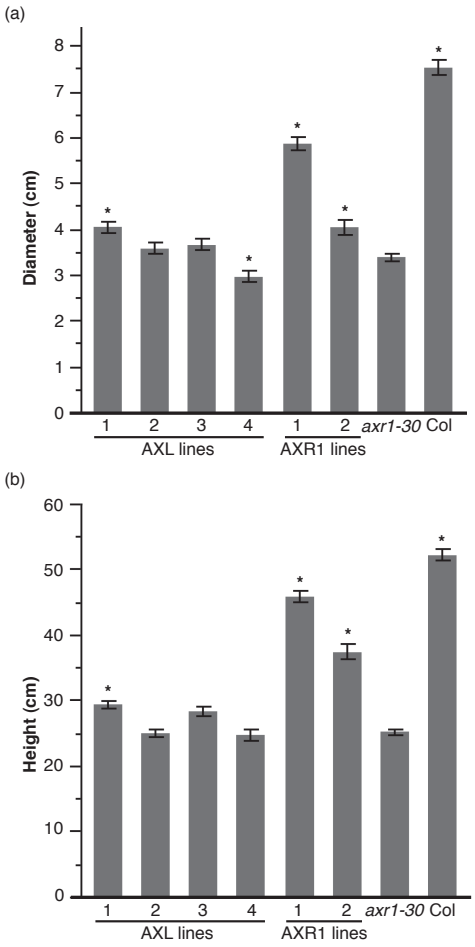

Figure 24. AXR1 corrects *axr1-30* adult phenotypic defects more than AXL1.

(a) Rosette diameter measurements on 28-day-old plants. Transgenic lines were grown for 28 days, then each was photographed and diameter was measured. Student's t-tests with Bonferroni adjustment ($\alpha = 0.00313$) were performed on log-transformed data combined from two replicates. Plant lines marked with an asterisk are significantly different from *axr1-30*. Error bars represent SE with minimally n = 29 measurements per line. (b) Inflorescence height measurements on 70-day-old plants. Transgenic lines were grown for 70 days and height was measured. Student's t-tests with Bonferroni adjustment ($\alpha = 0.00313$) were performed on log-transformed data combined from two replicates. Plant lines marked with an asterisk are significantly different from *axr1-30*. Error bars represent SE with minimally n = 24 measurements per line.

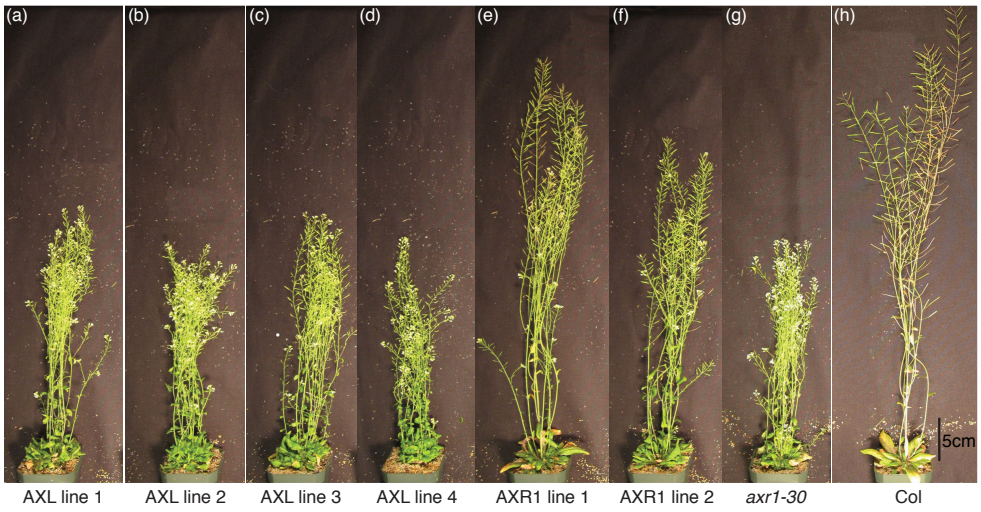

Figure 25. At day 70 post-plating, AXR1 corrects the inflorescence height defect of axr1-30 more than AXL1.

AXR1 and AXL lines were grown for 70 days and height was measured. Representative pictures of AXL lines (a-d), AXR1 lines (e-f), *axr1-30* (g), and Columbia (h) are shown. Scale bar represents 5 cm.

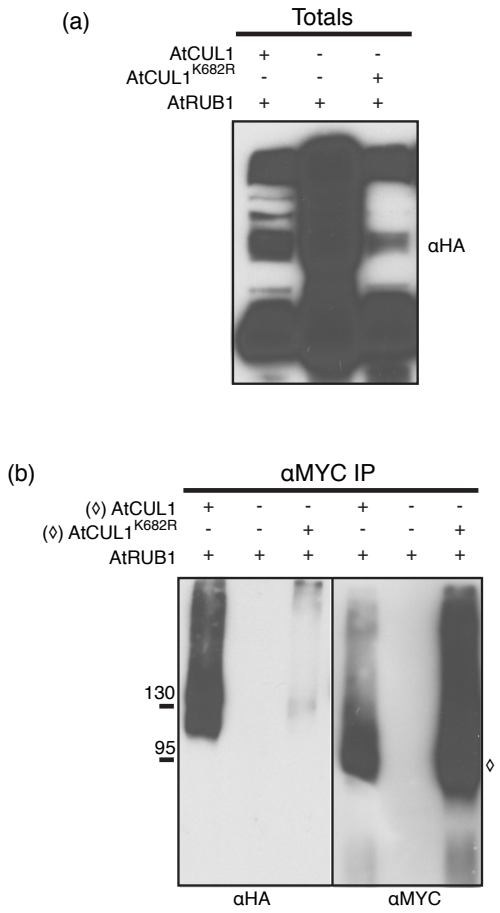

Figure 26. Comparison of RUB modification of MYC-CUL1 and MYC-CUL1^{K682R} in transient tobacco assays.

Gene constructs encoding 6HIS-3HA-RUB1 and MYC-tagged putative RUB-interacting proteins were co-infiltrated in tobacco leaves by *Agrobacterium*-mediated transformation. Anti-MYC IPs were carried out on soluble protein fractions, resolved on SDS-PAGE, and analyzed by anti-HA and anti-MYC immunoblot analyses. MYC-CUL1 was compared to the rubylation site mutant MYC-CUL1^{K682R} to establish assay specificity. Expression of 6HIS-3HA-RUB1 alone served as the background control for anti-MYC IPs. (a) Anti-HA immunoblots of total aliquots were done to establish expression of 6HIS-3HA-RUB1 in all samples. (b) Anti-MYC IPs of MYC-CUL1 and MYC-CUL1^{K682R} were successful (αMYC), but 6HIS-3HA-RUB1 readily modified only MYC-CUL1 (αHA). Background was low for 6HIS-3HA-RUB1 alone. The diamond symbol to the right of the blot in (b) indicates the predicted size of unmodified MYC-CUL1/CUL1^{K682R}. Representative blots are shown. Size markers are in kDa.

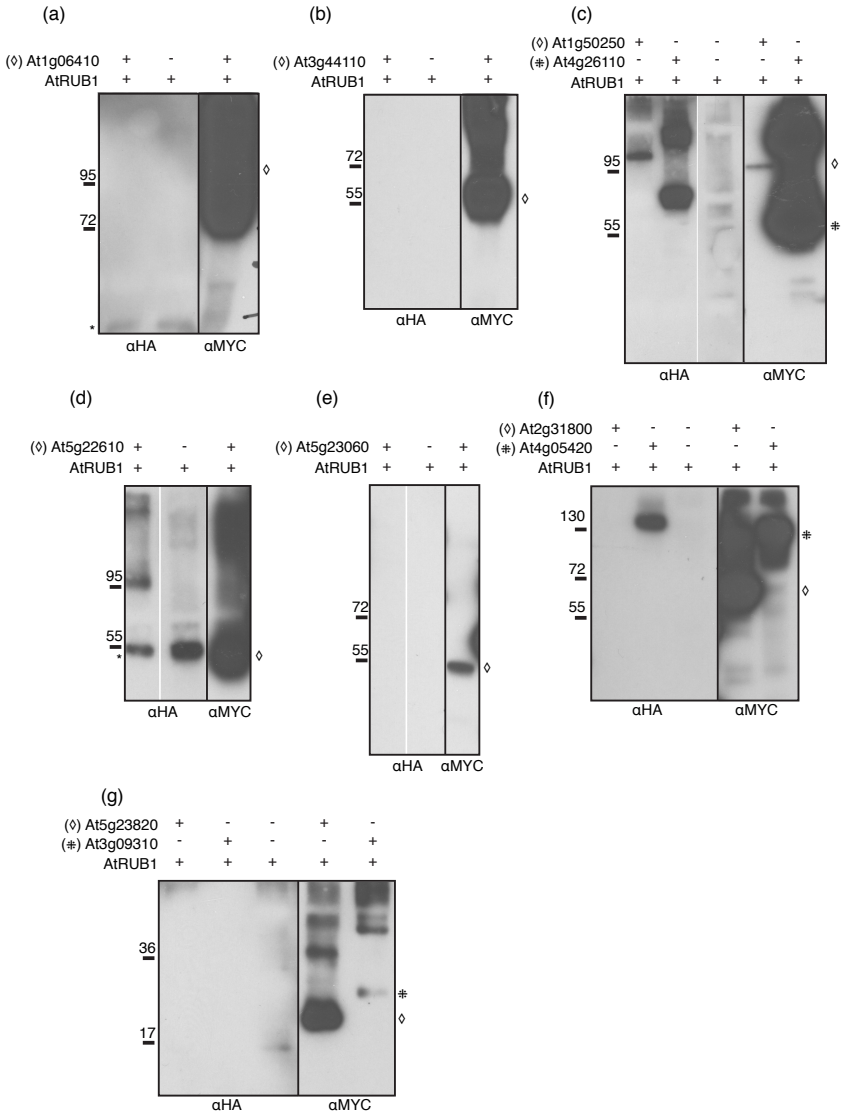

Figure 27. At1g50250, At4g26110, At5g22610, and At4g05420 encode proteins that interact with RUB1 in transient tobacco assays.

Plasmids for expression of 6HIS-3HA-RUB1 and MYC-tagged putative RUB-interacting proteins were co-infiltrated in tobacco leaves by *Agrobacterium*-mediated transformation. Anti-MYC IPs were carried out on soluble protein fractions, resolved on SDS-PAGE, and analyzed by anti-HA and anti-MYC westerns. Proteins encoded by (a) At1g06410, (b) At3g44110, (c) At1g50250 and At4g26110, (d) At5g22610, (e) At5g23060, (f) At2g31800 and At4g05420, and (g) At5g23820 and At3g09310 were tested. Slow-migrating anti-HA immunoreactive bands (indicative of RUB1-modified proteins) are present in anti-MYC IPs with (c) At1g50250 and At4g26110, (d) At5g22610, and (f) At4g05420, whereas the remaining samples (a) At1g06410, (b) At3g44110, (e) At5g23060, (f) At2g31800, and (g) At5g23820 and At3g09310 do not have anti-HA signal (a-g, αHA). The symbols to the right of each blot indicate the predicted sizes of the unmodified MYC-tagged proteins, with a symbol designated to the left of each construct name above. The asterisk found to the left of some blots indicates a background anti-HA immunoreactive background band at 55 kDa that was sometimes present. Size markers are in kDa.

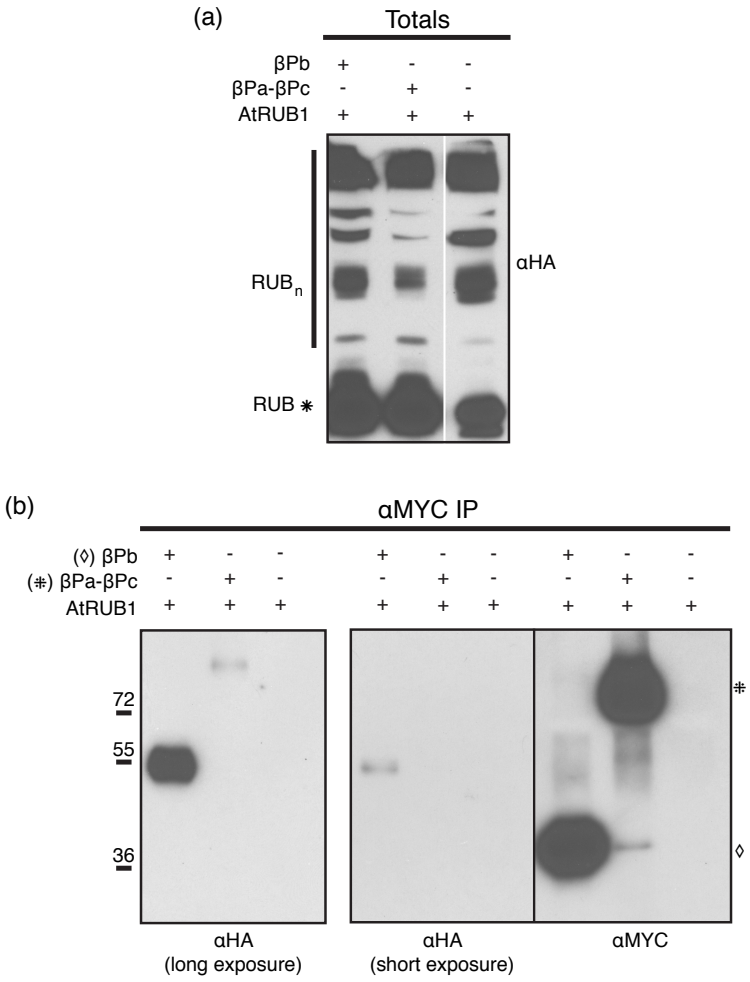

Figure 28. RUB modification status for split DDB1a (encoded by At4g05420) constructs: RUB modification for β-propeller domains βPb is greater than βPa-βPc.

Constructs encoding 6HIS-3HA-RUB1 and MYC-βPb or MYC-βPa-βPc proteins were co-infiltrated in tobacco leaves; expression of 6HIS-3HA-RUB1 alone served as the negative control. Anti-MYC IPs were done on soluble protein fractions, resolved on SDS-PAGE, and analyzed by anti-HA and anti-MYC immunoblot analyses. MYC-βPb was compared to MYC-βPa-βPc to determine specificity of RUB modification of DDB1a. (a) Anti-HA immunoblots of total aliquots were done to establish expression of 6HIS-3HA-RUB1 in all samples. (b) Anti-MYC IPs of MYC-βPb and MYC-βPa-βPc were successful (αMYC), but only MYC-βPb was readily modified by 6HIS-3HA-RUB1 (αHA). On long exposures of the αHA blot, a small proportion of MYC-βPa-βPc is RUB-modified, suggesting the preferred RUB modification site is found in the βPb subunit (αHA, compare βPb and βPa-βPc samples). Symbols to the right of the blot in (b) indicate the sizes of the unmodified MYC-tagged proteins, with a symbol designated to the left of each construct name.Size markers are in kDa.

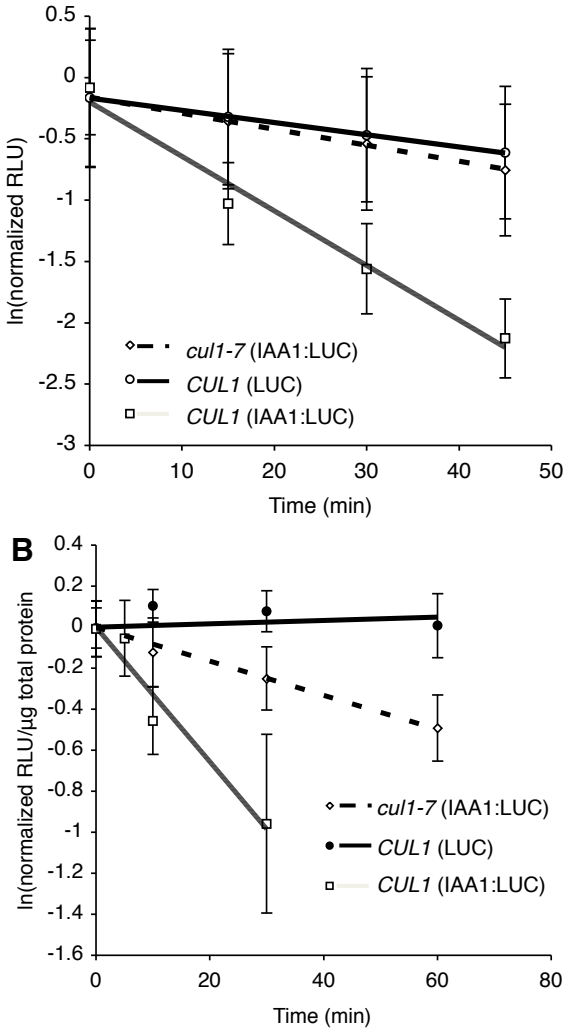

Figure 29. Degradation of IAA1-LUC is slowed in a mutant line called *cul1-7*.

(A). Single-seedling degradation assay. Experiment performed on 7-day-old seedlings. Zero represents the initial luciferase activity of seedlings in the initial plate reading. Values represent averages +/- one sd from a total of at least 56 seedlings from 2 independent experiments. $T_{1/2}$ (IAA1-LUC) = 15 and 53 min, respectively for *CUL1* and *cul1-7*. $T_{1/2}$ (LUC) = 70 min in *CUL1*.

(B) Pooled-seedling degradation assay. Values represent averages +/- standard deviation from a total of 9 replicates, from three independent experiments. $T_{1/2}$ (IAA1-LUC) = 21 and 83 min respectively for *CUL1* and *cul1-7*. Loss of LUC in *CUL1* is not detected.

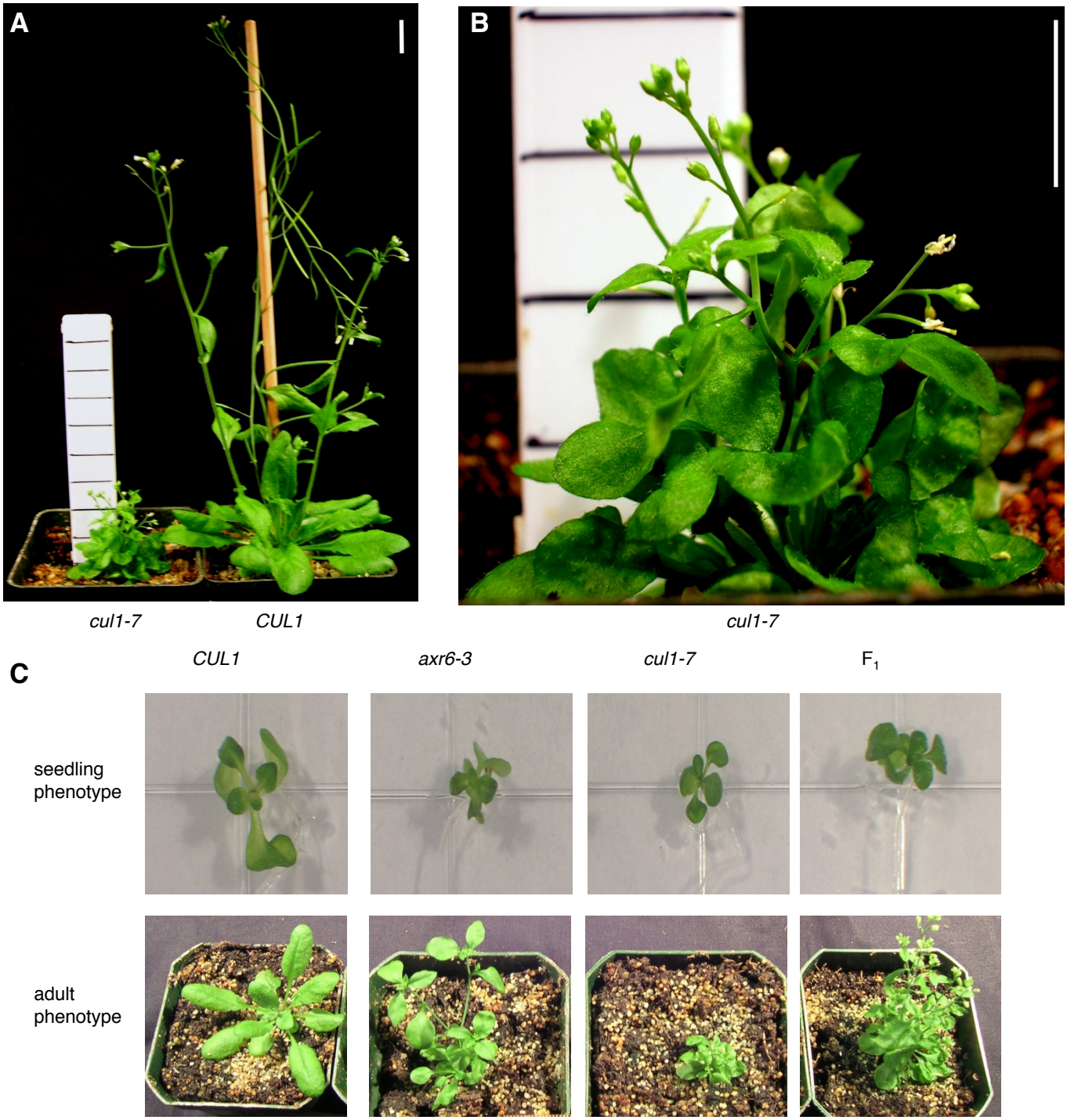

Figure 30. Morphological phenotypes of *cul1-7* in comparison to wild type and *axr6-3*.

(A) and (B) Aerial phenotype of *cul1-7*. (A) One week-old c*ul1-7* (left) and the progenitor line *CUL1* (right) seedlings grown on GM were transferred to soil and grown four weeks more under a 16h photoperiod. (B) Close up of *cul1-7* phenotype in (A). All scale bars represent 1 cm. (C) Allelism test of *cul1-7* with *axr6-3*. *cul1-7* was crossed crossed to *axr6-3*, and the resulting F_1 progeny were grown two weeks at 22°C under constant light on GM plates, genotyped, then transferred to soil for an additional six weeks.

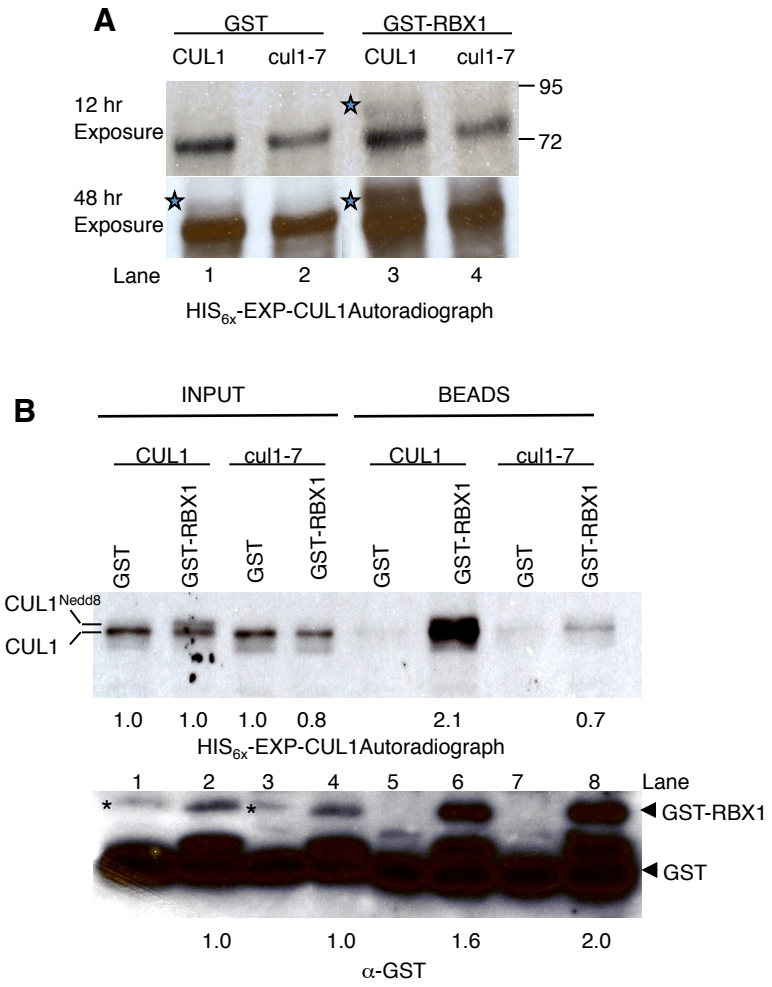

Figure 31. RBX1 interaction with cul1-7 is impaired.

(A) *In vitro* translations of HIS_{6x}-EXP-CUL1 and HIS_{6x}-EXP-cul1-7 in the presence of GST-RBX1. Proteins were translated *in vitro* and radio-labeled with ^{3}H-Leu. Reactions were supplemented with approximately 125 ng either GST or GST-RBX1. Stars were placed to the left of $CUL1^{Nedd8}$ bands. (B) Pulldown of *in vitro* translated HIS_{6x}-EXP-CUL1 and HIS_{6x}-EXP-cul1-7 with GST-RBX1. HIS_{6x}-EXP-CUL1 and HIS_{6x}-EXP-cul1-7 proteins were translated in reactions supplemented with approximately 500 ng of GST or GST-RBX1. Translations were incubated with glutathione-sepharose beads to collect GST-RBX1 complexes. Input represents 1% of the total for the autoradiogram and 4% for the anti-GST blot. Beads represents 75% of the total pulldown for the autoradiogram and 25% for the anti-GST blot. Inputs were either normalized to the amount of HIS_{6x}-EXP-CUL1 translated with GST for the autoradiograph or to amount of GST-RBX in HIS_{6x}-EXP-CUL1 translation for the anti-GST blot, and the amount in the pulldowns were normalized to their respective inputs. The asterisk represents a nonspecific, cross-reactive band. A GST cleavage product that co-purified with GST-RBX1 is also detectable in the GST-RBX1 lanes.

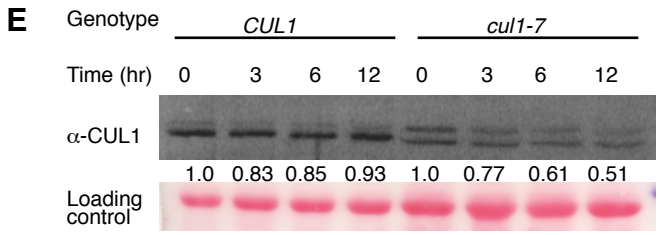

Figure 32. Degradation of cul1-7 is faster than CUL1.

CUL1 or cul1-7 protein degradation was examined in 7 day-old progenitor and *cul1-7* lines. The zero time-point represents a mock cycloheximide sample. Each lane represents 20 µg and 40 µg total protein for *CUL1* and *cul1-7*, respectively. CUL1 levels and image quantification were determined. Quantification denotes the amount of total CUL1 relative to 0 time-point for the given genotype.

(a)

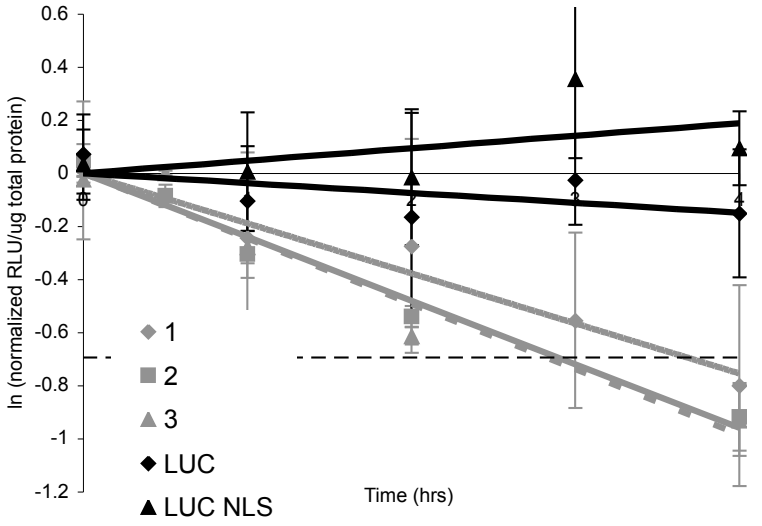

(b)

TG Line	Half-life (hrs)	R^2
ARF1:LUC line 1	3.7	1.0
ARF1:LUC line 2	2.7	1.0
ARF1:LUC line 3	2.9	0.9
LUC	>12	N/A
LUC:NLS	>12	N.A

(c)

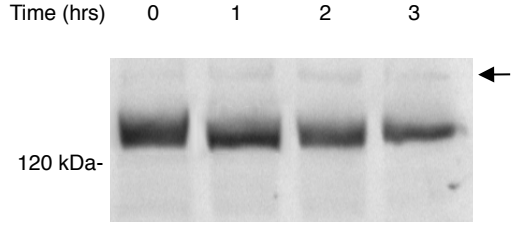

% protein	100	71	56	37
% activity	100	70	56	38

Figure 33. ARF1:LUC is degraded with a half-life of 2.7 to 3.7 hours.

(a) Natural log (ln) graph showing the degradation rate of ARF1:LUC in three independent transgenic lines (all grey lines; 1 – diamond, 2 – square, 3 – triangle) compared to LUC alone and LUC:NLS. Error bars represent the standard deviation from the mean. The dashed horizontal line indicates ln (0.5), which intersects the degradation curve at the half-life.
(b) Table of half-lives and R^2 for the data shown in (a).
(c) Anti-LUC western blot performed on equal total protein from a cycloheximide chase experiment using line 2. The LUC bands were quantified and the percentage of ARF1:LUC protein remaining at each time point relative to zero time point are give below. Arrow indicates the position of a cross-reacting band used as a loading control. LUC activity was determined from same extracts and expressed as percentage remaining relative to zero time point.

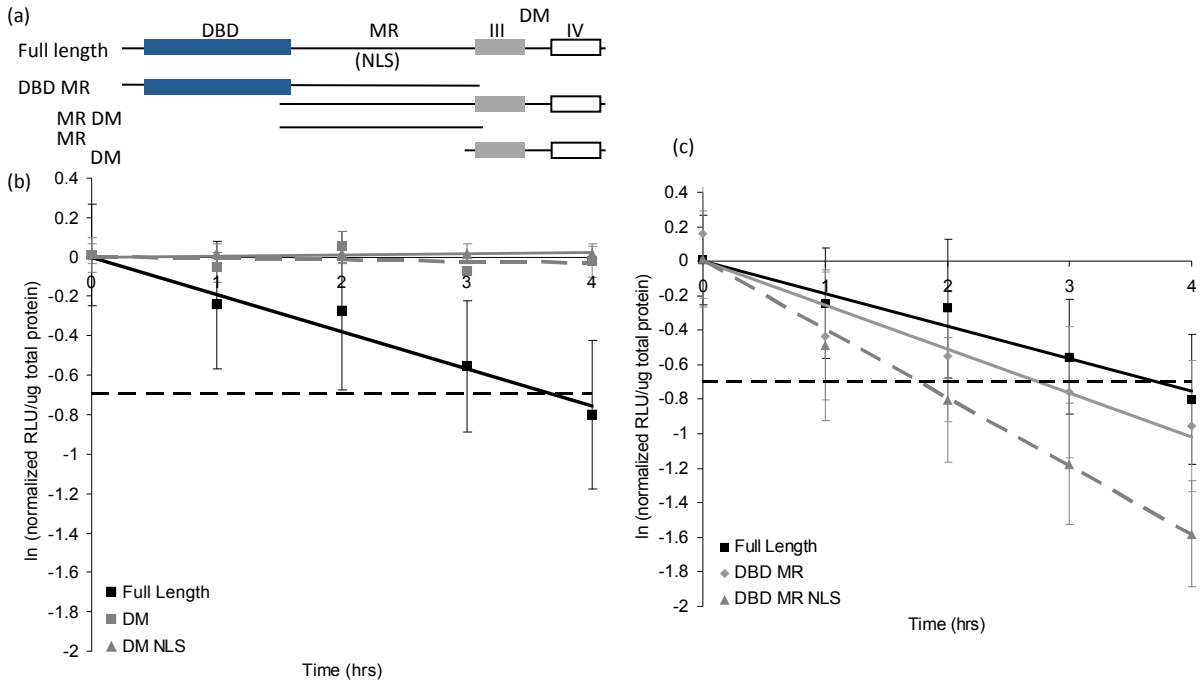

Figure 34. The MR of ARF1 is sufficient for conferring a ~3 hr half-life on LUC when ARF1 fusion proteins contain an exogenous NLS.

(a) A schematic illustration of the ARF1 segments fused to the N-terminus of LUC. When an NLS was present it was fused to the C-terminus of LUC. DBD – DNA binding domain, MR – Middle Region, DM – Domains III and IV, NLS – location of ARF1 predicted nuclear localization sequence. The names used to describe the segments are written to the left of the respective illustration.
(b) Graph of data acquired for cycloheximide chase experiments performed on ARF1:LUC full length, DM:LUC and DM:LUC:NLS. Error bars represent the standard deviation from the mean. The dashed horizontal line indicates ln (0.5), which intersects the degradation curve at the half-life.
(c) As in (b) but for ARF1:LUC (= Full Length), MR:LUC, MR:LUC:NLS and MRDM:LUC:NLS proteins.
(d) As in (b) but for ARF1:LUC (= Full Length), DBDMR:LUC and DBDMR:LUC:NLS.

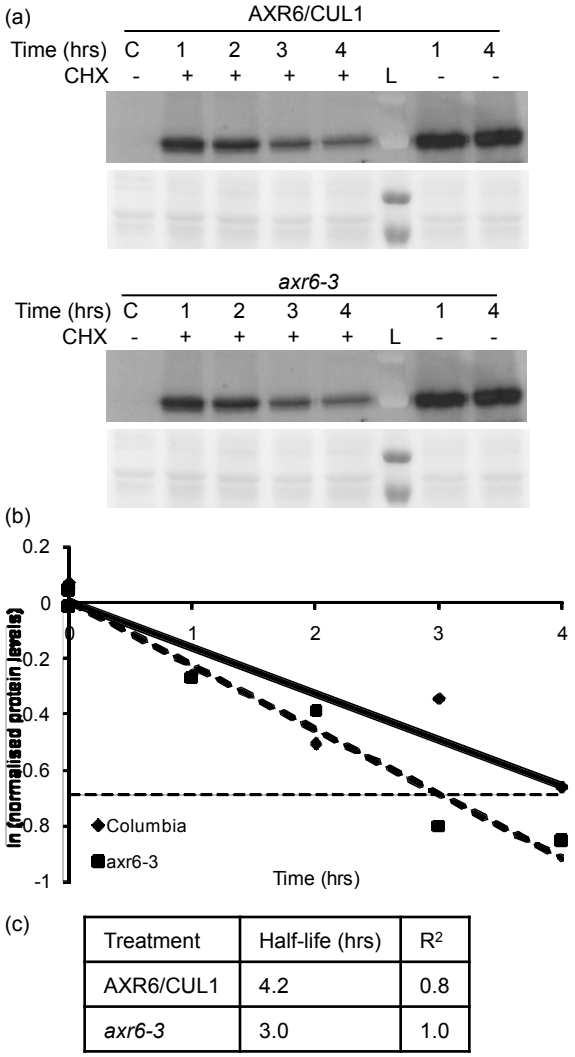

(c)

Treatment	Half-life (hrs)	R^2
AXR6/CUL1	4.2	0.8
axr6-3	3.0	1.0

Figure 35. The degradation rate of HA_3:ARF1 is not affected by mutation in *CUL1*.

(a) Anti-HA western blot on total protein extracts from seven-day-old transgenic seedlings line 1 in the *AXR6/CUL1* Columbia background (upper panel), or homozygous for the *axr6-3* mutation and expressing the HA_3:ARF1 fusion protein from the same insertion site as line 1 (lower panels), and treated with (+) or without (-) cycloheximide for the times indicated. Ponceau staining of the membranes to indicate protein loading. L is the marker lane with the 120 and 96 KDa proteins visible in each panel.
(b) Graph of the data obtained from the quantification of the western blot in (a). *axr6-3* are squares and dotted line, Columbia are diamonds and black line. The dashed horizontal line indicates ln (0.5), which intersects the degradation curve at the half-life.
(c) Half-lives and R^2 values calculated from data in (b).

Table 1 RUB conjugation components recovered by LC-MS/MS analysis of 3HA-RUB1 immunoprecipitations

Gene	Uniprot ID	AGI	Mass (Da)	Unique Peptides[a]	Total Unique Hits	Protein ID Probability[b]	% Coverage[c]
AXL1	Q9ZV69	At2g32410	57924.10	12	63	100%	33%
AXR1	P42744	At1g05180	60018.10	20	212	100%	56%
CUL1	Q94AH6 B9DGE3	At4g02570	86287.40	7	11	100%	12%
CUL4	Q8LGH4	At5g46210	91457.70	3	5	100%	5%
ECR1	O65041	At5g19180	50524.40	18	264	100%	48%
RCE1	Q9SDY5	At4g36800	20768.90	4	45	100%	28%
RUB1	Q9SHE7	At1g31340	8872.80	3	460	100%	50%

[a] Peptides are designated as unique if they differ in primary amino acid sequence and satisfy rules of parsimony.
[b] Protein ID probability is for the highest probability observed in 5 biological replicates.
[c] % coverage is cumulative for 5 biological replicates.

Table 2 Single peptide-based protein identifications from LC-MS/MS analysis of 3HA-RUB1 immunoprecipitations

Index	Gene	AGI	Sequence Identified	Peptide ID Probability	-log(e) Peptide Score	Precursor Ion m/z	Charge State	Sample
1	CUL1	At4g02570	(R)EAFEEYINSTVLPALR(E)	95%	4.23	926.48	2	C
2	CUL1	At4g02570	(K)IPLPPVDER(K)	95%	3.96	518.30	2	B
3	CUL1	At4g02570	(K)IPLPPVDER(K)	95%	3.52	518.30	2	B
4	CUL3a	At1g26830	(K)EIEQATEIPAADLK(R)	95%	6.52	764.40	2	A
5	CUL4	At5g46210	(K)VLSHTLLITELFQQLK(F)	95%	6.42	628.37	3	D
6	RCE2	At2g18600	(K)DISELNLPK(S)	95%	2.82	514.78	2	A
7	RCE2	At2g18600	(K)DISELNLPK(S)	95%	3.13	514.79	2	A

Table 3. Summary of putative RUB-interacting proteins identified from MS screen

Count	AGI #	Gene Symbol	Gene description	Sequence cloned	IP 6HIS-3HA-RUB1
1	At5g23820.1	none	MD-2-related lipid recognition domain-containing protein	cds	No
2	At3g44110.1	ATJ3	DNAJ homologue 3	cds	No
3	At1g06410	TPS7	trehalose-phosphatase/synthase 7	genomic	No
4	At1g50250.1	FTSH1	FTSH protease 1	cds	**Yes**
5	At3g24080.1	none	KRR1 family protein	n/a	n/a
6	At3g09310.1	none	unknown protein	cds	No
7	At5g23060.1	CaS	calcium sensing receptor	cds	No
8	At5g22610	none	F-box/RNI-like/FBD-like domains-containing protein	genomic	**Yes**
9	At4g26110.1	NAP1-1	nucleosome assembly protein1-1	cds	**Yes**
10	At2g31800.1	none	integrin-linked protein kinase family	cds	No
11	At4g05420.1	DDB1a	damaged DNA binding protein 1a	cds	**Yes**
12	At4g21100.1	DDB1b	damaged DNA binding protein 1b	n/a	n/a